

Copyright Warning & Restrictions

The copyright law of the United States (Title 17, United States Code) governs the making of photocopies or other reproductions of copyrighted material.

Under certain conditions specified in the law, libraries and archives are authorized to furnish a photocopy or other reproduction. One of these specified conditions is that the photocopy or reproduction is not to be “used for any purpose other than private study, scholarship, or research.” If a user makes a request for, or later uses, a photocopy or reproduction for purposes in excess of “fair use” that user may be liable for copyright infringement,

This institution reserves the right to refuse to accept a copying order if, in its judgment, fulfillment of the order would involve violation of copyright law.

Please Note: The author retains the copyright while the New Jersey Institute of Technology reserves the right to distribute this thesis or dissertation

Printing note: If you do not wish to print this page, then select “Pages from: first page # to: last page #” on the print dialog screen

The Van Houten library has removed some of the personal information and all signatures from the approval page and biographical sketches of theses and dissertations in order to protect the identity of NJIT graduates and faculty.

ABSTRACT

HYDROPHOBICALLY MODIFIED ISOSORBIDE DIMETHACRYLATES AS BIOMATERIALS FOR BISPHENOL A FREE DENTAL FILLINGS

by
Bilal Marie

Amalgam and Bisphenol A glycerolate dimethacrylate (BisGMA) are the main dental filling materials in use today. Because of the negative perception of amalgam and its lower esthetic appeal, as well as the desire to replace the endocrine disruptor Bisphenol A, which is the building block of BisGMA, there has been a critical need to search for safer alternatives to these dental filling materials.

Isosorbide is a sugar-based molecule generally recognized as safe. It has been extensively studied as a replacement to the Bisphenol A core in various materials. However, isosorbide is extremely hygroscopic, and water uptake in dental fillings causes expansion, plasticization and reduced mechanical properties.

Hydrophilic materials take up more water than hydrophobic ones. Therefore, modifying isosorbide with hydrophobic moieties such as hydroxy benzoates, can lead to improved and controlled water uptake and mechanical properties of the isosorbide dental resin.

A series of bio-based hydrophobically modified isosorbide dimethacrylates, with a *para*, *meta*, and *ortho* benzoate aromatic spacer, are synthesized, characterized, and evaluated as dental restorative resins. The new monomers, isosorbide 2,5-bis(glyceryloxybenzoate) dimethacrylates, are further mixed with triethylene glycol dimethacrylate (TEGDMA) at a 60:40 weight ratio, and evaluated for viscosity, degree of conversion, polymerization shrinkage, water sorption, glass transition temperature, flexural

strength, and modulus. BisGMA is prepared and evaluated as a reference. Isosorbide glycerolate dimethacrylate (ISDGMA), a hydrophilic isosorbide dimethacrylate control, is synthesized and evaluated as well.

The polymers derived from the hydrophobically modified isosorbide dimethacrylates show significant reduction in water sorption at 39-44 $\mu\text{g}/\text{mm}^3$ over poly(ISDGMA/TEGDMA) at 73 $\mu\text{g}/\text{mm}^3$, and improved network stability. Their flexural strength is also higher at 37-42 MPa in comparison to 10 MPa for poly(ISDGMA/TEGDMA) after immersion in a phosphate buffer solution for 24 hours.

The performance of the new materials is close to that of the reference poly(BisGMA/TEGDMA), whose water sorption is 26 $\mu\text{g}/\text{mm}^3$ and flexural strength is 52 MPa. The degree of monomeric conversion and glass transition temperature for the *ortho* derived isosorbide polymer at 52% and 85°C is also close to that of poly(BisGMA/TEGDMA) at 54% and 95°C, respectively. Therefore, this dissertation demonstrates the design and development of a potential BisGMA dental resin replacement.

**HYDROPHOBICALLY MODIFIED ISOSORBIDE DIMETHACRYLATES AS
BIOMATERIALS FOR BISPHENOL A FREE DENTAL FILLINGS**

**by
Bilal Marie**

**A Dissertation
Submitted to the Faculty of
New Jersey Institute of Technology
in Partial Fulfillment of the Requirements for the Degree of
Doctor of Philosophy in Materials Science and Engineering
Interdisciplinary Program in Materials Science and Engineering
December 2021**

Copyright © 2021 by Bilal Marie

ALL RIGHTS RESERVED

APPROVAL PAGE

**HYDROPHOBICALLY MODIFIED ISOSORBIDE DIMETHACRYLATES AS
BIOMATERIALS FOR BISPHENOL A FREE DENTAL FILLINGS**

Bilal Marie

Dr. Michael Jaffe, Dissertation Co-Advisor Date
Research Professor of Biomedical Engineering, NJIT

Dr. Nugehalli M. Ravindra, Co-Advisor Date
Professor of Physics, NJIT

Dr. Cristiano Dias, Committee Member Date
Associate Professor of Physics, NJIT

Dr. Murat Guvendiren, Committee Member Date
Assistant Professor of Chemical and Materials Engineering, NJIT

Dr. Keith Chenault, Committee Member Date
Group Leader, Applied Research, Ashland Inc, Bridgewater, NJ

BIOGRAPHICAL SKETCH

Author: Bilal Marie
Degree: Doctor of Philosophy
Date: December 2021

Undergraduate and Graduate Education:

- Doctor of Philosophy in Materials Science and Engineering
New Jersey Institute of Technology, Newark, NJ 2021
- Master of Science in Chemistry
Polytechnic Institute of New York University, Brooklyn, NY 2009
- Bachelor of Science in Biochemistry
The College of Staten Island, Staten Island, NY 2006

Major: Materials Science and Engineering

Publications and Patents:

Journal Articles

Marie, B.; Clark, R.; Gillece, T.; Ozkan, S.; Jaffe, M.; Ravindra, N.M. Hydrophobically Modified Isosorbide Dimethacrylates as a Bisphenol-A (BPA)-Free Dental Filling Material. *Materials* (2021) *14*, 2139

Tallon, M.A.; Rogan, Y.; Marie, B.; Clark, R.; Musa, O.M.; Khosravi, E. Monomer Sequencing and Microstructural Analysis on Polymers of Dimethyl Norbornene Dicarboxylate and 7-Oxanorbornene Dicarboxylic Derivatives Employing Ruthenium Catalysts by Ring-Opening Metathesis Polymerization. *Journal of Polymer Science Part A: Polymer Chemistry* (2014) *52*, 2477-2501

Mukherjee, N.; Sun, C.; Marie, B.; Jin, S.; Peetz, R.M. Soluble and Processable Conjugated Polyazines with Oligo(p-phenylene vinylene)s. *Tetrahedron Letters* (2008) *49*, 1037-1040

Patents

Marie, B.; Tallon, M.; Musa, O. Dihydroxy Lactam Based Polymer, Compositoins and Applications Thereof. WO 2020/154471 A1, 30 July 2020

Nguyen, T.; Lei, C.; Yang, H.; Marie, B. Cementing Fluid and Methods for Producing The Same. US 20150191642A1, 9 July 2015

I dedicate this dissertation to my beloved wife, Alaa, who has been a constant source of encouragement and support during this journey.

I also dedicate this work to my children, Amaya, Elyas, and Adam. I hope the sacrifices you endured for me to pursue this dream will be repaid to you with many opportunities of joy and success in your future.

This dissertation is also dedicated to my dear parents, my beloved brothers and sister, my extended family, and friends. Your support and encouragement of me goes beyond what the words can express.

مع فائق الحب و التقدير و الاحترام

بلال

ACKNOWLEDGMENT

I would like to express my sincere and deep gratitude to my co-advisors, Dr. Michael Jaffe, and Dr. Nuggehalli Ravindra for their continuous support, patience, guidance, and for providing me with such a great opportunity to learn and grow.

I would also like to thank my committee members, Dr. Keith Chenault, Dr. Cristiano Dias, and Dr. Murat Guvendiren for their support, guidance, and insightful comments.

I am very grateful to my mentors, Dr. Keith Silverman, and Dr. Michael Tallon (may you rest in peace), and my colleagues, Bret Clark, Tim Gillece, Dr. Seher Ozkan, Dr. Zheng Li, and Larry Feeley for their guidance, assistance, and encouragement.

I am also very appreciative to my lab mates and friends, Gabrielle Busto, and Richard Vincent, for their support and for keeping a watchful eye on my experiments.

TABLE OF CONTENTS

| Chapter | | Page |
|----------------|--|-------------|
| 1 | INTRODUCTION..... | 1 |
| 1.1 | Dental Caries..... | 1 |
| 1.2 | Historical Perspective of Dental Restoration Materials..... | 6 |
| 1.3 | Dental Ceramics..... | 8 |
| 1.4 | Dental Gold and Casting Alloys | 9 |
| 1.5 | Dental Amalgam..... | 10 |
| 1.6 | Dental Polymers..... | 12 |
| 1.7 | Resin-Based Composites..... | 14 |
| 1.7.1 | The Monomer System..... | 17 |
| 1.7.2 | The Polymerization Process..... | 21 |
| 1.7.3 | Evaluation..... | 31 |
| 1.8 | Isosorbide..... | 42 |
| 2 | HYPOTHESIS AND OBJECTIVES..... | 46 |
| 2.1 | Hypothesis..... | 46 |
| 2.2 | Specific Objectives..... | 48 |
| 2.2.1 | Objective 1..... | 48 |
| 2.2.2 | Objective 2..... | 48 |
| 3 | METHODS..... | 49 |
| 3.1 | Structure Elucidation and Thermal Analysis..... | 49 |
| 3.1.1 | Nuclear Magnetic Resonance..... | 49 |

TABLE OF CONTENTS
(Continued)

| Chapter | Page |
|--|-------------|
| 3.2 Sample Preparation..... | 53 |
| 3.3 Water Sorption..... | 53 |
| 3.4 Degree of double Bond Conversion..... | 54 |
| 3.5 Polymerization Shrinkage..... | 54 |
| 3.6 Glass Transition Temperature..... | 55 |
| 3.7 Flexural Strength and Modulus..... | 55 |
| 3.8 Statistical Analysis..... | 56 |
| 3.9 Hydrophobic Evaluation..... | 56 |
| 3.10 Viscosity Evaluation..... | 56 |
| 4 SYNTHESIS of ISOSORBIDE DIMETHACRYLATES..... | 57 |
| 4.1 Isosorbide 2,5-bis(glyceryloxy) dimethacrylate (ISDGMA)..... | 57 |
| 4.2 Isosorbide 2,5-bis(4-glyceryloxybenzoate) dimethacrylate (ISB4GBMA)..... | 60 |
| 4.3 Isosorbide 2,5-bis(3-glyceryloxybenzoate) dimethacrylate (ISB3GBMA)..... | 65 |
| 4.4 Isosorbide 2,5-bis(2-glyceryloxybenzoate) dimethacrylate (ISB2GBMA)..... | 66 |
| 5 RESULTS AND DISCUSSION..... | 68 |
| 5.1 Structural Analysis..... | 69 |
| 5.1.1 NMR Analysis of ISDGMA and Reaction Intermediates..... | 70 |
| 5.1.2 NMR Analysis of ISB4GBMA and Reaction Intermediates..... | 73 |

TABLE OF CONTENTS
(Continued)

| Chapter | Page |
|---|-------------|
| 5.1.3 NMR Analysis of ISB3GBMA and Reaction Intermediates..... | 76 |
| 5.1.4 NMR Analysis of ISB2GBMA and Reaction Intermediates..... | 79 |
| 5.1.5 NMR Comparison of the Isosorbide Cyclic Protons H3 and H4..... | 82 |
| 5.2 Hydrophobicity..... | 85 |
| 5.3 Viscosity..... | 86 |
| 5.4 Degree of Double Bond Conversion..... | 88 |
| 5.5 Polymerization Shrinkage..... | 90 |
| 5.6 Glass Transition Temperature..... | 91 |
| 5.7 Water Sorption..... | 94 |
| 5.8 Flexural Strength and Modulus..... | 98 |
| 6.0 SUMMARY AND FUTURE WORK..... | 102 |
| 6.1 Summary..... | 102 |
| 6.2 Future Work..... | 104 |
| APPENDIX A PROTON NMR SPECTRA..... | 106 |
| APPENDIX B ATR-FTIR SPECTRA..... | 108 |
| APPENDIX C EFFECT OF CURING DURATION ON WATER SORPTION OF P(ISDGMA/TEGDMA)..... | 114 |
| APPENDIX D DATA CORRELATIONS..... | 115 |
| REFERENCES..... | 117 |

LIST OF TABLES

| Table | Page |
|-------|--|
| 1.1 | 2017 Top 3 Global Prevalent Disorders..... 1 |
| 1.2 | Minimal Mechanical Requirements for Casting Alloys..... 10 |
| 1.3 | Estimated Mercury Concentration In Respiratory, Urinary, and Blood Systems..... 12 |
| 1.4 | Examples of Composite Classification Based On Filler Particle Size and Distribution..... 15 |
| 1.5 | Degree of Conversion for BisGMA, BisEMA, UDMA, and TEGDMA..... 33 |
| 1.6 | Degree of Conversion of BisGMA as a Function of TEGDMA Content..... 34 |
| 1.7 | Correlation of Degree of Conversion with Molecular Structure and Flexural Strength and Modulus 36 |
| 1.8 | Water Uptake % of BisGMA, UDMA, and TEGDMA..... 37 |
| 1.9 | Correlation of The Degree of Conversion with Polymerization Shrinkage..... 39 |
| 1.10 | Bisphenol A Content in Commercial BisGMA..... 41 |
| 2.1 | Glass Transition Temperature and Water Uptake of Cured Isosorbide Epoxies with Jeffamine..... 47 |
| 5.1 | Molecular Weight and Double Bond Concentration of ISB4GBMA, ISB3GBMA, ISB2GBMA, ISDGMA, BisGMA, and TEGDMA..... 68 |
| 5.2 | Contact Angle Measurements and cLogP Estimations of BisGMA, ISB4GBMA, ISB3GBMA, ISB2GBMA, and ISDGMA..... 85 |
| 5.3 | Glass Transition Temperature of P(BisGMA/TEGDMA), P(IB4GBMA/TEGDMA), P(ISB3GBMA/TEGDMA), P(ISB2GBMA/TEGDMA), and P(ISDGMA/TEGDMA) at 60:40 wt%..... 92 |

**LIST OF TABLES
(CONTINUED)**

| Table | Page |
|---|-------------|
| 5.4 cLogP Values for Isosorbide, Isosorbide Derivatives and BisGMA..... | 97 |
| 5.5 Water Uptake After 24 Hours and at 37°C for P(BisGMA/TEGDMA), P(ISB4GBMA/TEGDMA), P(ISB3GBMA/TEGDMA), P(ISB2GBMA/TEGDMA) and P(ISDGMA/TEGDMA)..... | 100 |
| D.1 Monomer Mixture Viscosity, Degree of Conversion, and Polymerization Shrinkage for P(BisGMA/TEGDMA), P(ISB4GBMA/TEGDMA), P(ISB3GBMA/TEGDMA), P(ISB2GBMA/TEGDMA), and P(ISDGMA/TEGDMA)..... | 115 |
| D.2 Degree of Conversion, Glass Transition Temperature, and Water Sorption for P(BisGMA/TEGDMA), P(ISB4GBMA/TEGDMA), P(ISB3GBMA/TEGDMA), P(ISB2GBMA/TEGDMA), and P(ISDGMA/TEGDMA)..... | 115 |
| D.3 Degree of Conversion and Flexural strength for P(BisGMA/TEGDMA), P(ISB4GBMA/TEGDMA), P(ISB3GBMA/TEGDMA), P(ISB2GBMA/TEGDMA), and P(ISDGMA/TEGDMA)..... | 116 |
| D.4 Degree of Conversion and Flexural Modulus for P(BisGMA/TEGDMA), P(ISB4GBMA/TEGDMA), P(ISB3GBMA/TEGDMA), P(ISB2GBMA/TEGDMA), and P(ISDGMA/TEGDMA)..... | 116 |

LIST OF FIGURES

| Figure | | Page |
|--------|--|------|
| 1.1 | Clinical and radiographic examination of the various stages of dental caries..... | 2 |
| 1.2 | Tooth structure and dental plaque..... | 3 |
| 1.3 | Initial clinical sign of dental caries in progress..... | 4 |
| 1.4 | A Schematic representation of a fluorapatite-like remineralized crystal surface..... | 5 |
| 1.5 | Dental caries balance..... | 6 |
| 1.6 | Etruscan denture 700 BC..... | 7 |
| 1.7 | Three implanted incisors made of seashells 800 AD | 7 |
| 1.8 | All-ceramic posterior bridge..... | 9 |
| 1.9 | High gold alloy a) inlay, b) only, c) partial crown | 10 |
| 1.10 | Dental amalgam filling..... | 11 |
| 1.11 | Resin-based composite filling..... | 13 |
| 1.12 | Cross-linked polymeric network..... | 14 |
| 1.13 | Schematic representation of silane bonding between fillers and polymer matrix..... | 17 |
| 1.14 | Silane coupling agent mechanism..... | 17 |
| 1.15 | Common dental dimethacrylates | 18 |
| 1.16 | Synthesis scheme of BisGMA..... | 19 |
| 1.17 | Synthesis scheme of TEGDMA..... | 20 |
| 1.18 | Synthesis scheme of UDMA..... | 20 |
| 1.19 | Mechanism of redox initiation by benzoyl peroxide/amine system..... | 22 |

LIST OF FIGURES
(Continued)

| Figure | | Page |
|---------------|---|-------------|
| 1.20 | Photoinitiation of camphorquinone and amines..... | 24 |
| 1.21 | Schematic representation of the polymerization process..... | 25 |
| 1.22 | The structural heterogeneity of dimethacrylate networks..... | 27 |
| 1.23 | Physical and chemical cross-linking as well as defects in the polymer network..... | 28 |
| 1.24 | BisGMA and BisEMA..... | 33 |
| 1.25 | Tan delta plots of 70:30 wt% P(BisGMA/TEGDMA) cured at different time intervals with corresponding degree of conversion percentage..... | 35 |
| 1.26 | Degradation products of BisGMA and TEGDMA..... | 40 |
| 1.27 | General scheme for the synthesis of isosorbide..... | 42 |
| 1.28 | 1,4:3,6-dianhydrohexitols..... | 42 |
| 1.29 | Intramolecular hydrogen bonding in isosorbide and isomannide..... | 43 |
| 1.30 | Isosorbide and Bisphenol A..... | 44 |
| 1.31 | Isosorbide based dental dimethacrylates..... | 44 |
| 2.1 | Hydrophobically modified isosorbide dimethacrylates with an aromatic spacer..... | 46 |
| 2.2 | Hydrophobically modified isosorbide epoxides with an aromatic spacer..... | 47 |
| 3.1 | Proton chemical Shifts..... | 52 |
| 4.1 | Synthesis scheme of ISDGMA..... | 57 |
| 4.2 | Synthesis scheme of ISB4GBMA..... | 60 |
| 4.3 | Synthesis scheme of ISB3GBMA..... | 65 |

LIST OF FIGURES
(Continued)

| Figure | | Page |
|---------------|--|-------------|
| 4.4 | Synthesis scheme of ISB2GBMA..... | 66 |
| 5.1 | Chemical structures of ISB4GBMA ISB3GBMA, ISB2GBMA, ISDGMA, BisGMA, and TEGDMA | 68 |
| 5.2 | ¹ H NMR spectrum of isosorbide in DMSO-d ₆ | 70 |
| 5.3 | ¹ H NMR spectrum of isosorbide diallyl ether in CDCl ₃ | 71 |
| 5.4 | ¹ H NMR spectrum of isosorbide diglycidyl ether in CDCl ₃ | 72 |
| 5.5 | ¹ H NMR spectrum of isosorbide 2,5-bis(glyceryloxy) dimethacrylate in CDCl ₃ | 73 |
| 5.6 | ¹ H NMR spectrum of isosorbide 2,5-bis(4-allyloxybenzoate) in CDCl ₃ | 74 |
| 5.7 | ¹ H NMR spectrum of isosorbide 2,5-bis(4-glycidyloxybenzoate) in CDCl ₃ | 75 |
| 5.8 | ¹ H NMR spectrum of isosorbide 2,5-bis(4-glyceryloxybenzoate) dimethacrylate in CDCl ₃ | 76 |
| 5.9 | ¹ H NMR spectrum of isosorbide 2,5-bis(3-allyloxybenzoate) in CDCl ₃ | 77 |
| 5.10 | ¹ H NMR spectrum of isosorbide 2,5-bis(3-glycidyloxybenzoate) in CDCl ₃ | 78 |
| 5.11 | ¹ H NMR spectrum of isosorbide 2,5-bis(3-glyceryloxymethacrylate) in CDCl ₃ | 79 |
| 5.12 | ¹ H NMR spectrum of isosorbide 2,5-bis(2-allyloxybenzoate) in CDCl ₃ | 80 |
| 5.13 | ¹ H NMR spectrum of isosorbide 2,5-bis(2-glycidyloxybenzoate) in CDCl ₃ | 81 |

LIST OF FIGURES
(Continued)

| Figure | Page |
|--|-------------|
| 5.14 ¹ H NMR spectrum of isosorbide 2,5-bis(2-glyceryloxybenzoate) Dimethacrylate in CDCl ₃ | 82 |
| 5.15 ¹ H NMR peak shape comparison of H3/H4 as a result of methacrylation in ISB4GBMA and ISB3GMA..... | 83 |
| 5.16 ¹ H NMR peak shape comparison of H3/H4 as a result of methacrylation in ISB2GBMA and ISDGMA..... | 84 |
| 5.17 Viscosity of BisGMA/TEGDMA, ISDGMA/TEGDMA, ISB4GBMA/TEGDMA, ISB3GBMA/TEGDMA, and ISB2GBMA/TEGDMA monomer mixtures (60:40 wt%) at 25°C and 200 rpm..... | 87 |
| 5.18 Degree of monomeric conversion of P(BisGMA/TEGDMA), P(ISB4GBMA/TEGDMA), P(ISB3GBMA/TEGDMA), and P(ISB2GBMA/TEGDMA) at 60:40 wt%..... | 89 |
| 5.19 Comparison of the degree of conversion between top and bottom specimen layers..... | 90 |
| 5.20 Polymerization shrinkage for P(BisGMA/TEGDMA), P(ISB4GBMA/TEGDMA), P(ISB3GBMA/TEGDMA), P(ISB2GBMA/TEGDMA), and P(ISDGMA/TEGDMA) at 60:40 wt%..... | 91 |
| 5.21 Tan delta curves for P(BisGMA/TEGDMA), P(ISB4GBMA/TEGDMA), P(ISB3GBMA/TEGDMA), P(ISB2GBMA/TEGDMA), and P(ISDGMA/TEGDMA) at 60:40 wt%..... | 92 |
| 5.22 Storage modulus as a function of temperature for P(BisGMA/TEGDMA), P(ISB4GBMA/TEGDMA), P(ISB3GBMA/TEGDMA), P(ISB2GBMA/TEGDMA), and P(ISDGMA/TEGDMA) at 60:40 wt%..... | 93 |
| 5.23 Water sorption of P(BisGMA/TEGDMA), P(ISB4GBMA/TEGDMA), P(ISB3GBMA/TEGDMA), P(ISB2GBMA/TEGDMA), and P(ISDGMA/TEGDMA) at 60:40 wt%..... | 95 |

LIST OF FIGURES
(Continued)

| Figure | Page |
|---|-------------|
| 5.24 SEM images at 150X and 2.5 kV of a) P(ISDGMA/TEGDMA), b) P(ISB2GBMA/TEGDMA), and c) P(BisGMA/TEGDMA) after buffer immersion for 7 days at 37°C..... | 96 |
| 5.25 Flexural strength analysis of P(BisGMA/TEGDMA), P(ISB4GBMA/TEGDMA), P(ISB3GBMA/TEGDMA), P(ISB2GBMA/TEGDMA), and P(ISDGMA/TEGDMA) at 60:40 wt% at RT..... | 99 |
| 5.26 Flexural modulus of P(BisGMA/TEGDMA), P(ISB4GBMA/TEGDMA), P(ISB3GBMA/TEGDMA), P(ISB2GBMA/TEGDMA), and P(ISDGMA/TEGDMA) at 60:40 wt% at RT..... | 101 |
| A.1 ¹ H- ¹ H COSY of isosorbide..... | 106 |
| A.2 ¹ H NMR Spectrum of BisGMA in CDCl ₃ | 107 |
| B.1 ATR-FTIR spectrum of isosorbide..... | 108 |
| B.2 ATR-FTIR spectrum of isosorbide 2,5-bis(glyceryloxy) Dimethacrylate..... | 109 |
| B.3 ATR-FTIR spectrum of isosorbide 2,5-bis(4-glyceryloxybenzoate) dimethacrylate..... | 109 |
| B.4 ATR-FTIR spectrum of isosorbide 2,5-bis(3-glyceryloxybenzoate) dimethacrylate..... | 110 |
| B.5 ATR-FTIR spectrum of isosorbide 2,5-bis(2-glyceryloxybenzoate) dimethacrylate..... | 110 |
| B.6 ATR-FTIR spectrum of ISDGMA/TEGDMA 60:40 wt%..... | 111 |
| B.7 ATR-FTIR spectrum of ISB4GBMA/TEGDMA 60:40 wt%..... | 111 |
| B.8 ATR-FTIR spectrum of ISB3GBMA/TEGDMA 60:40 wt%..... | 112 |

LIST OF FIGURES
(Continued)

| Figure | | Page |
|---------------|---|-------------|
| B.9 | ATR-FTIR spectrum of ISB2GBMA/TEGDMA 60:40 wt%..... | 112 |
| B.10 | ATR-FTIR spectrum of BisGMA/TEGDMA 60:40 wt%..... | 113 |
| C.1 | Water sorption of P(ISDGMA/TEGDMA) when cured at different time lengths..... | 114 |

CHAPTER 1

INTRODUCTION

1.1 Dental Caries

According to the 2017 Global Burden of Disease Study, oral disorders are the most prevalent among all age groups and both sexes, followed by headache disorders and tuberculosis, **Table 1.1**. Approximately 3.5 billion people are affected by oral diseases. Dental caries of permanent teeth is the most common condition affecting nearly 2.5 billion people, while more than 530 million children suffer from caries in their primary teeth [1].

Table 1.1 2017 Top 3 Global Prevalent Disorders

| Disorder | Prevalence (billions) 2017 count |
|-------------------|-------------------------------------|
| Oral disorders | 3.47 |
| Headache disorder | 3.07 |
| Tuberculosis | 1.93 |

Source : [1]

Dental caries, known also as tooth decay, is an infectious transmissible bacterial disease caused by acids from bacterial metabolism diffusing into the tooth enamel and dentin and dissolving the protective mineral, leading to cavitation, **Figure 1.1** [2].

Dental caries is largely caused by two major groups of cariogenic bacteria; they are *Streptococcus mutans* and *Lactobacilli* species. The bacteria are essentially introduced from one person to another, for example, from the mother to the child. They colonize the mouth and adhere to the tooth via the formation of dental plaque [3].

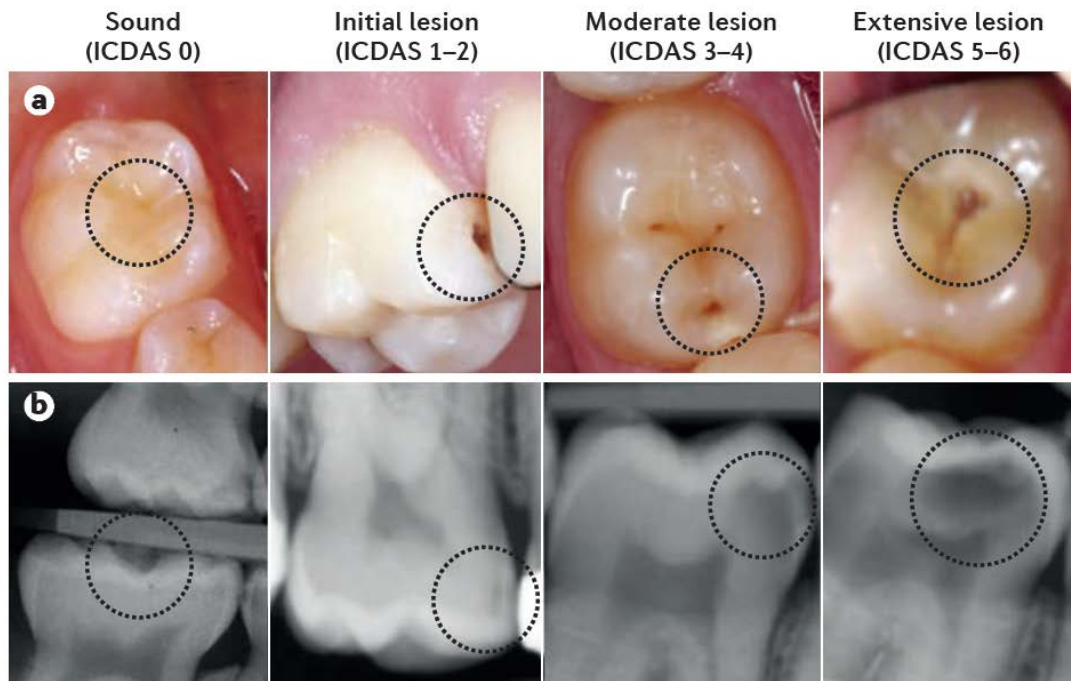


Figure 1.1 Clinical and radiographic examination of the various stages of dental caries.
 Note: ICDAS: international caries detection and assessment system.
 Source: [4]

The tooth is made up of three layers as shown in **Figure 1.2**. The top-most layer of the tooth crown is the enamel, which is the most mineralized and hardest layer. The second layer is the dentin, and it is softer than enamel due to a higher content of collagen and water. The center of the tooth is called the pulp and contains nerves and blood vessels that provide sensation to the tooth and keep it alive. The outermost layer of the tooth root is called cementum followed by dentin which encases the pulp tissue within the root canal [3].

Dental plaque is formed through a three-step process [5]. First, salivary molecules including glycoproteins, acidic proline rich proteins, mucins, and sialic acid coat the tooth enamel once it has been cleaned. Second, primary bacterial colonizers, mainly *Streptococcus sanguinis* and *Actinomyces viscosus*, adhere to the pellicle via cell to surface

interactions [6,7]. Third, other bacterial species such as *Streptococcus mutans* and *Lactobacilli* species adhere to the primary colonizers via cell to cell interactions, with further bacterial growth leading to the formation of the dental plaque biofilm [8].

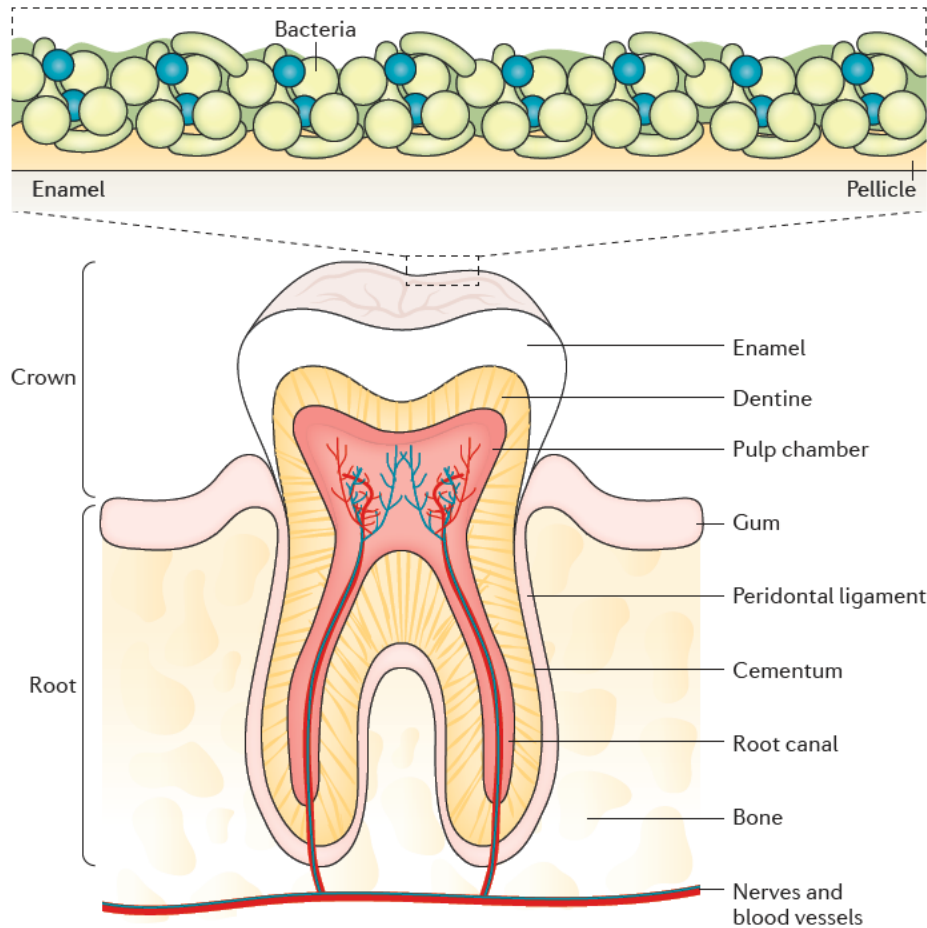


Figure 1.2 Tooth structure and dental plaque.

Source: [4]

The disease process is a continuing cycle of demineralization and remineralization of tooth enamel and dentin that can lead to cavitation. Sound enamel and dentin crystals are made up of a hydroxyapatite like mineral that can be easily dissolved in acids. The mineral contains carbonate ions that substitute for the phosphate ion in the crystal lattice, creating defects and calcium deficient regions which are more acid susceptible [2].

Demineralization begins when bacteria metabolize fermentable carbohydrates, producing a number of organic acids, including lactic, acetic, formic, and propionic acids, which diffuse into the dentin and enamel via the water between their crystals. When the acid reaches a susceptible site, it dissolves away the calcium and phosphate ions [9]. The early sign that dental caries is in progress is the presence of white spot lesion in the mouth, **Figure 1.3** [2].

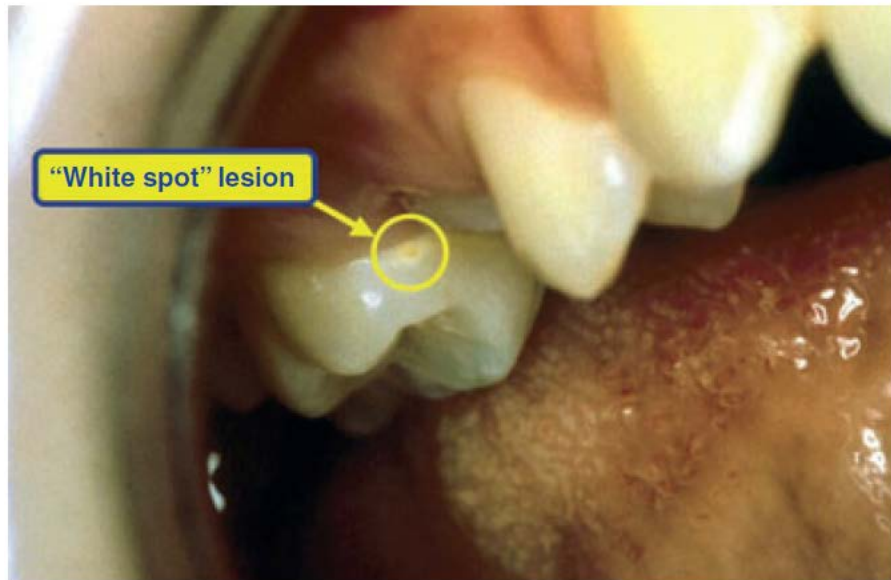


Figure 1.3 Initial clinical sign of dental caries in progress.
Source: [2]

Remineralization occurs when calcium and phosphate ions, primarily from saliva, along with fluoride ions, build on the existing crystal remnants. Depending on the fluoride content present, the fluoride ions adsorb onto the dental crystal surface, attracting calcium and then phosphate ions. The new crystal structure is fluorapatite-like and is much more acid-resistant than the original carbonated hydroxyapatite, **Figure 1.4** [9,10].

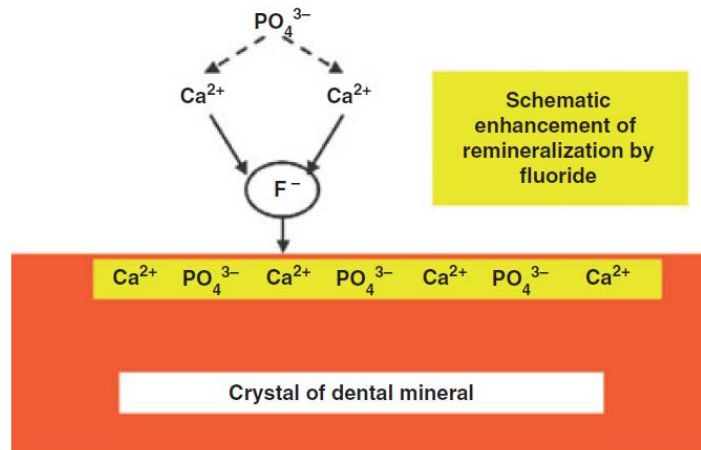


Figure 1.4 A Schematic representation of a fluorapatite-like remineralized crystal surface.
Source: [2]

Dental caries is a continuous dynamic disease process. As long as there are cariogenic bacteria, fermentable carbohydrates, and saliva present, the cycle of demineralization and remineralization continues in the mouth. If balance is not achieved and demineralization proceeds at a faster rate, then tooth decay and cavitation is the end result, **Figure 1.5** [2,3].

At the early stages of decay, the tooth may be treated with restorations. If the decay has reached the pulp, then root canal therapy is needed to remove the infected tissue. However, if the tooth is badly damaged, then tooth extraction is the final solution [11,12].

Dental materials can be classified as preventive, restorative, or auxiliary. Preventive materials include sealants with antibacterial effects. Restorative materials are synthetic components that are used to repair or replace tooth structure. They can be intracoronal, placed inside a prepared cavity, or extracoronal, placed around the tooth such as crowns. Auxiliary materials are used in the fabrication of dental prostheses and appliances but are not part of the device, such as dental impression materials [13,14].

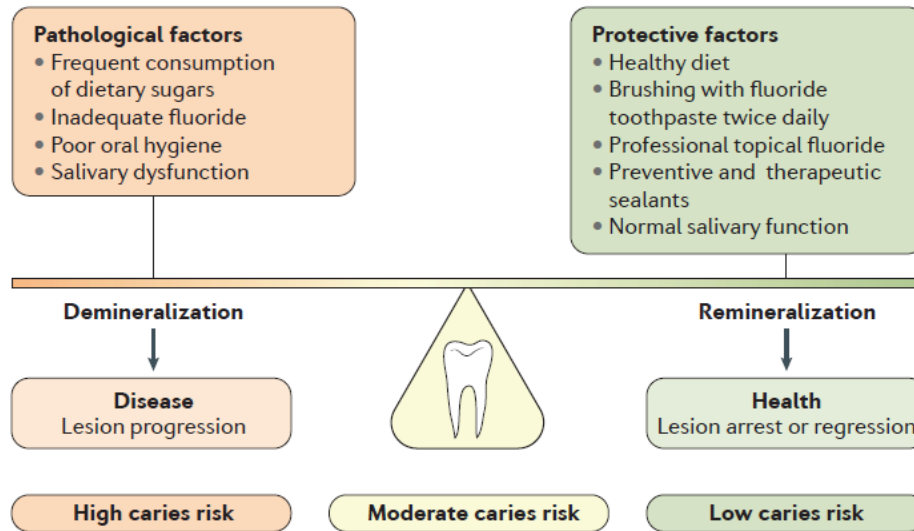


Figure 1.5 Dental caries balance.
Source: [4]

1.2 Historical Perspective of Dental Restoration Materials

Various natural and artificial materials were used in dental restorations in the past, and some of them evolved over time. This includes bones, ivory, gum, ceramics, and metals. Dental restoration is believed to have started around 3000 BC, when evidence of tooth implants was discovered in Egyptian mummies. However, the earliest documented tooth implant material is attributed to the Etruscans, where elephant and hippopotamus ivory was carved as partial dentures and bound to natural teeth using gold bands around 700 B.C, **Figure 1.6**. Phoenicians used gold bands and wires similarly. The Mayans used implants made of seashells around 600 A.D, **Figure 1.7** [13,15].

A process to make porcelain dentures was developed in 1774 by Duchateau and de Chemont. An individual porcelain tooth was made by Fonzi in 1808. The first amalgam was developed in France in 1816 by Taveau. Vulcanized rubber dentures were made after the material was invented in 1839. Gold foils were used in filling cavities in 1843 by

Giovanni d'Arco. Silicate cement was introduced in the early 20th century and was followed by methacrylate composites in 1962 [13,15,16].



Figure 1.6 Etruscan denture 700 BC.
Source: [13]



Figure 1.7 Three implanted incisors made of seashells 800 AD.
Source: [13]

The choice of dental restorative materials can depend on many factors, including the patient, the dentist, and tooth characteristics. Important parameters for choosing the proper dental restorative materials include strength, hardness, wear and chemical resistance, esthetic appearance, and biocompatibility [15].

Metals are mainly used in applications in which strength and durability are needed. Typical uses of metals include casting alloys, amalgams, and porcelain fused to metal (PFM) restorations. Ceramics are either used as stand-alone ceramic materials, or in conjunction with metals as PFM restorations. They are used where chemical durability and esthetics are important, especially as veneers and crowns. Polymeric materials are used as cements and as cavity fillings in combination with ceramic filler particles. Polymers are useful because of good esthetics and adhesion properties [15].

1.3 Dental Ceramics

Ceramics can match the esthetic appearance and function of missing teeth; they are biocompatible and wear resistant, and have long term color stability. Ceramics are categorized into all-ceramic and metal-ceramic (porcelain fused to metal) systems. All ceramic systems are made of glass ceramics or glass-infiltrated ceramics. Metal ceramics are feldspathic porcelain. Ceramic restorations are believed to fail due to their brittleness, and their inability to suppress crack propagation. Dental ceramics are mostly used as inlays, onlays, veneers and crowns, **Figure 1.8** [13,15].



Figure 1.8 All-ceramic posterior bridge.

Source: [13]

1.4 Dental Gold and Casting Alloys

Gold is one of the oldest dental restoration materials, and its use is continued today as pure gold and as dental casting alloys. The use of pure gold is limited to smaller cavities due to its lower mechanical resistance to masticatory forces [17].

Casting alloys are divided into all metal and porcelain fused to metal restorations. They are classified according to their metal type, high noble, noble, and predominantly base metal. High noble alloys contain more than 40 weight% of gold, and the rest is from the platinum group metals. Noble alloys contain more than 25% of noble metals while predominantly base metal alloys contain less than 25% of noble metals. Silver is not considered noble in dental applications. Casting alloys are also classified according to their mechanical properties to type I (low strength), type II (moderate strength), type III (high strength), and type IV (extra high strength), **Table 1.2** [15].

Casting alloys are used for inlays, onlays, full crowns, and partial dentures, **Figure 1.9**. They are biocompatible, corrosion- and tarnish-resistant, with good thermal and

esthetic properties. Metal alloys in porcelain, fused to metal castings, should have a thermal coefficient that is compatible to porcelain, form stable oxides to promote bonding to porcelain, and have minimum creep or sag during firing of porcelain [13,15].

Table 1.2 Minimal Mechanical Requirements for Casting Alloys

| Type | Strength | Yield Strength (MPa) | Elongation (%) | Application Examples |
|------|------------|----------------------|----------------|-----------------------------------|
| I | Low | 80 | 18 | Inlays |
| II | Moderate | 180 | 10 | Inlays/onlays |
| III | High | 270 | 5 | Onlays, Crowns |
| IV | Extra high | 360 | 3 | Crowns, bridges, partial dentures |

Source: [13]



Figure 1.9 High gold alloy a) inlay, b) onlay, c) partial crown.

Source: [17]

1.5 Dental Amalgam

Dental amalgam fillings have been extensively used for over two centuries due to their low cost, ease of use, durability and resistance to moisture, **Figure 1.10**. Dental amalgam contains about 45-50% mercury and is formed by reacting mercury with copper, silver, and tin. The quality of dental amalgam is dictated by its dimensional stability, compressive strength, low creep rate, and tarnish- and corrosion-resistance [13,15].



Figure 1.10 Dental amalgam filling.
Source: [13]

Mercury is considered toxic to the kidneys and the nervous system [18,19], and small amounts of the inorganic material may be released into the oral environment [20]. This depends on a number of factors including the size and number of restorations, composition, and chewing and grinding habits [21]. The major routes of mercury exposure are through inhalation of mercury vapors, ingestion of elemental mercury, or swallowing small pieces of amalgam. The estimated concentration of mercury in the respiratory, urinary and blood systems, based on the data from the world health organization, are presented in **Table 1.3**. As can be seen in **Table 1.3**, they are far below the safety limit of occupational mercury exposure [22].

Table 1.3 Estimated Mercury Concentration in Respiratory, Urinary, and Blood Systems

| Medium | Individual with typical number of fillings | Occupational exposure limit |
|----------------------------------|--|-----------------------------|
| Respiratory air concentration | 3-17 $\mu\text{g Hg/day}$ | 346 $\mu\text{g Hg/day}$ |
| Urinary concentration of mercury | 3.5 $\mu\text{g/L}$ | 100 $\mu\text{g/L}$ |
| Blood concentration | 3-5 $\mu\text{g/L}$ | 25 $\mu\text{g/L}$ |

Source: [22]

The US-FDA recently issued an epidemiological review of exposure to dental amalgam mercury and did not find sufficient evidence correlating this exposure with adverse health outcomes [23]. However, the negative perception of amalgam and its lower esthetic appeal, in addition to the Minamata convention to minimize mercury production, usage, and environmental impact, are leading reasons for patients and governments to limit its use [21,24].

1.6 Dental Polymers

The early uses of polymers as dental materials started with natural rubber and was followed by vulcanized rubber as denture bases in 1853. Gutta-Percha, a plant exudate rich in *trans*-poly(isoprene), was used for cavity fillings, temporary crowns, and permanent restorations in the 1890s [15,16].

Silicate cement was the first tooth colored material used in esthetic dentistry in the late 19th century. However, it had several drawbacks such as pulp irritation potential, desiccation, and solubility. Therefore, poly(methyl methacrylate) was developed and used by 1940 as crowns, inlays, fixed dental prostheses, and denture bases. The development of low-and room-temperature curing allowed for the use of direct resin dental fillings in the

1950s. The resin was based on the mixture of methyl methacrylate, poly(methylmethacrylate), and the crosslinker ethylene glycol dimethacrylate. Early resin systems suffered from high polymerization shrinkage that led to marginal leakage and secondary caries. Therefore, further developments were made to incorporate and bind filler ceramic particles to new resins. This led to the development of BisGMA (Bisphenol A glycidyl methacrylate) in 1956 and UDMA (urethane dimethacrylate) in 1974. Similarly, polymerization-based curing methods progressed from self-curing to ultraviolet light curing and to blue light-curing [13,15,16].

Polymeric materials are used in various dental applications, such as denture bases and teeth, dental bonding agents, cementing and luting materials, cavity fillings, brackets and bracket bonding resins and cements, custom trays, and impression materials, **Figure 1.11** [15]. The focus of this dissertation is on dental resins for direct filling restorations.



Figure 1.11 Resin-based composite filling.
Source: [25]

1.7 Resin-Based Composites

Dental restorative resin-based composites are a new class of materials that were developed in the late 1950s. They are of significant interest due to their good performance, esthetic appeal, and ability to match the color of natural tooth [15].

Resin based composites are described as interconnected heterogenous materials with three distinct phases. The first phase is a continuous phase consisting of the photopolymerizable organic matrix. The second is a higher-modulus dispersed phase of fillers with different types, sizes, morphologies, and shapes. The third is an interfacial phase that binds the continuous and dispersed phases together [26].

The organic matrix consists of either individual or blends of aromatic, aliphatic, and urethane dimethacrylate monomers, a photo initiator system, and stabilizers [27]. Dental monomers cross-link into a three-dimensional polymeric network that should provide high monomeric degree of conversion, low water uptake and polymerization shrinkage, as well as good mechanical properties, **Figure 1.12** [15,27,28].

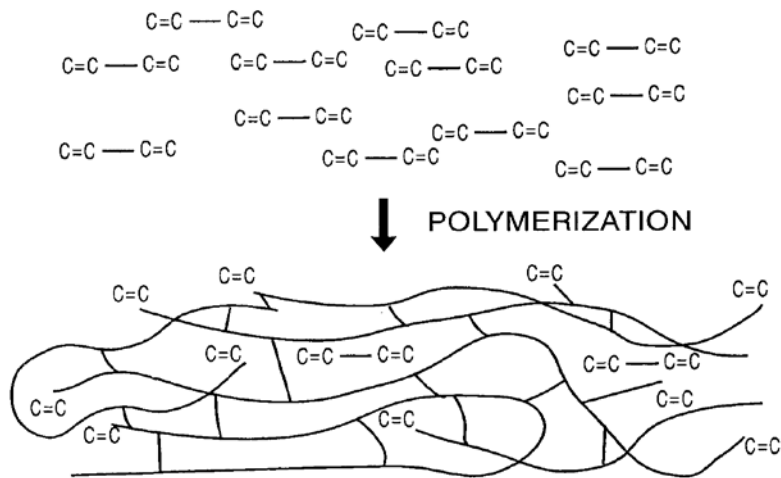


Figure 1.12 Cross-linked polymeric network.

Source: [29]

Fillers are introduced to reinforce and strengthen composites, and to lower polymerization shrinkage and thermal expansion. They are dispersed in the crosslinked polymeric network and constitute about 30-70% by volume or 50-85% by weight of the composite. Some of the common fillers are fused quartz, aluminum silicate, lithium aluminum silicate, barium, zirconium, and zinc glasses [13]. Composites can be classified in accordance with their filler's particle size and distribution, with many composites having a combination of different sizes to tailor performance. Some examples are summarized in

Table 1.4.

Table 1.4 Examples of Composite Classification Based on Filler Particle Size and Distribution

| Class of composite | Particle size | Clinical use |
|------------------------------|--|---|
| Traditional (large particle) | 1-50 μm glass or silica | High stress areas |
| Hybrid (large particle) | 1) 1-20 μm glass 2) 40 nm silica | High stress areas requiring improved polishability |
| Hybrid (midfilled) | 1) 0.1-10 μm glass 2) 40 nm silica | High stress areas requiring improved polishability |
| Hybrid (minifilled) | 1) 0.1-2.0 μm glass 2) 40 nm silica | Moderate stress areas requiring optimal polishability |
| Nanohybrid | 1) 0.1-2.0 μm glass 2) \leq 100 nm nanoparticles | Moderate stress areas requiring optimal polishability |

Source: [13]

Increased filler loadings improve compressive and tensile strength, toughness, and modulus of elasticity, which translate into better clinical composite performance. As the filler volume fraction reaches 70%, the abrasion and fracture resistance of the composite approach those of natural tooth. The polymerization shrinkage decreases as well in

proportion to filler volume fraction, because higher filler content reduces the overall resin content and fillers do not participate in the polymerization process. Similarly, increased filler loadings reduce the overall coefficient of thermal expansion of the composite to levels near that of natural tooth. As a result, less interfacial stresses are produced due to volumetric changes when consuming hot and cold foods. Finally, fillers impart radiopacity which aids in the detection of secondary caries, leaking margins, and surface wear [13,26].

The adhesion of the polymer matrix to the filler can occur via hydrogen bonding, ionic interaction, van der Waals forces, ionic or covalent bonding, and interpenetrating polymer network formation. This improves the physical and mechanical properties of the composite by allowing the lower moduli polymer network to transfer stresses to the higher moduli fillers. A properly bonded polymer/filler interface can also inhibit or reduce leaching by preventing water from penetrating [13,26] into the filler.

Adhesion can occur via coupling agents, which are difunctional surface active compounds that are used to bond the inorganic filler to the polymer matrix. Organosilanes are the most common coupling agents, **Figure 1.13**. This includes γ -methacryloxypropyl trimethoxysilane whose mechanism is depicted in **Figure 1.14**. The coupling mechanism is as follows: the methoxy functionality is hydrolyzed in the presence of water to silanol, which will react and bond with other silanol functionalities on the filler. The methacrylate functionality of the coupling agent will react with the resin once it is polymerized, thus creating a bonding between the two interfaces [13].

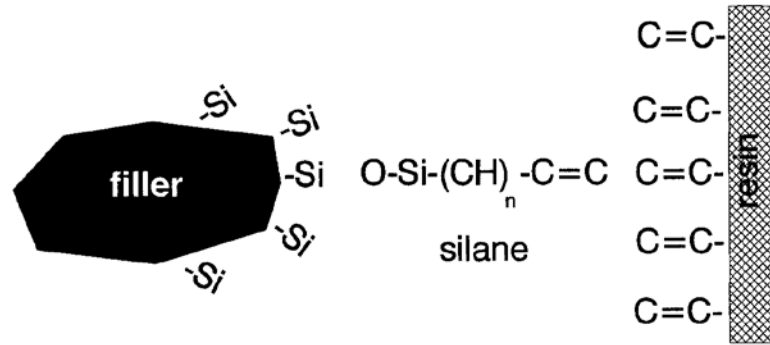


Figure 1.13 Schematic representation of silane bonding between fillers and polymer matrix.

Source: [29]

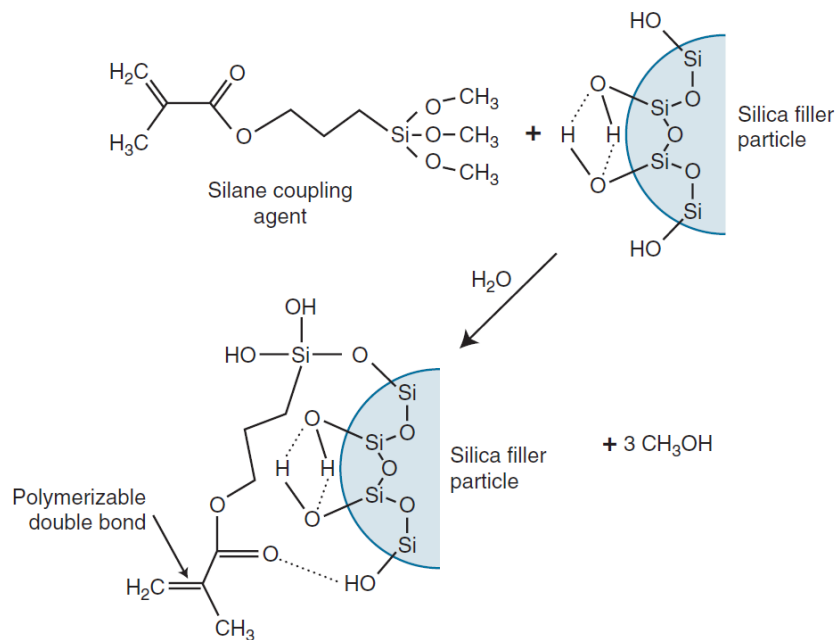


Figure 1.14 Silane coupling agent mechanism.

Source: [13]

1.7.1 The Monomer System

The molecular structure of the dimethacrylate monomer impacts the crosslink density, morphology of the network, and the overall properties of the polymeric network. For example, oligoethers and aliphatic hydrocarbons increase the overall elasticity, while

aromatic and cycloaliphatic groups increase stiffness [30]. The length of the dimethacrylate molecule dictates the theoretical cross-link density; the shorter the molecule, the higher the cross-link density, and the lower the possibility of chain reorganization [31]. Physical cross-links on the other hand, such as through hydrogen bonding, reduce rotational motion and increase stiffness [31].

There are various dimethacrylate monomers that are used for direct dental restorations; the most common ones are shown in **Figure 1.15**. They include 2,2-bis[4-(2-hydroxy-3-methacryloyloxypropoxy)phenyl]propane, BisGMA. Triethylene glycol dimethacrylate. TEGDMA. 1,6-bis-(methacryloyloxy-2-ethoxycarbonylamino)-2,4,4-trimethylhexane, UDMA.

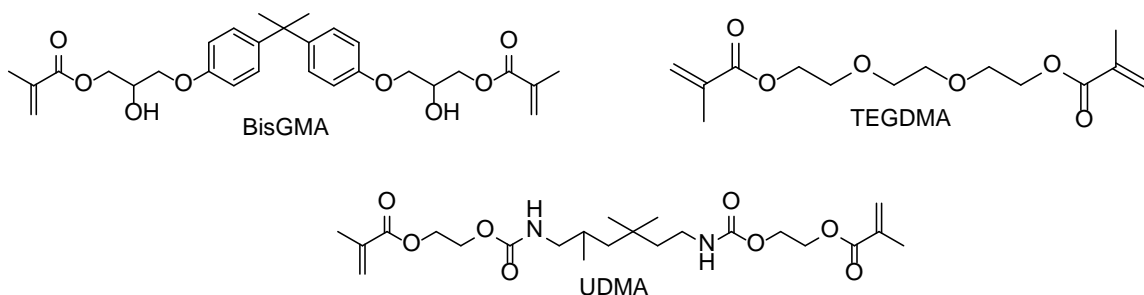


Figure 1.15 Common dental dimethacrylates.

BisGMA was designed and synthesized specifically for dental restorations by Bowen in 1956 [32]. It is typically synthesized as the reaction product of either bisphenol-A with glycidyl methacrylate or, bisphenol A diglycidyl ether with methacrylic acid, **Figure 1.16** [33]. Its stiff and bulky aromatic core imparts high polymeric modulus and low shrinkage, and the hydroxyl groups provide good adhesion to the tooth enamel

[30,34,35]. However, it has a high viscosity of 1200 Pa·s due to intermolecular hydrogen bonding between its hydroxyl groups and the presence of π - π interactions, thus limiting its handling, degree of monomeric conversion, and the amount of filler that can be incorporated. As a result, it is usually mixed with a diluent such as TEGDMA which has a viscosity of 0.01 Pa·s [36].

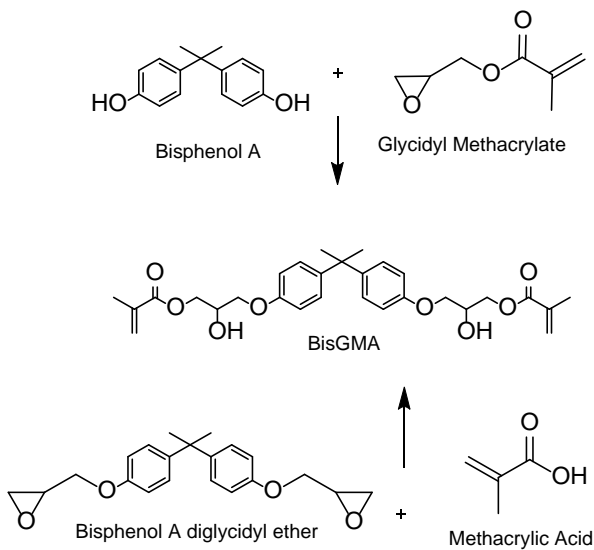


Figure 1.16 Synthesis scheme of BisGMA.

TEGDMA is used a dental diluent due to its low viscosity. It is the synthesis product of triethylene glycol and methacrylic acid, **Figure 1.17** [33]. Its flexible and hydrophilic ether linkages are reported to increase water sorption and polymerization shrinkage [37,38].

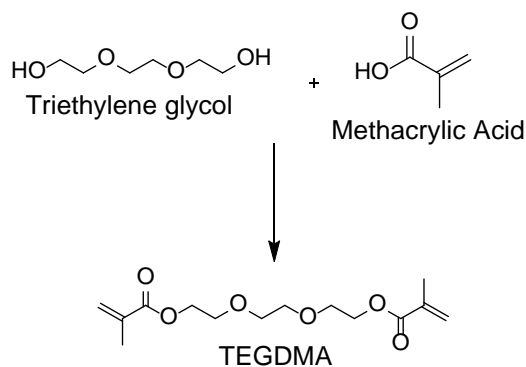


Figure 1.17 Synthesis scheme of TEGDMA.

UDMA was developed by Foster and Walter in 1974 as a response to BisGMA and its high viscosity [39]. It is the synthesis product of 2,4,4-trimethylhexamethylene diisocyanate and 2-hydroxyethyl methacrylate, **Figure 1.18** [33]. It has a low viscosity of 6.75 Pa·s due to its aliphatic spacer group. But it imparts toughness, good durability, and adhesion to the tooth enamel due to the presence of the urethane group and hydrogen bonding [30,40-43].

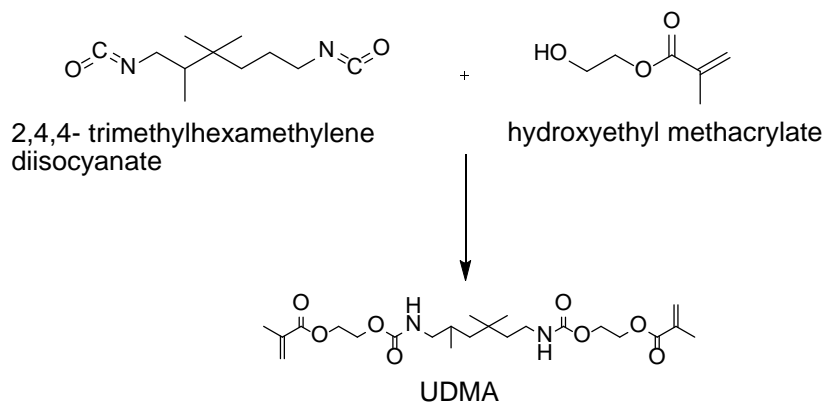


Figure 1.18 Synthesis scheme of UDMA.

1.7.2 The Polymerization Process

1.7.2.1 The Activation Mechanism. Dental dimethacrylate polymerization can be activated either chemically or photochemically. In chemically initiated polymerizations, the monomers are supplied as two pastes, one of which contains benzoyl peroxide as the initiator, while the other contains aromatic tertiary amines as the reducing agent, such as *N,N*-dimethyl-*p*-toluidine. In addition, butyl hydroxytoluene is added as a stabilizer to control the start of the polymerization [44].

When the two components are mixed together, the amines react with benzoyl peroxide through the formation of a complex by means of electron transfer from the unshared pair of the nitrogen to the peroxide, which also leads to the formation of the benzoate anion. The complex homolyzes into an amine radical cation and benzoyloxy radical. The benzoate anion extracts a proton from the amine cation to make benzoic acid. An alkyl amine radical is then formed upon the transfer of an electron from carbon to nitrogen. The newly formed radicals can then initiate polymerization, **Figure 1.19** [44-46].

There are several drawbacks that are associated with chemical activation of dental dimethacrylates such as the entrapment of air which leads to voids and weakening of the polymeric network. In addition, any trapped oxygen can react with free radicals and inhibit polymerization. Finally, there is a limited control of work time once the two components are mixed together. Therefore, chemical activation is used for restorations or large foundation structures that are not readily cured by light activation [13].

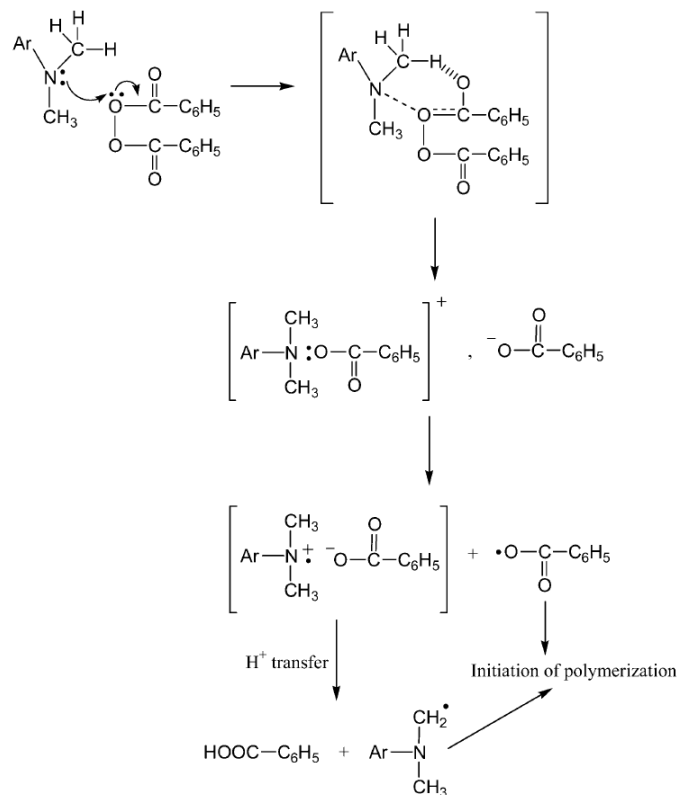


Figure 1.19 Mechanism of redox initiation by benzoyl peroxide / amine system.
Source: [44]

The photochemical activation of dental dimethacrylates typically occurs by means of free radical photo polymerization using the photo-initiator camphorquinone (CQ) in the blue region of visible light [47]. Camphorquinone is an α -diketone with a UV absorption in the region of 200-300 nm due to the π,π^* transition, and a visible light absorption in the region of 400-500 nm due to n,π^* transition. The molar extinction coefficient of the π,π^* transition ($\epsilon_{250 \text{ nm}}$) is $10,000 \text{ M}^{-1} \text{ cm}^{-1}$, and for the n,π^* transition ($\epsilon_{468 \text{ nm}}$) is $40 \text{ M}^{-1} \text{ cm}^{-1}$ [48]. Camphorquinone has an absorbance peak around 469 nm and is typically mixed with tertiary amines as co-initiators to improve its effectiveness [49]. Polymerization co-initiators are chemical compounds that interact with camphorquinone and generate reactive species that are able to initiate and sustain the polymerization process. Dimethylamino

ethyl methacrylate and ethyl-4-dimethylaminobenzoate are examples of such co-initiators [50].

Upon absorption of light, there is a transition of an electron from the localized non-bonding orbital (n) of one of the oxygen atoms of CQ to the antibonding orbital (π^*) of the carbonyl group to form the singlet activated state (S_1). This electronic transition ($n \rightarrow \pi^*$) is characterized by a much lower molar absorptivity than other transitions, and it does not involve the reversal of electron spin [50,51]. Then by intersystem crossing (a non-radiative isoenergetic transition from a singlet electronic state to a triplet state or vice versa), it causes the formation of the triplet state (T_1) [52]. While in T_1 , CQ interacts with an amine to generate an excited state complex, called the exciplex [48]. The exciplex is a heterodimeric, short-lived species that forms in the excited state but dissociates in the ground state.

In the exciplex state, the electron donor amine transfers an electron from the nitrogen's lone pair to the activated carbonyl of CQ, which acts as an electron acceptor. Then via an intermolecular hydrogen abstraction from the amine by CQ, free radicals can form, **Figure 1.20**. These radicals are the amino alkyl radicals which can initiate free radical polymerization, and the camphorquinone ketyl radicals which can deactivate or terminate the polymerization [52,53]. The hydrogen abstraction from amines by the triplet CQ state to form free radicals is much faster than the reaction of CQ alone with the monomer. Therefore, amines are added as co-initiators [48,51].

There are a number of advantages that are associated with light curing, such as avoiding porosity of chemical activation, having longer work time and faster curing procedure [13].

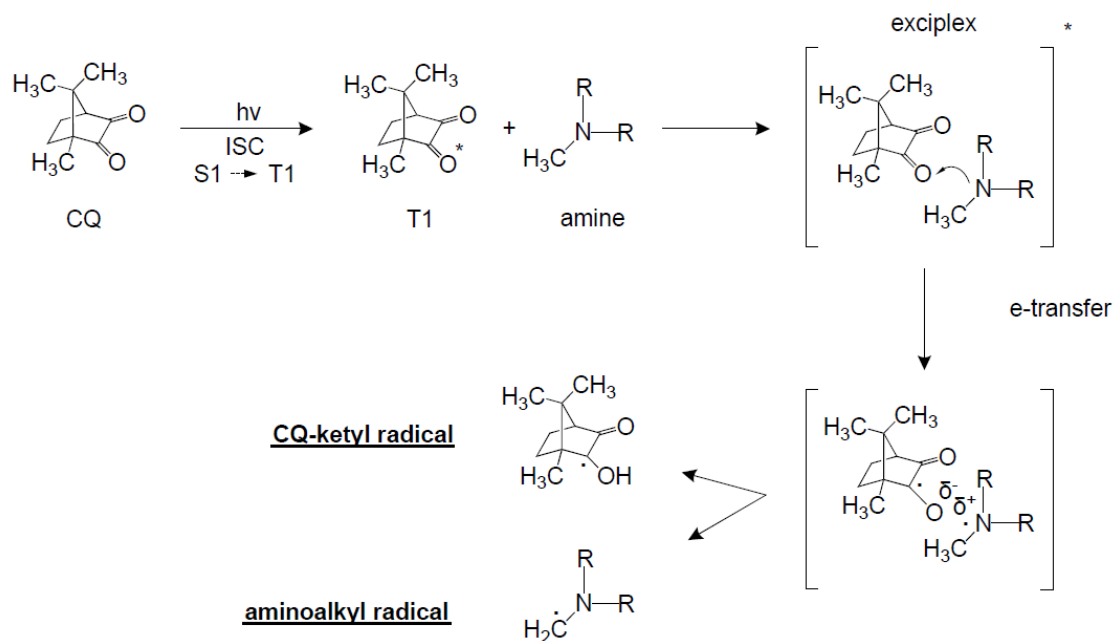


Figure 1.20 Photoinitiation of camphorquinone and amines.
 Source: [53]

1.7.2.2 Polymer network development. The free radicals created by the camphorquinone amine system attack and open the double bond (C=C) of the methacrylate group, and cause a chain reaction polymerization characterized by initiation, propagation, and termination, **Figure 1.21** [54].

Dimethacrylate monomers can bind to four other monomers or polymer chain ends creating a highly crosslinked covalently bonded network. The extent of polymerization, or double bond conversion, can be quantified by determining the ratio of the remaining unreacted double bonds to the initial double bond amount; this is termed as the degree of conversion [54].

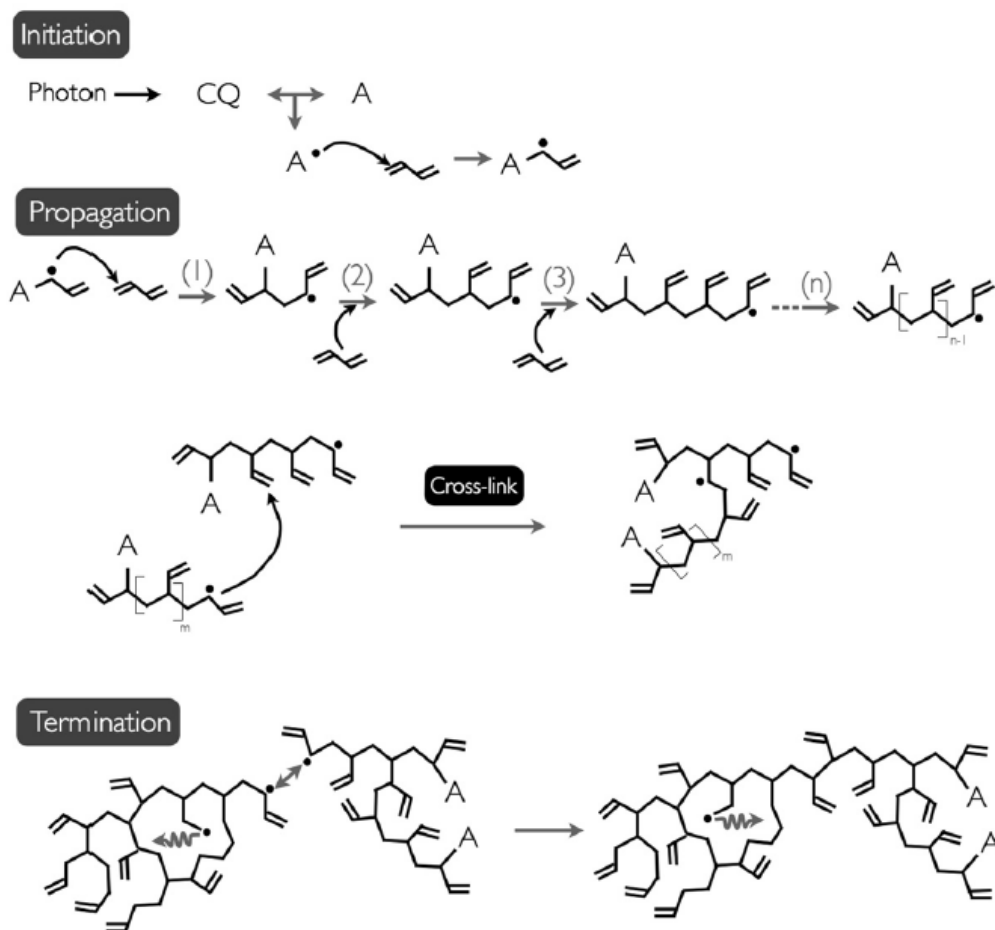


Figure 1.21 Schematic representation of the polymerization process.

Note: CQ: camphorquinone, A: tertiary amine, [•] indicates a radical species. (1), (2), (3), and (n) represent the theoretical steps of linear monomer addition. n and m: large amount of monomer units. A trapped radical is illustrated in the termination section and segmental mobility is represented by a twisting gray arrow. A double gray arrow indicates radicals about to react together (bimolecular termination).

Source: [54]

The monomer system exists mainly as a homogenous liquid solution prior to polymerization. At the beginning of the photopolymerization process, the degree of monomeric conversion and cross-link density increase rapidly as the ratio of free monomers decrease in comparison to the growing polymer phase. This includes the formation of polymer backbone chains, cross-links, and pendant reactive groups. The formation of a cross-linked network causes a rapid increase in the system's viscosity and

changes its state from a viscous liquid to an elastic gel; this point is called gelation [30,55].

The mobility restriction caused by an increase in the viscosity at the gel point mostly affects free radicals at the growing polymer chain ends, but free monomers can still diffuse easily. As a result, bimolecular termination, in which free radicals react with each other [56], slows while new growth centers are still being created by initiation. As the rate of free radical concentration increases, the rate of polymerization increases, and the system is in an auto-acceleration stage [54,57].

As the reaction proceeds further, the viscosity of the system becomes very high and the diffusion becomes very limited, even for monomers. At this point, the rate of polymerization decreases, and the system is in an auto-deceleration stage. The state of the system then changes from rubbery to glass at a point called vitrification. Vitrification leads to the entrapment of photo-initiators, free radicals, monomers, and pendant double bonds. As a result, the system cannot achieve a complete monomeric degree of conversion [54,58].

The polymeric network is largely seen as spatially heterogeneous clusters with various degrees of cross-linking density, **Figure 1.22** [59]. This heterogeneity arises from the polymerization process, where there is an initial formation of independent microgel domains advancing ahead of the surrounding polymer matrix. These domains can gradually form denser network structures through vitrification within the individual domains as the polymerization progresses. The vitrification within the individual domains creates microscopic localized gradient regions of higher and lower cross-link density that vary in proportions throughout the polymerization process. This heterogeneity can create glassy regions at relatively low levels of conversion as well as rubbery regions at the limiting conversion point [30,60].

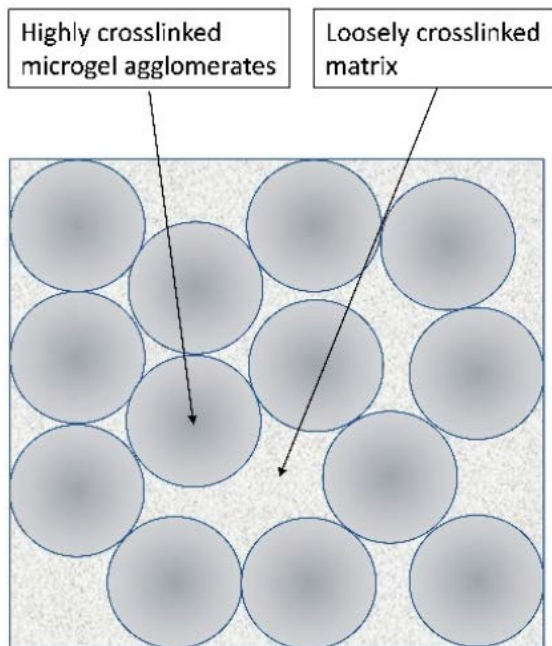


Figure 1.22 The structural heterogeneity of dimethacrylate networks.
Source: [59]

Network defects such as entanglements, loops, pendant groups, and pendant chains can arise as a result of the monomer structure or polymerization process. The presence of long and flexible monomers can cause network entanglement. On the other hand, monomers that are relatively compact and flexible are more prone to engage in cyclization reactions than monomers that are rigid and extended. Cyclization reactions occur when a propagating chain radical reacts with a pendant reactive group creating a loop. The pendant reactive group can be either already attached to the same chain, creating a primary cycle, or attached to another chain that has previously been connected to the first by a cross-link, creating a secondary cycle. These cyclization reactions produce ineffective cross-links. Lastly, pendant methacrylate groups and chains are caused by incomplete monomeric conversion, **Figure 1.23** [30,59].

Loops, pendant groups, and pendant chains can act as plasticizers and weaken the polymer matrix. They do so by decreasing the overall cross-link density and network tightness and by increasing the rotational movement of the chains. On the other hand, entanglements provide further network restraints and increase the network's tightness [59].

Alternatively, chemical cross-linking resulting from a high degree of monomeric conversion and physical cross-linking through hydrogen bonding can enhance the network's stability and performance [59].

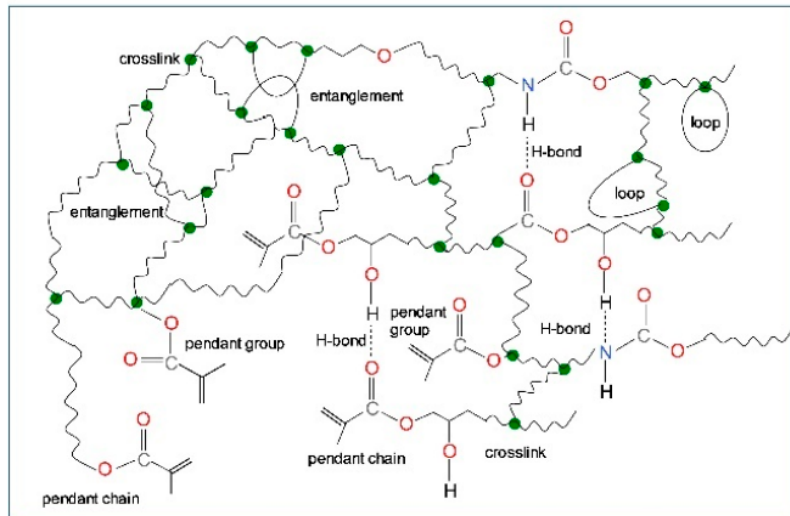


Figure 1.23 Physical and chemical cross-linking as well as defects in the polymer network.
Source: [59]

1.7.2.3 Photopolymerization Efficiency. The efficiency of the photopolymerization system is affected by intrinsic and extrinsic factors. Intrinsic factors include the photoinitiation system, monomer and filler viscosity, and optical properties of the resin/filler mixture. The extrinsic factors include light curing units, emission spectrum, light guide tip positioning, and curing temperature [54].

1.7.2.3A Intrinsic Factors. In the photoinitiation system, the concentration of the photo-initiator and co-initiator can have an impact on the polymerization efficiency. The degree of conversion is usually higher with higher concentrations up to an optimum level, due to an increase in the rate of polymerization. When the concentrations are increased beyond the optimum level, the degree of conversion decreases due to excessive absorption of light by the photo-initiator and co-initiator at the sample surface, resulting in less light transmission through the layers of the sample and lower polymerization rate. The optimal concentration of the photoinitiation system depends on the materials and the desired properties [54,61,62].

A number of photo-initiators, other than camphorquinone, can be used to improve the photopolymerization efficiency. For example, phenylenpropanedione (PPD) and mono- or bis-acylphosphine oxides (MAPO and BAPO) have higher molar absorptivity than camphorquinone and thus have a higher probability of light absorption in their optimal range. In addition, MAPO and BAPO can generate several free radicals per molecule while CQ can generate only one radical. MAPO and BAPO are being studied further as possible replacements for CQ [54,63,64].

The initial viscosity of the monomer system can affect the reaction kinetics and the degree of conversion. Viscous monomers tend to impede molecular motion and reduce the degree of conversion. Similarly, variations in the filler-resin contact area can create local areas of high viscosity due to higher filler loading, favoring early vitrification. The viscosity is affected by the composition and molecular structure of the monomer, and filler type [54,65,66].

The optical properties of the composite can limit light transmission through the

sample. For example, light can be either reflected at the surface [67,68] or absorbed by pigments or photo-initiators [69,70]. Fillers can reduce light transmission by reflection at the filler-resin interface due to refractive index mismatch [71,72]. Filler particles can also scatter light, depending on a number of factors, including their size [73].

The thickness of the resin-based composite layer during photopolymerization has an impact on the material property and the degree of conversion. Resin-based composite layers, that are more than 2 mm thick result in significant light absorption and scattering, rather than light penetration [74]. The studies by Rueggeber et al. [75,76], Price et al. [77] and Flury et al., [78] found a significant reduction in the degree of conversion and hardness of cured resin-based composites that were more than 2.5 mm thick. Therefore, incremental layering of dental fillings is used for cavities requiring fillings that exceed 2 mm thick [74].

1.7.2.3B Extrinsic Factors. The early visible light curing units were broad spectrum halogen filled quartz bulbs with a tungsten filament that required a filter to isolate the required wavelength (400-500 nm) [79,80]. The current light sources use light-emitting diodes, with a spectrum narrower than halogen lights, which can be more effective for camphorquinone initiation [81]. On the other hand, polywave light-emitting diodes, with two or more wavelength ranges, can be used for a broader range of initiators [82]. In choosing the right light curing unit, there should be an optimal spectrum match between the unit and the photo-initiator. This not only ensures efficient polymerization but avoids excessive temperature rise in the dental pulp. Since photons that are absorbed but do not initiate polymerization are transformed into heat and can irritate or damage dental tissue [83].

The position of the light-curing tip can affect the total energy reaching the composite surface, with reduction in energy resulting from increased distance between the composite surface and the light-curing tip [84]. Price et al. reported a significant reduction in microhardness by increasing the distance from 2 mm to 9 mm [85]. Therefore, it is better to minimize the distance as much as possible, or extend curing time or irradiation level [74].

An increase in the degree of conversion, hardness, and polymerization rate was observed when resin-based composites were cured at the oral temperature of 35°C in comparison to room temperature cure at 22°C [86]. The increase in polymerization temperature leads to lower viscosity of the resin-based system and improves molecular mobility, allowing higher reaction rate prior to vitrification [87].

For the photo-curing system to be clinically effective, it must have very rapid curing durations (30-40 seconds) for each layer. The light intensity and the associated spectrum should not harm the oral tissue. The heat of polymerization must be low to avoid any damage to the tissue as well [34,47].

1.7.3 Evaluation

1.7.3.1 Degree of Conversion. The degree of double-bond conversion of monomers is an important parameter for dental resins. It correlates with other material characteristics such as monomer elution, volumetric shrinkage, wear resistance, and mechanical properties [54]. The unreacted double bonds may either be in the form of free monomers or pendant groups. Free monomers can leach into the oral environment and irritate the soft tissue. Pendant groups lower the overall chemical cross-linking density and affect the

network's mechanical properties. However, near complete monomeric conversion can result in an increase in polymerization shrinkage since chains are brought closer together [34,88].

The chemical structure of the monomer influences the degree of double-bond conversion. Molecules with a stiff structure and low elasticity have a lower degree of conversion than molecules with higher elasticity and longer distance between the methacrylate groups. The addition of a diluent helps to increase the degree of conversion through a reduction in the overall viscosity and an improvement in reaction diffusion [54,59].

The degree of double bond conversion is never complete but is typically between 50-75% in resin-based composites due to vitrification [54,59]. The degree of conversion can be measured through Fourier Transform Infrared and Raman Spectroscopy, Differential Scanning Calorimetry, and solid state Nuclear Magnetic Resonance. Fourier-Transform Infrared Spectroscopy (FTIR) is the most common technique, allowing detection of the absorbance of the double-bond stretching of the methacrylate functionality (C=C) at 1636 cm^{-1} before and after polymerization. In order to obtain accurate measurements, the absorption of a band that does not change as a result of polymerization is used as an internal standard. The vibrational stretching of the (C=C) in the aromatic ring in the $1620\text{-}1565\text{ cm}^{-1}$ is the typical internal standard. The difference in the absorbance band of the vinyl group of the methacrylate functionality before and after curing, with respect to the internal standard, indicates the percentage of double bond conversion, **Equation 1.1** [89-92]. In this equation, $A_{(C=C)}$ is the absorbance of the double bonds of the vinyl group, A_{is} is the absorbance of the internal standard band.

$$\text{Degree of conversion} = \left[1 - \frac{\frac{A(c=c)_{polymer}}{A_{is}}}{\frac{A(c=c)_{monomer}}{A_{is}}} \right] \times 100\% \quad (1.1)$$

The work of Sideridou et al. [34] showed the degree of conversion in a set of dimethacrylate homopolymers to increase in the following order, BisGMA<UDMA<Bis-EMA<TEGDMA. BisGMA is a stiff molecule with limitations in rotational movement and has the lowest degree of conversion. BisEMA lacks the hydroxyl groups of BisGMA and contains additional ethoxylated groups for added flexibility and rotational movement, **Figure 1.24**. UDMA is characterized by high elasticity and hydrogen bonding and, as such, has moderate degree of conversion. TEGDMA is fully aliphatic with a high degree of conversion due to its high flexibility, **Table 1.5**.

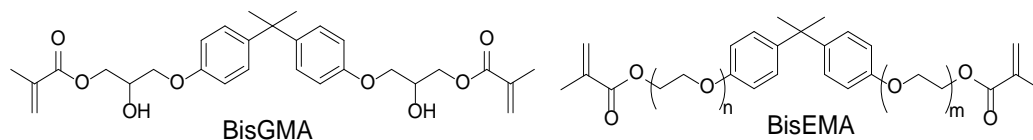


Figure 1.24 BisGMA and BisEMA.

Table 1.5 Degree of Conversion for BisGMA, BisEMA, UDMA, and TEGDMA

| Monomer | Mw | Viscosity (Pa's) | DC polymer |
|----------------|-----|------------------|------------|
| BisGMA | 511 | 1200 | 39 |
| BisEMA (n+m=4) | 540 | 0.9 | 52.2 |
| UDMA | 470 | 23.1 | 69.6 |
| TEGDMA | 286 | 0.011 | 75.7 |

Note: Mw (molecular weight), DC (Degree of conversion)

Source: [34]

Pfeifer et al. [31] investigated the effect of the diluent, TEGDMA, at various concentrations on the degree of conversion of BisGMA. The degree of conversion of BisGMA improved with increasing content of TEGDMA and lower viscosity of the mixture, **Table 1.6**.

Table 1.6 Degree of Conversion of BisGMA as a Function of TEGDMA Content

| BisGMA/TEGDMA mol% | Degree of conversion % | Viscosity (Pa.s) |
|--------------------|------------------------|------------------|
| 100% BisGMA | 50.2 | - |
| 80/20 | 60.9 | 31.67 |
| 60/40 | 67.9 | 2.680 |
| 40/60 | 72.4 | 0.333 |
| 20/80 | 80.8 | 0.047 |
| 100% TEGDMA | 81.3 | 0.015 |

Source: [31]

1.7.3.2 Degree of Cross-linking. The polymer network can be either chemically or physically cross-linked. A chemical cross-link occurs when the radical reacts with a pendant double bond on a different kinetic chain [93]. Physical cross-linking occurs by means of hydrogen bonding between polymer chains [59].

The degree of cross-linking can impact the structural stability and mechanical properties of the resin-based composite [94]. The less cross-linked the material, the more it swells and degrades in solvents [95]. A number of methods to measure the degree of cross-linking directly are being developed [59]. However, the degree of cross-linking can be inferred indirectly from the glass transition temperature; as cross-linking increases, mobility decreases, and the glass transition temperature increases. Additionally, the degree of cross-linking can be evaluated through material softening in ethanol and comparing surface hardness before and after ethanol storage [54].

1.7.3.3 Glass Transition Temperature. The glass transition temperature (T_g) is the temperature at which amorphous polymers undergo a transition from the glassy to the rubbery state. It is an important property of the cured polymeric matrix and can be measured by differential scanning calorimetry or mechanical analysis. The T_g of dental composites must be above the range of intraoral temperatures. Materials with lower T_g values can soften and fail during clinical procedures [96].

Stansbury et al. correlated the glass transition temperature, taken as the maximum $\tan \delta$ peak, with the degree of conversion, **Figure 1.25** [30]. As the polymerization progresses, the proportion of the free monomer decreases with respect to the growing polymer phase, which is made up of chains, cross-links, and pendant groups. Therefore, as the degree of conversion increases, the maximum $\tan \delta$ and the breadth of the curve increase.

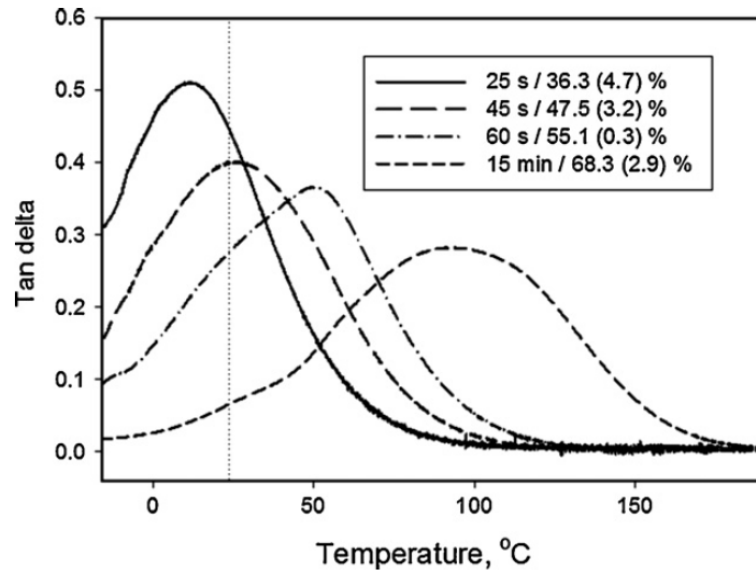


Figure 1.25 Tan delta plots of 70:30 wt% poly(BisGMA/TEGDMA) cured at different time intervals with corresponding degree of conversion percentage.

Source: [31]

1.7.3.4 Mechanical Properties. The mechanical properties of resin-based composites are evaluated in terms of flexural strength and modulus. The flexural strength of the materials should be as high as possible, while the elastic modulus should match the surrounding tissue to avoid inadequate stress-transfer on loading. The flexural strength and modulus are typically calculated through a three-point bending test [54].

Gajewski et al. related the degree of conversion with molecular structure and flexural strength and modulus for the homopolymers of BisGMA, BisEMA, UDMA, and TEGDMA, **Table 1.7** [97]. Although TEGDMA had the highest degree of conversion at 82.5%, its flexural strength was the second highest at 99.1 MPa. TEGDMA is susceptible to cyclization, which increases the degree of conversion but does not necessarily increase the overall strength. A higher degree of conversion that leads to a higher degree of cross-linking will lead to improved mechanical strength [58].

Table 1.7 Correlation of Degree of Conversion With Molecular Structure and Flexural Strength and Modulus

| Monomer | DC% | FS (MPa) | FM(GPa) |
|---------|------|----------|---------|
| BisGMA | 34.5 | 72.4 | 1.0 |
| BisEMA | 75.5 | 87.3 | 1.1 |
| UDMA | 72.4 | 133.8 | 1.8 |
| TEGDMA | 82.5 | 99.1 | 1.7 |

Note: DC, Degree of Conversion, FS, Flexural Strength, FM: Flexural Modulus

Source: [97]

1.7.3.5 Water Sorption. Dental composite resins are in a continuous interaction with the saliva in the wet intraoral environment. As a result, various interactions occur, such as hydrolysis [98] and degradation of polymer network bonds and resin-filler interfaces [99], which can lead to leaching of residual monomers [100,101].

The extent to which a material is affected by water interactions depends on polymer hydrophilicity, solubility, cross-linking density, and porosity, as well as filler content and morphology [99,102,103].

Water absorption into the resin is a diffusion-controlled process. Water molecules enter the polymer network through porosity and intermolecular spaces, thus occupying free volume in the resin [38,103-107]. Water uptake by the composite resin can result in swelling, plasticization and weakening of mechanical properties [99,108].

Hydrophilicity depends on monomer structure, polymer composition and polymerization linkage. Therefore, BisGMA, TEGDMA, and UDMA all take up different amounts of water depending on their structural differences, **Table 1.8** [99]. TEGDMA is believed to take up more water due to the presence of the hydrophilic ether linkages, and flexibility of its network. BisGMA and UDMA, despite their hydrogen bonding, take up less water than TEGDMA. In BisGMA, aromatic groups increase the hydrophobicity of the material and limit water uptake. In UDMA, the high cross-link density due to hydrogen bonding of the urethane groups limits water uptake as well [38].

Table 1.8 Water Uptake % of Homopolymers of BisGMA, UDMA, and TEGDMA

| Resin | Water sorption $\mu\text{g}/\text{mm}^3$ |
|--------|--|
| BisGMA | 33.49 (0.2) |
| UDMA | 29.46 (0.16) |
| TEGDMA | 69.51 (0.32) |

Source: [109]

Polymer networks of high cross-link density have lower water uptake. The covalent cross-linking keeps polymer chains within close proximity, reducing the available volume for water diffusion [99]. However, when the cross-linker is hydrophilic, it can facilitate more water uptake, due to its compatibility with water [110].

While porosity and micro-voids can serve as sites that enhance water uptake and elution [111], composite filler content can minimize water uptake by reducing the overall volume for water to be absorbed [112].

Hygroscopic expansion of a dental composite due to water absorption can weaken the mechanical properties and increase wear rate [113-116]. Some of the properties affected are strength, elastic modulus, hardness, and dimensional stability [117-119]. Plasticization occurs when the polymer chains are separated from one another and chain interaction is weakened. The rate of plasticization matches the rate of water uptake and reaches a maximum once saturation is achieved [117].

The hygroscopic expansion can make up for the loss of volume due to polymerization shrinkage [120-124]. However, if the material takes up significant amounts of water, then expansion can exceed shrinkage and lead to microcracks or cracked cusps in restored teeth due to expansion stress [118,121,125]. Hydrophilic materials are prone to taking up water in excess of polymerization shrinkage [126-128], while hydrophobic materials may take up just the right amount of water to alleviate polymerization shrinkage [121].

1.7.3.6 Polymerization Shrinkage. Polymer systems shrink because as monomers polymerize, they become covalently bonded and more restricted with lower degrees of freedom, thus occupying less space [41,129]. The extent of polymerization shrinkage depends on the degree of conversion, functionality and molecular weight of the monomer system [41]. Pfifer et al. showed how polymerization shrinkage increases with the degree of conversion prior to leveling off for a BisGMA/TEGDMA mixture at 60:40 weight percent, **Table 1.9** [31] .

Polymerization shrinkage is associated with micro-leakage, gap formation, enamel crack propagation, and postoperative sensitivity [130]. It causes stresses within the matrix and at its interface with the tooth. Flexion and crack formation of the tooth structure can occur as a result of inward pull [131-133], or the composite resin can de-bond from the tooth surface with the formation of gaps leading to secondary caries [134-136].

Table 1.9 Correlation of the Degree of Conversion with Polymerization Shrinkage

| Exposure time (s) | Degree of Conversion (%) | Volume Shrinkage (%) |
|-------------------|--------------------------|----------------------|
| 10 | 44.5 | 4.4 (0.2) |
| 20 | 53.1 | 5.0 (0.5) |
| 30 | 56.5 | 5.8 (0.4) |
| 60 | 60.5 | 5.7 (0.1) |
| 600 | 67.9 | 6.0 (0.7) |

Source: [31]

1.7.3.7 Biocompatibility. The biocompatibility of dental materials ensures minimal or no adverse health effects due to the materials' interaction with the oral environment [137]. However, resin-based composites are in continuous interaction with the oral mucosa and pulpal tissue where they can exhibit cytotoxic and genotoxic effects [138,139]. For example, UDMA and TEGDMA can induce apoptosis in dental pulp [140,141].

Polymer networks can also degrade through enzymatic attacks in the oral environment [142]. This causes a reduction in wear resistance, and elution of monomers or molecules from the surface of the material [143-145]. It is believed that polymer degradation occurs only at the network surface due to the large size of the enzymatic proteins. However, surface degradation can lead to further degradation, and this is dependent on the polymer network [146].

The inflammatory enzyme cholesterol esterase (CE), and the salivary enzyme, pseudocholinesterase (PCE), can cause the breakdown of BisGMA and TEGDMA [147]. The degradation products are mainly methacrylic acid, bishydroxypropoxyphenyl propane (bisHPPP), and triethylene glycol, **Figure 1.26**.

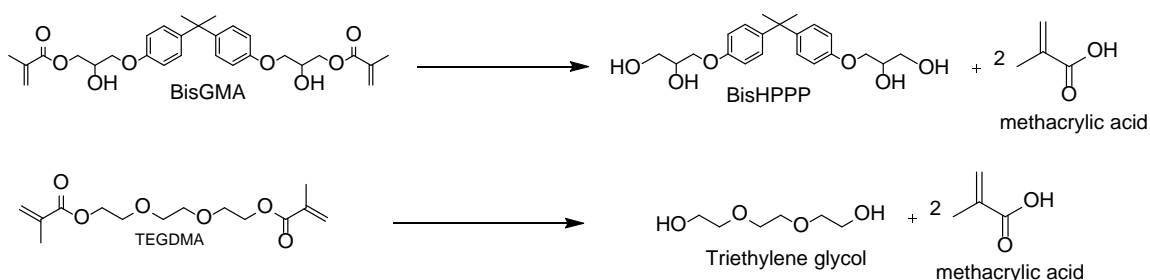


Figure 1.26 Degradation products of BisGMA and TEGDMA.

BisGMA might not undergo a direct hydrolysis to Bisphenol A (BPA) due to the presence of the ether linkage. Bisphenol A can be present as a byproduct in BisGMA, and

can elute into the oral environment, **Table 1.10** [148,149]. BPA is a suspected estrogen mimic [150]. Increased levels of BPA exposure have been linked to various adverse health outcomes such as reduced fertility, altered childhood behavior and neurodevelopment, cardiovascular disorders and altered gene expression [151]. Therefore, the use of BPA has been either banned or decreased. As such, there has been growing interest in replacing the BPA core with a safer, alternative material, such as isosorbide.

Table 1.10 Bisphenol A Content in Commercial BisGMA

| Manufacturer | Bisphenol A ($\mu\text{g/g}$) |
|--------------|---------------------------------|
| ShinNakamura | 130.0 |
| Polysciences | 43.4 |
| Freeman | 42.6 |

Source: [149]

1.8 Isosorbide

Isosorbide is a sugar-based molecule classified as GRAS, generally recognized as safe. In recent years, it has attracted significant interest due to its biocompatibility and potential to replace petroleum-based monomers. It is the product of starch degradation into D-glucose, followed by hydrogenation into D-sorbitol and, finally, the dehydration to D-isosorbide, **Figure 1.27** [152].

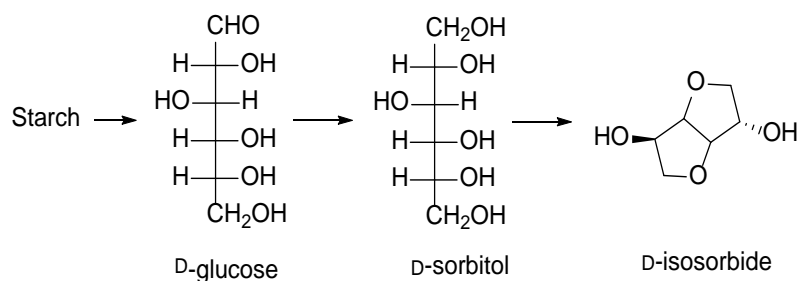


Figure 1.27 General scheme for the synthesis of isosorbide.

Isosorbide is made up of two *cis*-fused tetrahydrofuran rings that exhibit a puckered conformation (120°). The hydroxyl substitution at carbons 2 and 5 distinguish isosorbide from the other two isomers, isomannide and isoidide. Specifically, isosorbide has an *exo* and *endo* substitution at carbons 2 and 5, respectively. While isomannide has both substitutions as *endo*, isoidide has both substitutions as *exo*, **Figure 1.28** [152-154].

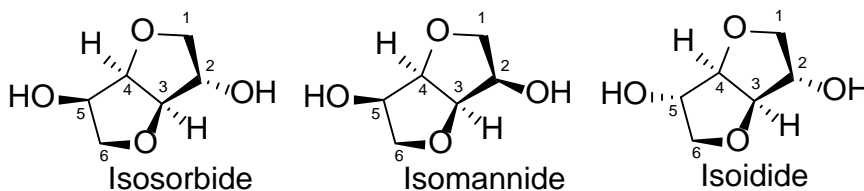


Figure 1.28 1,4:3,6-dianhydrohexitols.

The difference in configuration of the 2 and 5 hydroxyls results in different chemical and physical properties [155]. The *endo* hydroxyl groups form intramolecular hydrogen bonds with the ring-oxygen in the opposite ring, while the *exo* hydroxyl groups do not hydrogen-bond intramolecularly, **Figure 1.29** [152-154].

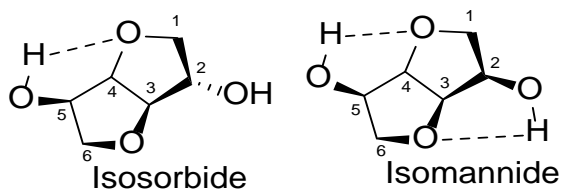


Figure 1.29 Intramolecular hydrogen bonding in isosorbide and isomannide.

Isosorbide and its derivatives have been explored in various health-related areas. For example, aspirin prodrugs in the form of isosorbide-2-aspirinate-5-salicylate completely hydrolyze upon interaction with plasma to release acetylsalicylic acid and salicylic acid [156,157]. The efficacy and safety of isosorbide mononitrate to prevent angina is well documented, and the potential of isosorbide mononitrate to prevent bleeding was also studied [158,159]. Isosorbide-based esters that can easily bind to and be hydrolyzed by human butyrylcholinesterases provide a template for the design of enzyme inhibitors [160]. Biodegradable polyurethane and polyester microporous scaffolds, based on isosorbide, have also been explored for tissue engineering [161,162].

Isosorbide, with its two-ring structure and hydroxyl functionality, mimics BPA, **Figure 1.30**. As such, it has been a topic of interest as BPA replacement, especially in dental materials. **Figure 1.31** shows some of the isosorbide dimethacrylate materials that have been developed up to date as potential BisGMA replacements.

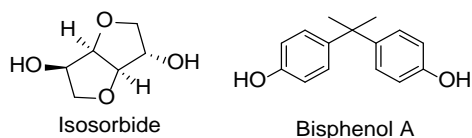


Figure 1.30 Isosorbide and Bisphenol A.

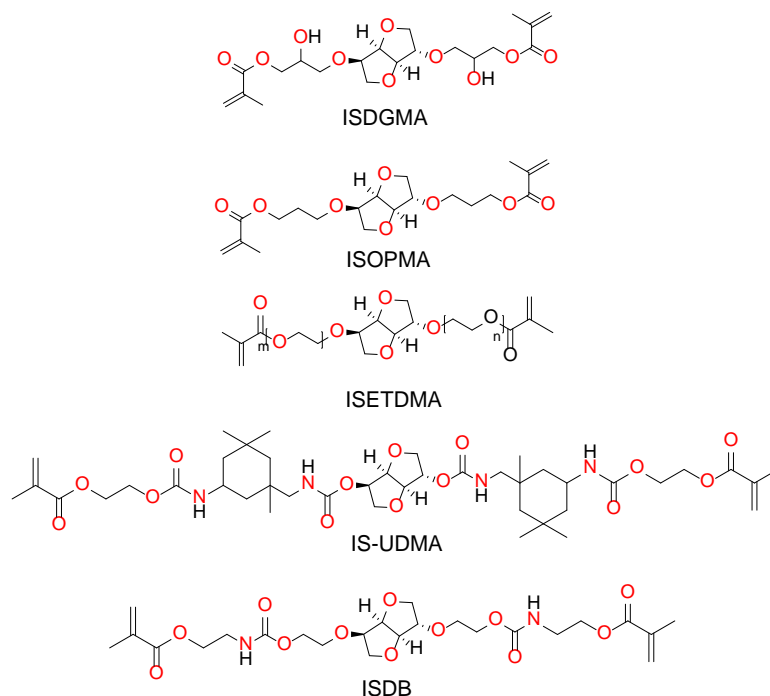


Figure 1.31 Isosorbide-based dental dimethacrylates.

Łukaszczyk et al. and Shin et al. reported the synthesis of ISDGMA [163,164], a monomer that mimics BisGMA and is made by direct methacrylation of isosorbide diglycidyl ether. Łukaszczyk et al. evaluated the performance of ISDGMA as a dental resin, while Shin et al. evaluated its performance as a resin-based composite. The reported water sorption for the homopolymer of ISDGMA was as high as $170 \mu\text{g}/\text{mm}^3$, while, for the copolymer of ISDGMA and TEGDMA, it was $100 \mu\text{g}/\text{mm}^3$, as reported by Łukaszczyk et al. [163].

Kim et al. reported on isosorbide 2,5-bis(propoxy) dimethacrylate (ISOPMA) and compared it to ISDGMA [165]. The water sorption of the polymer derived from ISOPMA, upon elimination of the hydroxyl groups, was lower than that of the polymer derived from ISDGMA.

Duarte et al. developed a urethane based isosorbide dimethacrylate (IS-UDMA) and evaluated it as a resin based composite [166]. The water sorption of the homopolymer was close to that of the BisGMA control but its flexural strength was much lower.

Vasifihasel et al. and Łukaszczyk et al. reported on the synthesis of an ethoxylated isosorbide dimethacrylate (ISETDMA) [167,168]. Łukaszczyk et al. evaluated its performance as a potential diluent due to its low viscosity of 0.062 Pa·s in comparison to 12.4 Pa·s for ISDGMA, and 1200 Pa·s for BisGMA. Since the viscosity of ISETDMA is near that of TEGDMA at 0.011 Pa·s, it can serve as a potential bio-replacement diluent.

Jun et al. developed an isosorbide dimethacrylate (ISDB) based on isocynoethyl methacrylates and evaluated its performance as a dental sealant [169]. Water sorption for samples containing ISDB in comparison to BisGMA were slightly higher but acceptable for that application.

This dissertation investigates the development of isosorbide dimethacrylates for dental applications.

CHAPTER 2

HYPOTHESIS AND OBJECTIVES

2.1 Hypothesis

The objective of this dissertation was to synthesize and develop a series of bio-based hydrophobically modified dental dimethacrylates based on isosorbide. Specifically, *para*, *meta*, and *ortho* benzoate spacers were introduced between the isosorbide core and the methacrylate functionality. This generated isosorbide 2,5-bis(4-glyceryloxybenzoate) dimethacrylate (ISB4GBMA), isosorbide 2,5-bis(3-glyceryloxybenzoate) dimethacrylate (ISB3GBMA), and isosorbide 2,5-bis(2-glyceryloxybenzoate) dimethacrylate (ISB2GBMA), **Figure 2.1**.

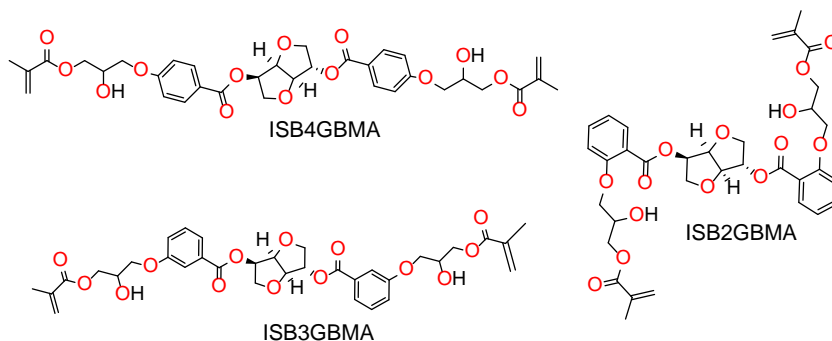


Figure 2.1 Hydrophobically modified isosorbide dimethacrylates with an aromatic spacer.

The performance of the new hydrophobically modified isosorbides was evaluated as dental filling materials and compared to the BisGMA reference and ISDGMA control. The new monomers were expected to result in lower water uptake and improved mechanical properties, relative to ISDGMA, as a result of the hydrophobic modification, but water uptake and mechanical properties comparable to those of BisGMA. The evaluation of the resins was carried out as copolymers with TEGDMA.

This concept was previously addressed by the Jaffe group [170]. In that study, the water uptake of an isosorbide thermoset was reduced, and mechanical properties were improved as a result of incorporating a hydrophobic moiety into the backbone of the polymer when cross-linked with different amines, **Figure 2.2**, and **Table 2.1**.

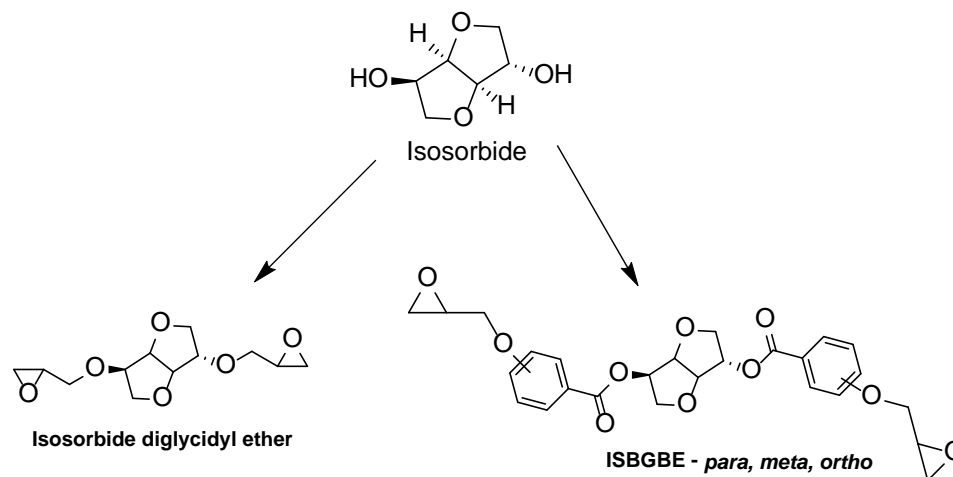


Figure 2.2 Hydrophobically modified isosorbide epoxides with an aromatic spacer.

Table 2.1 Glass Transition Temperature and Water Uptake of Cured Isosorbide Epoxies with Jeffamine

| Epoxy material | Tg | Water uptake ratio % |
|-----------------------------|-----|----------------------|
| Isosorbide diglycidyl ether | 48 | 18% |
| ISB2GB | 78 | 2.20% |
| ISB3GB | 95 | 0.55% |
| ISB4GB | 107 | 2.60% |

Note ISBGB: isosorbide 2,5-bis(glycidyl oxybenzoate), 2=*meta* substituted, 3=*ortho* substituted, 4=*para* substituted

Source: [170]

The choice of aromatic groups is based on the 2-,3- and 4-hydroxy benzoic acids. 2-Hydroxybenzoic acid is usually referred to as salicylic acid, which is the precursor to acetylsalicylic acid (aspirin). Isosorbide has been previously modified with acetylsalicylic

acid to make isosorbide aspirin prodrugs [157]. Therefore, modifying isosorbide with the benzoates is not believed to alter the safety nature of the sugar molecule.

In this approach, the aromatic groups were esterified to the isosorbide core. While this approach may render the bond susceptible to hydrolysis by esterases, it is believed to be a good starting point to differentiate the performance of the various isosorbide benzoate dimethacrylates. Based on this study, the best performing material will be chosen for further modification.

2.2 Specific Objectives

2.2.1 Objective 1: Synthesis and characterization of ISDGMA and the ISBGBMA series

- **Sub-objective 1:** The synthesis of ISDGMA was reported in the literature and was followed accordingly and used as a control material along with BisGMA. The hydrophobically modified isosorbide monomers (ISBGBMA) were synthesized through a 5-step scheme that will be discussed in detail in chapter 4.
- **Sub-objective 2:** Isosorbide and its derivatives were characterized by means of proton NMR for structure elucidation.

2.2.2 Objective 2: Sample preparation and evaluation

- **Sub-objective 1:** Monomer mixtures based on ISDGMA, ISBGBMA monomers, and BisGMA, along with the diluent TEGDMA, were prepared and photocured.
- **Sub-objective 2:** The cured resins were evaluated for the degree of monomeric conversion, glass transition temperature, polymerization shrinkage, water sorption, flexural strength, and modulus.

CHAPTER 3

METHODS

3.1 Structure Elucidation and Thermal Analysis

Structure elucidation and characterization was performed by utilizing Fourier Transform Nuclear Magnetic Resonance (FT-NMR) for proton analysis using a 400 MHz FT-NMR. Attenuated Total Reflectance Fourier-Transform Infrared Spectroscopy (ATR – FTIR) was used for functional group characterization. Dynamic Mechanical Analysis (DMA) was used for glass transition temperature evaluation.

3.1.1 Nuclear Magnetic Resonance

Nuclear magnetic resonance (NMR) spectroscopy is an absorption technique based on how nuclei behave under the influence of an external magnetic field. The various nuclei in a sample, under controlled experimental conditions, can absorb electromagnetic radiation. This absorbed energy can then be measured by the NMR spectrometer by plotting the frequency of the nuclei signal versus the signal intensity and this generates an NMR spectrum [171].

All nuclei carry a charge, and with some nuclei this charge spins on the nuclear axis and generates a magnetic dipole along the axis. Nuclei are NMR-active if they have an odd atomic number (# of protons)-e.g., ^1H , ^{14}N , ^{19}F and ^{31}P , or if they have an odd atomic mass (# of protons + neutrons)-e.g., ^{13}C . [171,172]. Nuclei that contain a magnetic dipole moment can be analyzed by NMR.

When nuclei are placed in an external magnetic field, the direction of the nuclear spin becomes defined by the direction of the magnetic field. The nuclear magnetic moment

of spin assumes two orientations, either opposed to- or along the magnetic field. The magnetic moment precesses about the field like a gyroscope at an angle, with a characteristic frequency, the Larmor frequency (ω_0) defined by **Equation 3.1**. Where γ is the magnetogyric ratio and B_0 is the applied magnetic field [171].

$$\omega_0 = \gamma B_0 \quad (3.1)$$

The magnetogyric ratio γ is the proportionality constant and relates the nuclear magnetic moment μ and the spin number I for a specific nucleus according to **Equation 3.2**, where h is Planck's constant [172,173].

$$\gamma = 2\pi\mu/hI \quad (3.2)$$

If the nuclei in a sample are irradiated with a radio frequency source perpendicular to the external magnetic field during the precession process, the nuclei precessional angle will be influenced. If the power from the radio frequency source is equivalent to that of the Larmor frequency, the nuclei will absorb the energy and be promoted to the less favorable higher energy state. This energy absorption is called resonance because the frequency of the precession and the applied energy resonate or coincide. The energy absorption will increase the precessional angle and tilt the nuclei toward the horizontal plane perpendicular to the external magnetic field. If a detector is aligned horizontally in the direction of the nuclei, the x and y components of the magnetization can be measured. The data generated is a free induction decay (FID) time domain versus energy absorption

spectrum and is converted into the frequency domain versus energy absorption profile mathematically through Fourier transform [172].

The exact frequency where each nucleus absorbs energy depends on its chemical and physical environment. The magnetic field of the nucleus is usually shielded or attenuated by the presence of surrounding electrons that precess and generate opposing magnetic fields. Therefore, the effective field on the nucleus can be either lower (shielded) or higher (deshielded) than the applied magnetic field [171,173].

Since different nuclei will have different frequencies depending on the field strength, the frequencies are converted to a dimensionless scale for spectra comparison. This scale is defined as the chemical shift scale, and it is expressed in parts per million, **Equation 3.3**, where the chemical shift is expressed as δ , and where ν_{sample} is the frequency of the sample, and $\nu_{\text{reference}}$ is the frequency of the reference standard such as tetramethyl silane [171]. An example of proton chemical shift groups is provided in **Figure 3.1**.

$$\delta = \frac{\nu_{\text{sample}} - \nu_{\text{reference}}}{\nu_{\text{reference}}} \times 10^6 \quad (3.3)$$

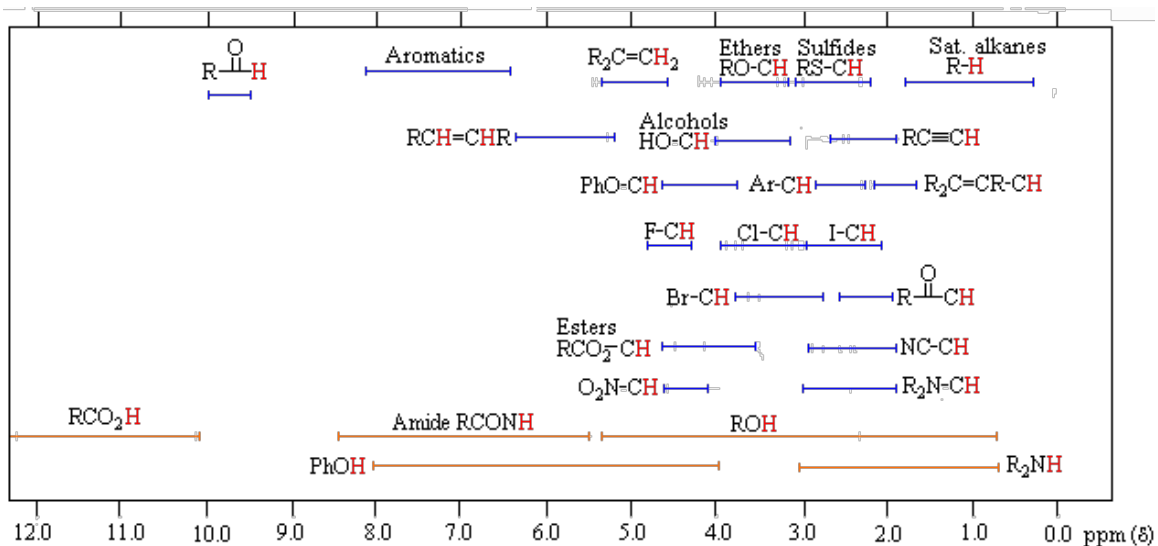


Figure 3.1 Proton chemical shifts.

Source: [174]

Chemically equivalent protons are those that behave identically in the same magnetic field and generate the same (equivalent) chemical shift signal. In contrast, chemically nonequivalent protons are those that behave differently in the same magnetic field. As such, with nonequivalent protons, spin-spin coupling can occur. Non-equivalent protons can share the same carbon (geminal coupling – 2 bonds length) or they can be on an adjacent carbon (vicinal coupling – 3 bonds length). The spin-spin coupling results in the splitting pattern of the proton signal according to $n+1$, where n is the number of the other nonequivalent protons. The distance between the peaks reflects the coupling constant and is measured in Hz. Further, the height of the peaks in the split proton signal follows pascals triangle pattern. For example, a doublet has two peaks with identical heights (1:1), while a triplet has a 1:2:1 peak height ratio [172].

If the proton is affected by two different types of non-identical protons, for example ($n+m$), then the splitting pattern of the proton signal will be according to $(n+1)(m+1)$ with two coupling constants. For instance, a proton coupled to two different protons will

appear as a doublet of a doublets. The number of protons responsible for any NMR signal can be determined from the area integration under the signal peak [172].

3.2 Sample Preparation

Samples were prepared by mixing each of the isosorbide dimethacrylate monomers, or the reference material (BisGMA), with the diluent TEGDMA in a 60:40 weight ratio. Camphorquinone and 2-(dimethylamino)ethyl methacrylate were added at 0.4% and 1.0% by weight respectively [163]. The final mixture was poured into a stainless-steel mold of the desired shape and bonded between two microscope slides prior to curing. Samples were cured using an AZDENT (1900 mW/cm²) LED blue curing light, with an 8 mm light guide tip, operating in the wavelength range of 400-500 nm. The light curing tip was placed 5 cm above the mold. This technique was adapted as a general means to compare the different resins.

Samples for water sorption were cured for 40 seconds once each on the top and bottom sides, except for ISDGMA/TEGDMA samples which were cured for 40 seconds twice on each side for reasons to be addressed in the discussion section. All other evaluations were done on samples cured for 40 seconds twice on each side.

3.3 Water Sorption

A minimum of five disk samples for each sample series with dimensions 1 mm thick x 15 mm diameter were prepared to measure the water sorption (WS) in accordance with ISO4049 [175]. Upon curing, they were placed in an oven at 37°C to obtain a constant mass. Then they were immersed in 10 ml of phosphate buffer solution (DPBS, pH 7.1) at

37°C for 7 days. Water sorption was measured as represented in **Equation 3.4**, where m_7 is the weight after 7 days of immersion, m_0 is the weight prior to immersion, and V_0 is the initial volume of the specimen.

$$WS (\mu\text{g}/\text{mm}^3) = \frac{m_7 - m_0}{V_0} \quad (3.4)$$

3.4 Degree of Double Bond Conversion

ATR-FTIR was used to calculate the degree of conversion (DC) of the top and bottom layers of cured rectangular samples with dimensions 2 mm x 6 mm x 38 mm, according to **Equation 3.5** [89]. The degree of conversion will be the difference in height of the methacrylate vinyl group at ($\nu=1636 \text{ cm}^{-1}$) between the monomer and the polymer, with respect to the height of the internal standard of the C=C aromatic stretching at ($\nu=1610 \text{ cm}^{-1}$).

$$DC\% = \left[1 - \frac{\frac{A(c=c) \text{ methacrylate}}{A(c=c) \text{ aromatic}} \text{ polymer}}{\frac{A(c=c) \text{ methacrylate}}{A(c=c) \text{ aromatic}} \text{ monomer}} \right] \times 100\% \quad (3.5)$$

3.5 Polymerization Shrinkage

A pycnometer was used to determine the mass, volume, and corresponding densities of the cured specimens. Polymerization shrinkage (PS%), as a result of volumetric shrinkage, was calculated according to **Equation 3.6**, where d_p is the density of the polymer, d_m is the

density of the monomer mixture [129].

$$\text{PS}(\%) = \frac{d_p - d_m}{d_p} \times 100\% \quad (3.6)$$

3.6 Glass Transition Temperature

Glass transition temperature was determined by dynamic mechanical analysis using a 2 mm x 6 mm x 38 mm specimen and a 3-point bending test. The temperature range was -40°C to 200°C, with a heating rate of 10°C/min and an oscillation frequency of 1 Hz. Glass transition temperature was determined from the maximum of the tan delta curve [176].

3.7 Flexural Strength and Modulus

Flexural strength was calculated using a modified ISO 4049 method, with a sample size of 2 mm x 6 mm x 38 mm. The analysis was done using a TA-XT Plus texture analyzer, with a 50 kg load cell at a rate of 1.2 mm/min. Sample sets were divided into two parts. One part was measured after immersion in a PBS buffer solution for 24 hours at 37°C, while the other part was measured after being placed in an oven at 37°C for 24 hours.

Flexural strength (σ , MPa) was calculated according to **Equation 3.7**, where F is the maximum load exerted on the specimen at the point of fracture (N), l is the distance between the supports (mm), b is the width of the specimen (mm), and h is the thickness of the specimen (mm). Flexural modulus was determined from the slope in the linear region between 0.05-0.25% strain, similar to ISO 178 [177].

$$\sigma = \frac{3Fl}{2bh^2} \quad (3.7)$$

3.8 Statistical Analysis

One way ANOVA analysis, considering the monomer/TEGDMA mixture as the single factor, with a Tukey post hoc test at a preset alpha of 0.05 was used to determine a 95% data significance using IBM SPSS Statistics software, version 27.

3.9 Hydrophobic Evaluation

The contact angle measurement of each monomer was determined through a drop shape analyzer using a Kruss-DSA30S instrument. In this test, a solution mixture of each monomer in methylene chloride was prepared, and a small film was casted on the surface of a microscope slide. Once methylene chloride evaporated, a drop of water was placed at the film surface and its image was recorded. The recorded image was then analyzed by the instrument software and a contact angle measurement was determined.

The logarithm of the 1-octanol/water partition coefficient was estimated using Chem-Draw Prime (version 17.1).

3.10 Viscosity Evaluation

Viscosity measurements of monomer mixtures were done using a Brookfield LV viscometer at 200 RPM and at 25°C.

CHAPTER 4

SYNTHESIS OF ISOSORBIDE DIMETHACRYLATES

4.1 Isosorbide 2,5-bis(glyceryloxy) dimethacrylate (ISDGMA)

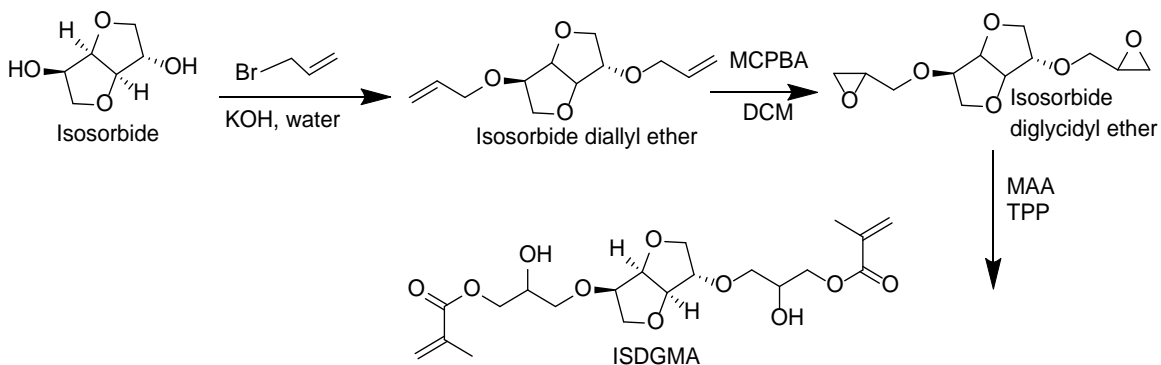


Figure 4.1 Synthesis scheme of ISDGMA.
2,5-bis(2-hydroxy-3-methacryloyloxypropoxy)-1,4:3,6-dianhydro-D-sorbitol

Step 1: Preparation of isosorbide diallyl ether

| | |
|---------------------|------------------|
| Isosorbide | 73 g (0.5 mol) |
| Allyl bromide | 173 ml (2.0 mol) |
| Potassium hydroxide | 67 g (1.2 mol) |
| DI Water | 67 ml |

A three-neck round-bottom flask equipped with a Teflon paddle stirrer, a condenser, a thermocouple, and a heating mantle was set up. Isosorbide (73 g), potassium hydroxide (67 g), and 67 ml of DI water were charged and heated to 65°C. Allyl bromide (173 ml, 2.0 mol) was charged dropwise over one hour and the reaction was run for 24 hours.

The reaction mixture was then neutralized with a few milliliters of 12N hydrochloric acid and extracted three times with 120 ml of dichloromethane. The combined

dichloromethane extracts were washed three times with 150 ml of saturated sodium bicarbonate solution, followed by three washes with 150 ml of DI water.

The dichloromethane was then dried over anhydrous magnesium sulfate, and the salt was removed by vacuum filtration. The product was then concentrated by removing dichloromethane using a rotary evaporator and purified by vacuum distillation at a vapor temperature range of 92-96°C and under a vacuum of 0.03 mm of mercury to prepare isosorbide diallyl ether as a liquid (80% yield and >98% purity by NMR).

Step 2: Preparation of isosorbide diglycidyl ether

| | |
|--|-------------------|
| Isosorbide 2,5-bis(diallylether) | 56.6 g (0.25 mol) |
| 3-Chloroperoxybenzoic acid (75%) MCPBA | 138 g (0.60 mol) |
| Methylene chloride (DCM) | 700 ml |

A 1,000-ml round bottom flask equipped with a Teflon paddle stirrer, a condenser, and a nitrogen line was set up. Isosorbide 2,5-bis(diallylether) (56.6 g) and 400 ml of dichloromethane were mixed and charged into the flask. Then, 138 g of 75% 3-chloroperoxybenzoic acid were placed in a 500-ml addition funnel and charged in a dropwise fashion over one hour. The reaction was run for 48 hours at room temperature.

The precipitated 3-chlorobenzoic acid was then filtered off, and the reaction mixture was stirred with 50 g of potassium carbonate for three hours to neutralize any remaining 3-chlorobenzoic acid. The reaction mixture was filtered again, and the product was concentrated using a rotary evaporator to remove dichloromethane. The final product was purified by column chromatography (ethyl acetate/hexanes, 80:20 w/w) to form a clear liquid (73% yield and >98% pure by NMR).

Step 3: Preparation of isosorbide 2,5-bis(glyceryloxy) dimethacrylate

| | |
|-------------------------------------|------------------------|
| Isosorbide 2,5-bis(diglycidylether) | 20 g (0.077 mol) |
| Methacrylic acid (MAA) | 75 ml (0.89 mol) |
| Triphenylphosphine (TPP) | 0.15 g (0.57 mmol) |
| 4-Methoxyphenol (MeHQ) | 12.5 mg (0.1 mmol) |
| Phenothiazine | 12.5 mg (63 μ mol) |

A 100-ml round bottom flask equipped with a Teflon paddle stirrer, a condenser, a thermocouple, and a heating mantle was set up. Isosorbide diglycidyl ether (20 g), triphenylphosphine (0.15 g), 4-methoxyphenol (12.5 mg), phenothiazine (12.5 mg) and 75 ml of methacrylic acid were charged. The reaction mixture was heated to 76°C and stirred for 24 hours. The product was then concentrated under vacuum (0.4 mm mercury) at 50°C to remove about 75% of unreacted methacrylic acid.

The crude was then mixed with 250 ml of dichloromethane and transferred to a 500-ml separatory funnel, where it was washed three times with 100 ml of saturated sodium carbonate solution. It was washed three times with 100 ml of DI water. The organic layer was then mixed with anhydrous magnesium sulfate to remove traces of water and then filtered and concentrated using a rotary evaporator. The final product was purified by column chromatography (ethyl acetate/hexanes, 95:5 w/w) and stabilized with 500 ppm of MeHQ (82% yield and >85% disubstituted by NMR – addressed further in discussion).

4.2 Isosorbide 2,5-bis(4-glyceryloxybenzoate) dimethacrylate (ISB4GBMA)

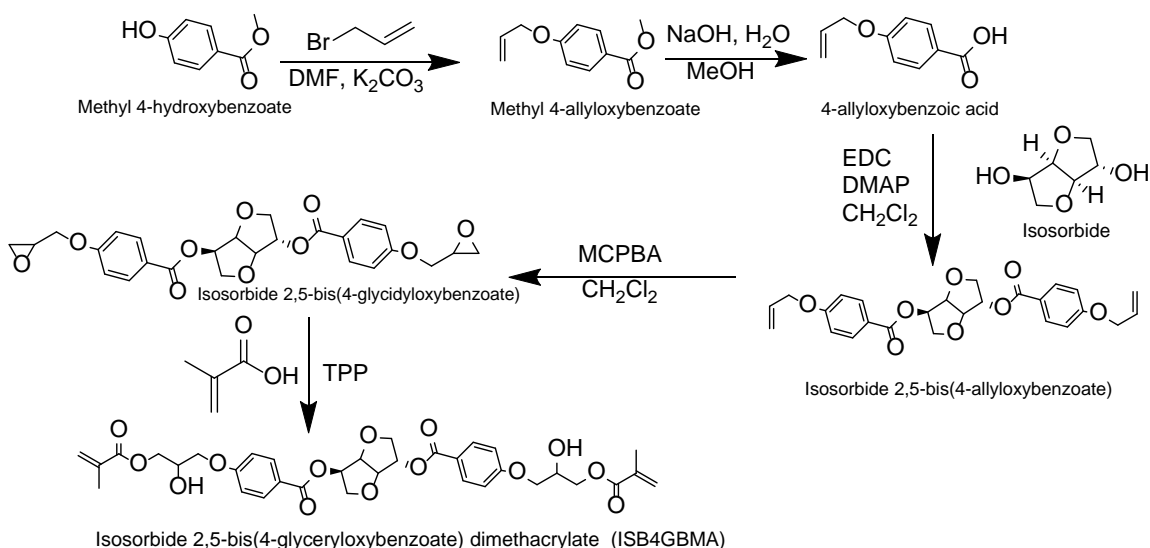


Figure 4.2 Synthesis scheme of ISB4GBMA.

1,4:3,6-dianhydro-D-sorbitol 2,5-bis[4-(2-hydroxy-3-methacryloyloxypropoxy)benzoate]

Step 1. Preparation of methyl 4-(allyloxybenzoate)

| | |
|--------------------------------------|-------------------------|
| Methyl 4-hydroxybenzoate | 152 g, 1.00 mol |
| Allyl bromide | 133 g, (95 ml, 1.1 mol) |
| Dimethylformamide (DMF) | 600 ml |
| Anhydrous potassium carbonate powder | 276 g (2.0 mol) |

A 2,000-ml 3-neck Morton round-bottom flask equipped with a Teflon paddle stirrer, a condenser, and a nitrogen line was set up. Methyl 4-hydroxybenzoate (152 g) and 600 ml of DMF were charged to the flask and stirred to dissolve methyl 4-hydroxybenzoate. Allyl bromide (133 g, 95 ml) were charged via dropwise addition over one hour. The reaction was run for 48 hours. Then, 1000 ml of DI water was added and stirred for one hour to dissolve the precipitated potassium chloride salt, which was then removed by filtration.

The product was transferred to a 2,000-ml separatory funnel and extracted with 250 ml of methylene chloride three times. The organic layer was isolated and mixed with a spoonful of anhydrous magnesium sulfate to remove residual water. The product was concentrated by removing methylene chloride through a rotary evaporator, then distilled at 100°C and collected at a vapor temperature range of 86-89°C under a vacuum range of 0.04-0.05 mm of mercury to yield methyl 4-(allyloxybenzoate) as a liquid (92% yield, >98% purity by NMR).

Step 2: Preparation of 4-allyloxybenzoic acid

| | |
|---------------------------|-------------------|
| Methyl 4-allyloxybenzoate | 164 g, 0.855 mole |
| Potassium hydroxide | 80 g, 1.42 mole |
| Methanol | 500 ml |
| DI water | 500 ml |

A 2,000-ml round Morton flask equipped with a Teflon paddle stirrer, a condenser, a nitrogen line, a thermocouple, and a heating mantle was set up. Methyl 4-allyloxybenzoate (164 g) and 500 ml of methanol were charged. The contents were then stirred and heated to reflux. Potassium hydroxide (80 g) were dissolved in 500 ml of DI water and charged to the flask. The mixture was then heated under reflux for 48 hours. The reaction product was cooled, and 100 ml of concentrated hydrochloric acid was added to precipitate the free acid. The precipitate was filtered, and the product was concentrated by removing the water/methanol mixture using a rotary evaporator. The final product was recrystallized in

750 ml of ethanol to yield a white solid of 4-allyloxybenzoic acid (87% yield, >98% purity by NMR, melting point 163-164°C).

Step 3: Preparation of isosorbide 2,5-bis(4-allyloxybenzoate)

| | |
|---|-------------------|
| Isosorbide | 73 g (0.50 mol) |
| 4-Allyloxybenzoic acid | 178 g (1.0 mol) |
| 1-Ethyl-3-[3-dimethylaminopropyl]carbodiimide hydrochloride (EDC) | 191 g (1.0 mol) |
| 4-Dimethylaminopyridine (DMAP) | 12.6 g (0.10 mol) |
| Dichloromethane (DCM) | 1200 ml |

A 2,000-ml 3-neck Morton flask equipped with a Teflon paddle stirrer, a condenser, and a nitrogen line was set up and dried by heating with a torch to remove any traces of moisture. The reaction set up was then cooled in a bucket of ice to about 0-5°C; then, 73 g of isosorbide, 600 ml of methylene chloride, and 12.6 g of DMAP were charged and stirred. EDC (91 g) was dissolved in 600 ml of dichloromethane and transferred to a 1,000-ml addition funnel. The EDC/DCM mixture was charged via dropwise addition over one hour. The reaction was run for 48 hours, and the precipitated urea byproduct was removed by filtration.

The product mixture was then transferred to a 2,000-ml separatory funnel and washed three times using 100 ml of 15% hydrochloric acid solution in each wash, to remove the basic DMAP. The extracted organic layer was then washed with 200 ml of saturated sodium carbonate twice to remove any traces of acid. It was mixed with a spoonful of anhydrous magnesium sulfate to remove any traces of water. After filtering off

the desiccant, the product was concentrated by removing dichloromethane on the rotary evaporator to leave an off-white solid material, which was recrystallized with 800 ml of ethanol (65% yield, >89% pure by NMR, melting point 91-92°C).

Step 4: Preparation of isosorbide 2,5-bis(4-glycidyloxybenzoate)

| | |
|--|----------------------|
| Isosorbide 2,5-bis(4-allyloxybenzoate) | 221.4 g (0.476 mole) |
| 3-Chloroperbenzoic acid (75%) MCPBA | 220 g (0.95 mole) |
| Dichloromethane (DCM) | 1200 ml |
| Anhydrous potassium carbonate | 100 g |

A 2,000-ml 3-neck Morton flask equipped with a Teflon paddle stirrer, a condenser, and a nitrogen line was set up. Isosorbide 2,5-bis(4-allyloxybenzoate) (221.4 g) and 600 ml of dichloromethane were charged, stirred, and cooled to 0-5°C. 3-Chloroperbenzoic acid (75%, 220 g) and 600 ml of dichloromethane were charged to flask via dropwise addition over one hour. The reaction was run for 48 hours, and the precipitated 3-chlorobenzoic acid was removed by filtration. The filtrate was then charged to a 1,000-ml round bottom flask and mixed with 100 g of anhydrous potassium carbonate to remove any residual peracid. The precipitate was later removed by filtration and the filtrate mixed with anhydrous magnesium sulfate to remove traces of water. The product was concentrated by removing dichloromethane on the rotary evaporator and recrystallized with 300 ml of ethyl acetate to yield an off white solid (60% yield and >98% pure by NMR, melting point 112-113°C).

Step 5: Preparation of Isosorbide 2,5-bis(4-glyceryloxybenzoate) dimethacrylate

| | |
|--|----------------------|
| Isosorbide 2,5-bis(4-glycidylloxybenzoate) | 20 g (0.04 mole) |
| Methacrylic acid | 100 ml (1.19 mole) |
| Triphenylphosphine | 0.30 g (1.14 mmol) |
| 4-Methoxyphenol | 10 mg (0.81 mmol) |
| Phenothiazine | 10 mg (50 μ mol) |

A 100-ml round bottom flask equipped with a Teflon paddle stirrer, a condenser, a thermocouple, and a heating mantle was set up. Isosorbide 2,5-bis(4-glycidylloxybenzoate) (20g), triphenylphosphine (0.30 g), 4-methoxyphenol (10 mg), phenothiazine (10 mg) and 100 ml of methacrylic acid were charged to the flask. The contents were heated to 76°C and stirred for 24 hours. The reaction mixture was then concentrated by removing about 75% of unreacted methacrylic acid at 50°C and 0.4 mm of mercury.

The concentrated mixture was then diluted with 250 ml of dichloromethane and transferred to a 500-ml separatory funnel. Then, the mixture was washed three times with 100 ml of saturated sodium carbonate solution to remove any remaining acid. The organic layer was then washed four times with 100 ml of DI water and mixed with anhydrous magnesium sulfate to remove any traces of water.

The product solution was then filtered and concentrated by removing excess dichloromethane using a rotary evaporator. The residue was purified by column chromatography (ethyl acetate/hexanes, 70:30 w/w) to obtain a thick paste (69% yield, >98% purity by NMR).

4.3 Isosorbide 2,5-bis(3-glyceryloxybenzoate) dimethacrylate (ISB3GBMA)

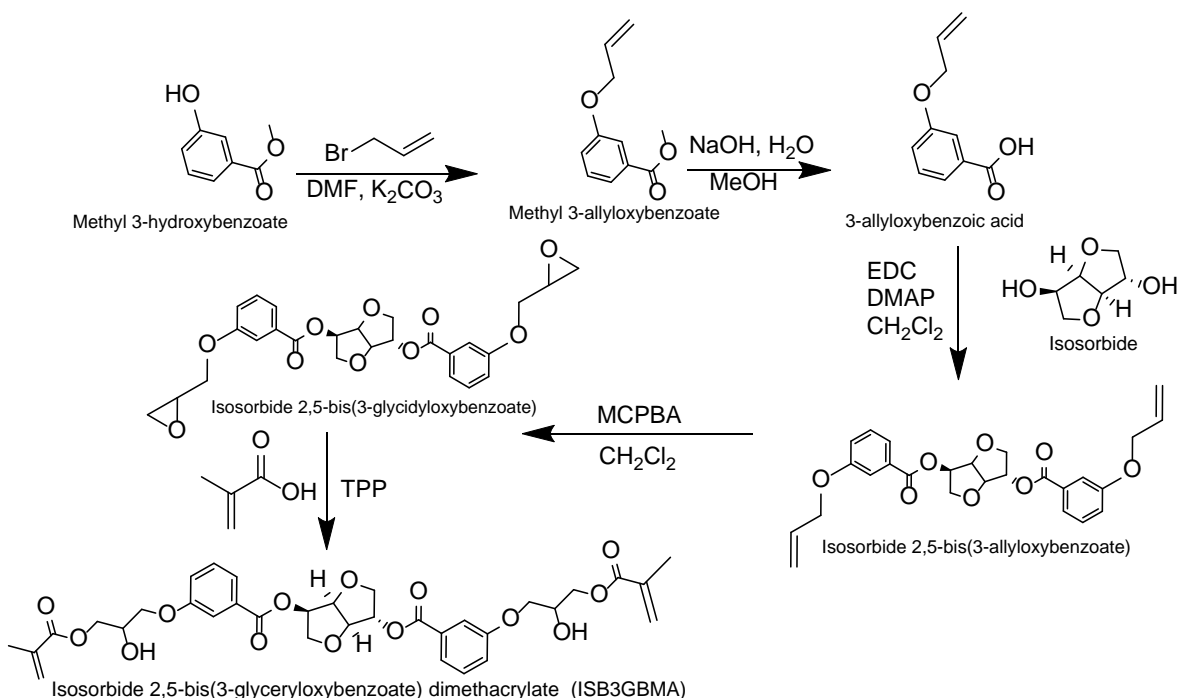


Figure 4.3 Synthesis scheme of ISB3GBMA.

1,4:3,6-dianhydro-D-sorbitol 2,5-bis[3-(2-hydroxy-3-methacryloyloxypropoxy)benzoate]

Isosorbide 2,5-bis(3-glyceryloxybenzoate) dimethacrylate was synthesized via a 5-step reaction as depicted in **Figure 4.3**, in a fashion similar to that used for ISB4GBMA. The melting point of 3-allyloxybenzoic acid was 74-75°C. Isosorbide 2,5-bis(3-allyloxybenzoate) was a liquid and was purified by column chromatography (ethyl acetate/hexanes, 1:1 w/w).

Isosorbide 2,5-bis(3-glycidyloxybenzoate) was a paste and was purified by column chromatography as well (ethyl acetate/hexanes, 2:1 w/w). ISB3GBMA was purified by column chromatography (ethyl acetate/hexanes, 70:30 w/w) and obtained as a paste (76% yield, >98% pure by NMR).

4.4 Isosorbide 2,5-bis(2-glyceryloxybenzoate) dimethacrylate (ISB2GBMA)

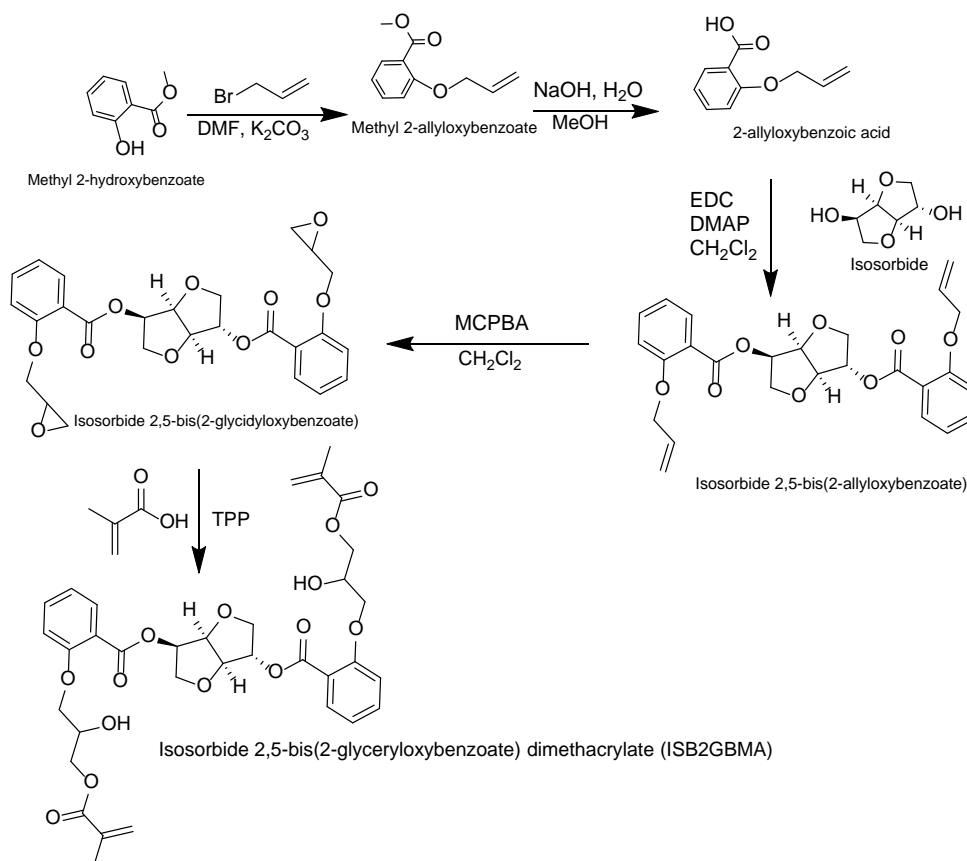


Figure 4.4 Synthesis Scheme of ISB2GBMA.

1,4:3,6-dianhydro-D-sorbitol 2,5-bis[2-(2-hydroxy-3-methacryloyloxypropoxy)benzoate]

Isosorbide 2,5-bis(2-glyceryloxybenzoate) dimethacrylate was synthesized via a 5-step reaction as shown in **Figure 4.4**, in a fashion similar to that used for ISB4GBMA and ISB3GBMA. The melting point of 2-allyloxybenzoic acid was 58-59°C. Isosorbide 2,5-bis(2-allyloxybenzoate) was a liquid and was purified by column chromatography (ethyl acetate/hexanes, 1:1 w/w).

Isosorbide 2,5-bis(2-glycidyloxybenzoate) was purified by column chromatography (ethyl acetate: hexanes, 2:1 w/w) and obtained as a paste.

ISB2GBMA was purified by column chromatography (ethyl acetate/hexanes, 7:3 w/w) and obtained as a paste as well (79% yield, >96% pure by NMR).

CHAPTER 5
RESULTS AND DISCUSSION

The analysis and evaluation of the different dental dimethacrylate monomers, depicted in **Figure 5.1** and **Table 5.1**, are explored in this chapter. Their physical and chemical nature will play an important role in their performance.

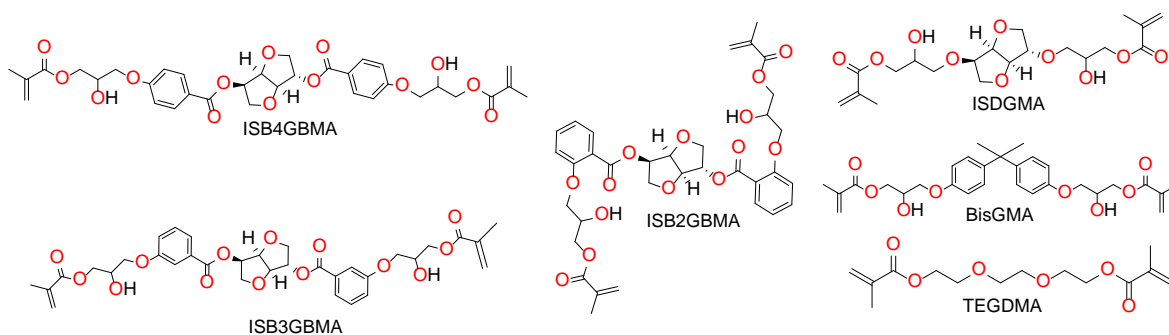


Figure 5.1 Chemical structures of ISB4GBMA, ISB3GBMA, ISB2GBMA, ISDGMA, BisGMA, and TEGDMA.

Table 5.1 Molecular Weight and Double Bond Concentration of ISB4GBMA, ISB3GBMA, ISB2GBMA, ISDGMA, BisGMA, and TEGDMA

| Structure | ISB4-GBMA | ISB3-GBMA | ISB2-GBMA | ISD-GMA | Bis-GMA | TEG-DMA |
|-------------|-----------|-----------|-----------|---------|---------|---------|
| Mw (g/mol) | 670.66 | 670.66 | 670.66 | 430.45 | 512.60 | 286.32 |
| DB (mol/Kg) | 2.98 | 2.98 | 2.98 | 4.65 | 3.90 | 6.99 |

Note: Mw, molecular weight. DB, double bond concentration

5.1 Structural Analysis

The synthesis of ISDGMA and the *para*, *meta*, and *ortho* isomers of ISBGBMA was followed by proton NMR spectral analysis. Isosorbide is the core building block for these dimethacrylate monomers. As such, it is important to elucidate its structure by NMR to better understand the subsequent degree of substitution.

Isosorbide has a total of 8 chemically nonequivalent protons bound to carbon. The degree of substitution can be determined from the integration ratio of either the isosorbide cyclic protons (H2/H5) bonded to the C₂ and C₅ carbons or, the isosorbide cyclic bridge protons (H3/H4) bonded to the C₃ and C₄ carbons, **Figure 5.2**. Depending on the nature of the substitution, the H2/H5 signals either can be distinguishable, or they can be indistinguishable and overlap with other isosorbide protons. On the other hand, the H3/H4 signals are more resolvable and are used regularly to determine the degree of substitution. H3 is adjacent to H2 and H4, but it is coupled only to H4 and thus appears as a doublet. On the other hand, H4 is adjacent to H3 and H5 and coupled to both H3 and H5 and thus appears as a doublet of a doublets. Isosorbide proton NMR assignments were verified through ¹H-¹H correlation spectroscopy (COSY), and the spectrum is provided in the appendix, **Figure A.1**.

In the structural analysis of the isosorbide derivatives, the key focus will be on the major peaks identifying the desired compound. Further spectroscopic analysis by means of carbon, ¹H-¹H COSY, ¹H-¹³C heteronuclear single quantum correlation (HSQC), and ¹H-¹³C heteronuclear multiple bond correlation (HMBC) spectroscopy is needed to confirm the additional proton assignments.

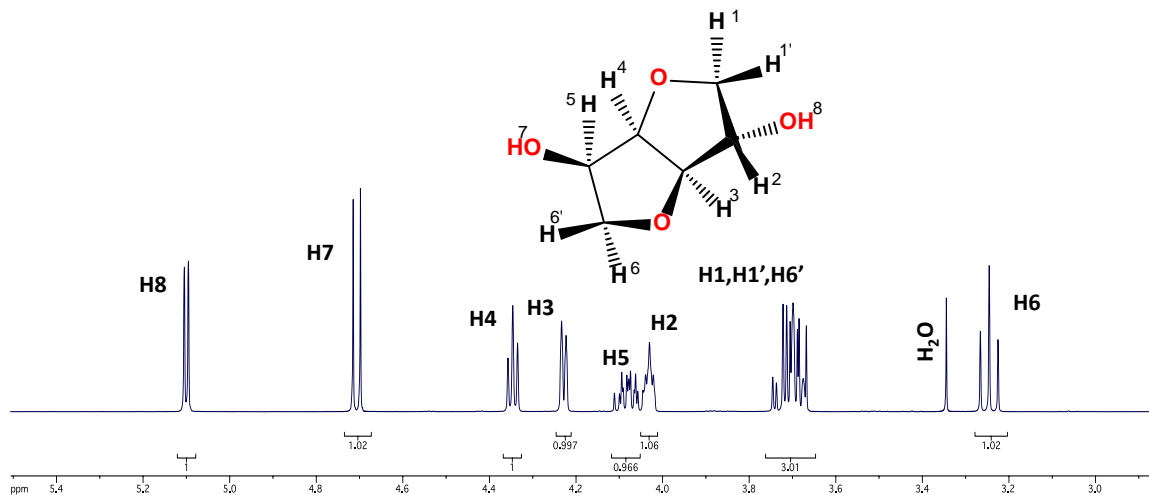


Figure 5.2 ^1H NMR spectrum of isosorbide in DMSO-d_6 .

^1H NMR (DMSO-d_6 , δ -ppm): 5.10 (d, $J = 3.7$ Hz, 1H-H8), 4.71 (d, $J = 6.7$ Hz, 1H-H7), 4.35 (t, $J = 4.4$ Hz, 1H-H4), 4.23 (d, $J = 4.1$ Hz, 1H-H3), 4.11-4.06 (m, 1H-H5), 4.05-4.01 (m, 1H-H2), 3.75-3.67 (m, 3H-H1, H1', H6'), 3.25 (t, $J = 8.2$ Hz, 1H-H6).

5.1.1 NMR Analysis of ISDGMA and Reaction Intermediates

The ^1H NMR spectrum of isosorbide diallyl ether (ISDAE) is shown in **Figure 5.3**. The proton integration ratio of the isosorbide cyclic protons H3/H4 at 4.46 and 4.58 ppm to the allyl methine protons Hc/Hc' at 5.94-5.79 ppm is 1:1:2.16. This means that, for every isosorbide core, there are two allyl methine protons, and this confirms that two allyl groups are attached to isosorbide in ISDAE.

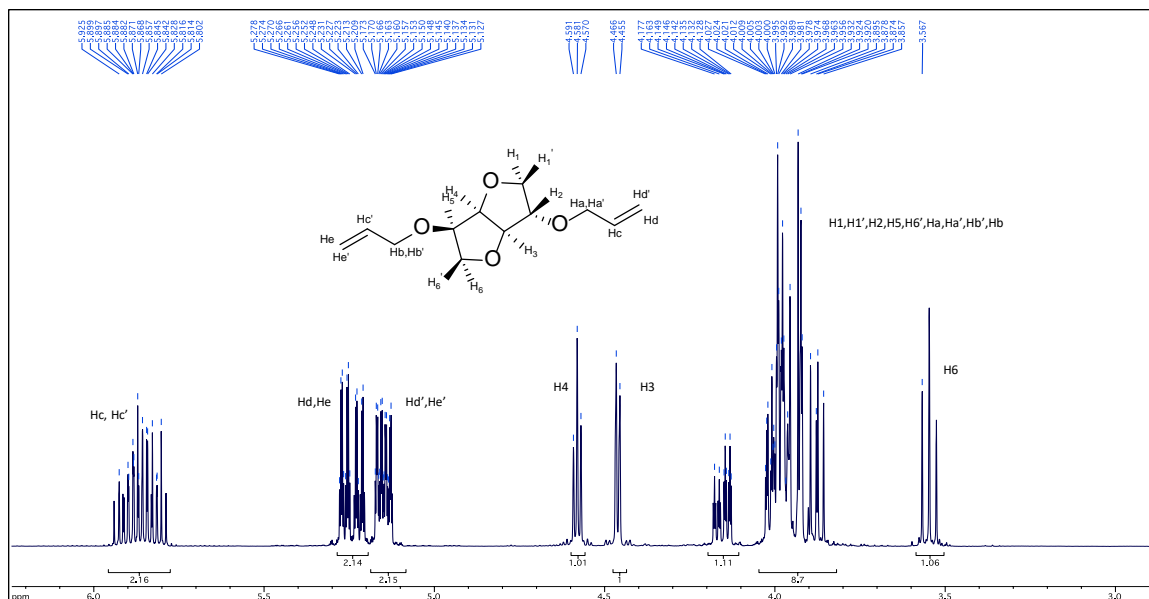


Figure 5.3 ^1H NMR spectrum of isosorbide diallyl ether in CDCl_3 .

^1H NMR (CDCl_3 , δ -ppm): 5.94-5.79 (m, 2H-Hc/Hc'), 5.28-5.21 (m, 2H-Hd,He), 5.17-5.13 (m, 2H-Hd',He'), 4.58 (t, $J = 4.4$ Hz, 1H-H4), 4.46 (d, $J = 4.3$ Hz, 1H-H3), 4.18-4.13 (m, 1H) and 4.03-3.86 (m, 9H) – (H1,H1',H2,H5,H6',Ha,Ha',Hb,Hb'), 3.55 (t, $J = 8.3$ Hz, 1H-H6).

Figure 5.4 depicts the ^1H NMR spectrum of isosorbide diglycidyl ether. The allyl vinyl protons in the ISDAE profile shifted upfield upon epoxidation. The new epoxide protons appear at 2.58-2.51 ppm for Hd/He, 2.75-2.72 for Hd'/He', and 3.13-3.06 ppm for Hc/Hc'. The integration ratio of the isosorbide cyclic protons H3/H4 to the epoxide protons is about (1:1:2:2:2), which means that, for every isosorbide core, there exists 6 epoxide protons, and this confirms that two glycidyl groups are attached to isosorbide in ISDGE.

The epoxidation changes the splitting pattern of the cyclic protons H3/H4. H3 now appears as two doublets, and H4 appears as a multiplet. This is probably due to the presence of the epoxide ring at the endo and exo sites of isosorbide.

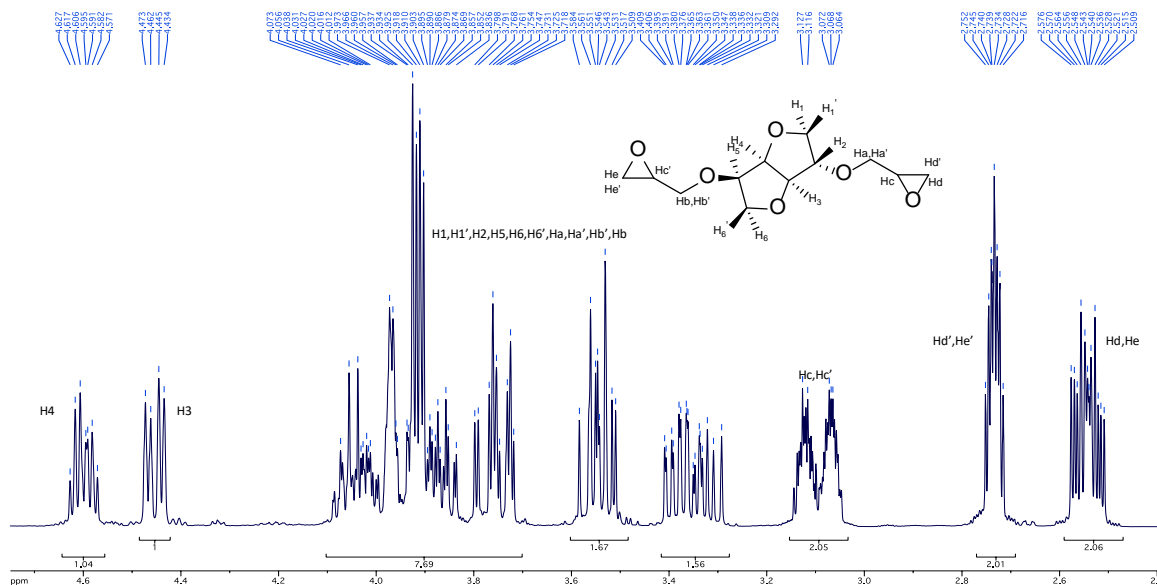


Figure 5.4 ^1H NMR spectrum of isosorbide diglycidyl ether in CDCl_3 .

^1H -NMR (CDCl_3 , δ -ppm): 4.63 (m, 1H-H4 isosorbide), 4.45 (dd, $J = 11.0$, 4.4 Hz, 1H-H3 isosorbide), 4.07-3.72 (m, 8H), 3.58-3.51 (m, 1.5H), 3.41-3.29 (m, 1.5H) - (H1,H1',H2,H5,H6,H6',Ha,Ha',Hb,Hb'), 3.13-3.06 (m, 2H-Hc,Hc'), 2.75-2.72 (m, 2H-Hd',He'), 2.58-2.51 (m, 2H-Hd,He).

The epoxide proton signals in the isosorbide diglycidyl ether spectrum disappear to give rise to glyceryloxy peaks, and methacrylate protons appear in ISDGMA at 5.58, 6.11, and 1.93 ppm, indicating methacrylation, **Figure 5.5**. The integration ratio of the isosorbide cyclic protons H3 to H4 is 1:1, which indicates equal substitution at the isosorbide core.

However, we believe bis-methacrylation (branching) to be also present as indicated by the integration ratio of the isosorbide cyclic protons to the newly formed methacrylate protons. The integration ratio of H3/H4 to the methacrylate vinyl protons ($\text{H}_{i,i'}/\text{H}_{j,j'}$) and the methacrylate methyl protons (H_g/H_f) is (1:1:2.4:2.4:7.1) instead of (1:1:2:2:6); this demonstrates the possibility of bis-methacrylation of up to 15 mole %.

The proton signal at 5.0 ppm was reported by Łukaszczyk [163] to be that of the methine proton of the glycerol moiety (Hc/Hc') where bis-methacrylation had occurred. However, Fujisawa studied the NMR spectrum of BisGMA and Iso-BisGMA (where

epoxide ring opening and methacrylation occurs at the more substituted carbon) and referred that peak to the glyceryl methine in Iso-BisGMA [178]. The ^1H NMR spectrum of BisGMA is provided in the appendix, **Figure A.2**.

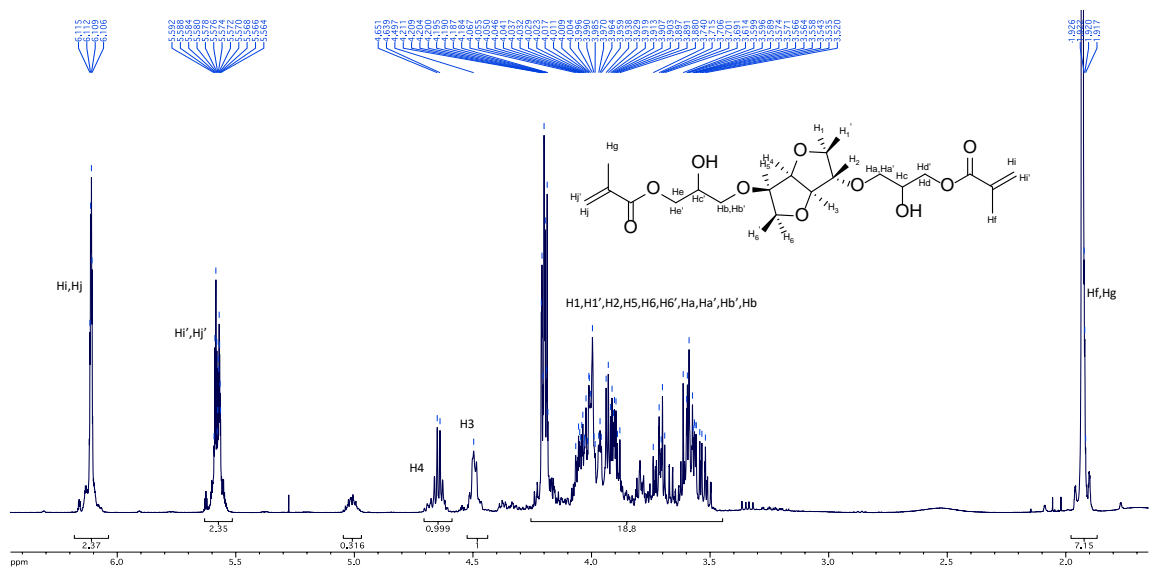


Figure 5.5 ^1H NMR spectrum of isosorbide 2,5-bis(glyceryloxy) dimethacrylate in CDCl_3 . ^1H NMR (CDCl_3 - δ , ppm): 6.11 (m, 2.4H-Hi,Hj), 5.58 (m, 2.4H- Hi',Hj'), 4.64 (m, 1H-H4), 4.50 (m, 1H-H3), 4.21-4.35 (m, 16-19H-H1,H1',H2,H5,H6,H6',Ha,Ha',Hb,Hb', Hc,Hc', Hd,Hd',He,He'), 1.93 (m, 6-7H-Hf,Hg).

5.1.2 NMR Analysis of ISB4GBMA and Reaction Intermediates

The ^1H NMR spectrum of isosorbide 2,5-bis(4-allyloxybenzoate) is presented in **Figure 5.6**. The integration ratio of the isosorbide cyclic protons H3 and H4 at 4.96 and 5.01 ppm to the allyl methine protons Hd/Hi at 6.09-5.97 ppm is (1:1:2) indicating that the desired product had been made.

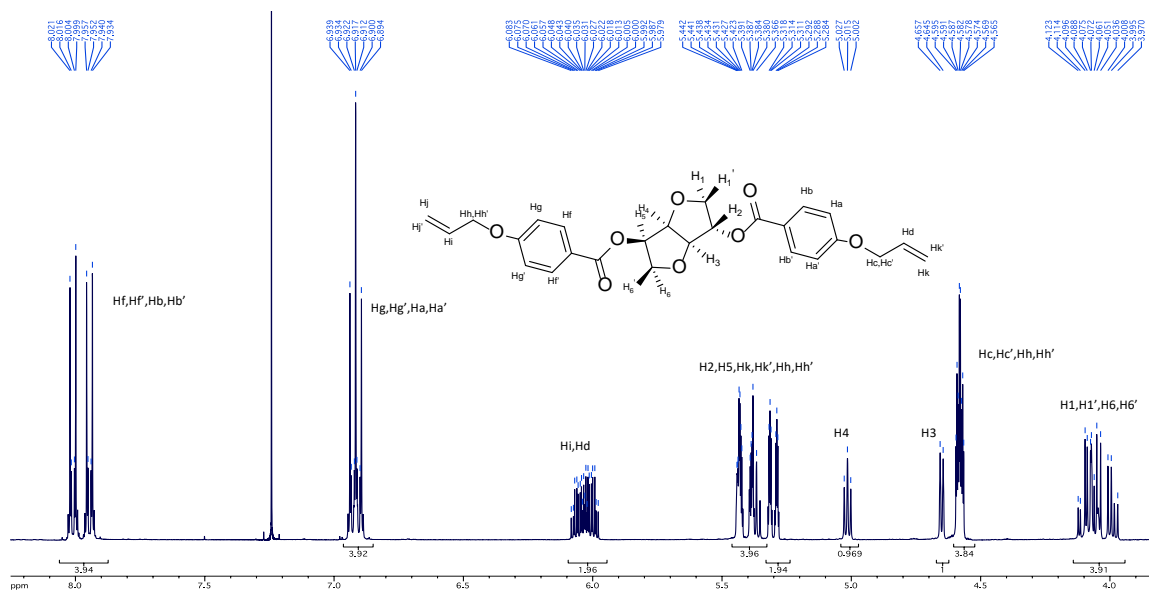


Figure 5.6 ¹H NMR spectrum of isosorbide 2,5-bis(4-allyloxybenzoate) in CDCl₃. ¹H-NMR (CDCl₃, δ-ppm): 8.02-7.93 (2d, *J* = 9.02, 9.03 Hz, 4H-Hf,Hf',Hb,Hb'), 6.94-6.89 (m, 4H-Hg,Hg',Ha,Ha'), 6.03 (m, 2H-Hi,Hd), 5.44-5.37 (m, 4H) and 5.30 (m, 2H) - (H₂,H₅,Hk,Hk',Hh,Hh'), 5.01 (t, *J* = 5.0 Hz, 1H-H₄), 4.96 (d, *J* = 4.7 Hz, 1H-H₃), 4.58 (m, 4H-Hc,Hc',Hh,Hh'), 4.12-3.97 (m, 4H-H₁,H_{1'},H₆,H_{6'}).

The ¹H NMR spectrum of isosorbide 2,5-bis(4-glycidyoxybenzoate) is shown in **Figure 5.7**, where the allyl vinyl protons have shifted upfield to 3.36 ppm for Hd/Hi, 2.92 ppm for Hk/Hj, and 2.76 ppm for Hk'/Hj' upon epoxidation. The ratio of integration of the isosorbide cyclic protons H₃/H₄ to the epoxide protons is (1:1:2:2) which indicates complete epoxidation and disubstitution. The isosorbide H₂/H₅ protons are more pronounced at 5.44 and 5.37 ppm, where H₂ appears as a doublet and H₅ as a doublet of a doublets. H₂ is coupled to H_{1'}, while H₅ is coupled to H₆ and H₄. Their ratio of integration is 1:1 which also indicates dual substitution at the isosorbide core.

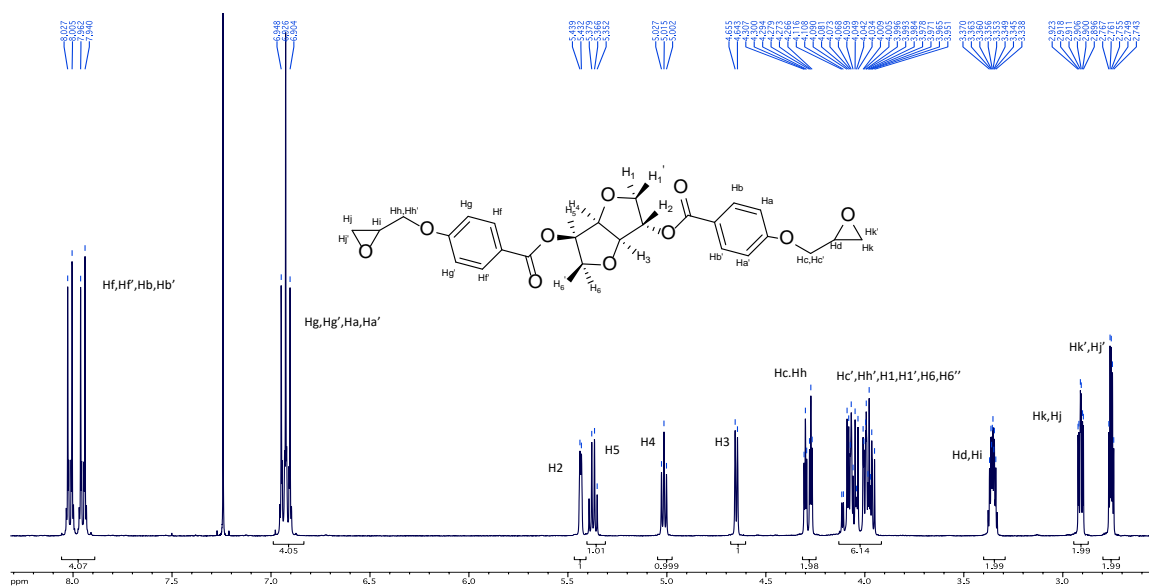


Figure 5.7 ^1H NMR spectrum of isosorbide 2,5-bis(4-glycidyoxybenzoate) in CDCl_3 . ^1H -NMR (CDCl_3 , δ -ppm): 8.03-7.93 (2d, $J = 8.78, 8.8$ Hz, 4H-Hb,Hb',Hf,Hf'), 6.93 (m, 4H- Hg,Hg',Ha,Ha'), 5.44 (d, $J = 3.0$ Hz, 1H-H2), 5.37 (q, $J = 5.5$ Hz, 1H-H5), 5.01 (t, $J = 5.1$ Hz, 1H-H4), 4.65 (d, $J = 4.7$ Hz, 1H-H3), 4.29 (dt, $J = 11.0, 2.7$ Hz, 2H-Hc,Hh), 4.12-3.95 (m, 6H-Hc',Hh',H1,H1',H6,H6'), 3.36 (m, 2H-Hd,Hi), 2.92 (m, 2H-Hk,Hj), 2.76 (m, 2H-Hk',Hj').

Figure 5.8 shows the NMR spectrum of the final product, isosorbide 2,5-bis(4-glycidyoxybenzoate) dimethacrylate. The integration ratio of the isosorbide cycle protons H3 to H4 and H2 to H5 is about 1:1, which indicates dual substitution. The ratio of integration of either of the dual cyclic protons to the methacrylate vinyl protons is (1:1:2:2), indicating that the desired product is made without any bis-methacrylation or branching. The methine proton signal at 5.3 indicates the possibility of the formation of Iso-ISB4GBMA, similar to Iso-BisGMA.

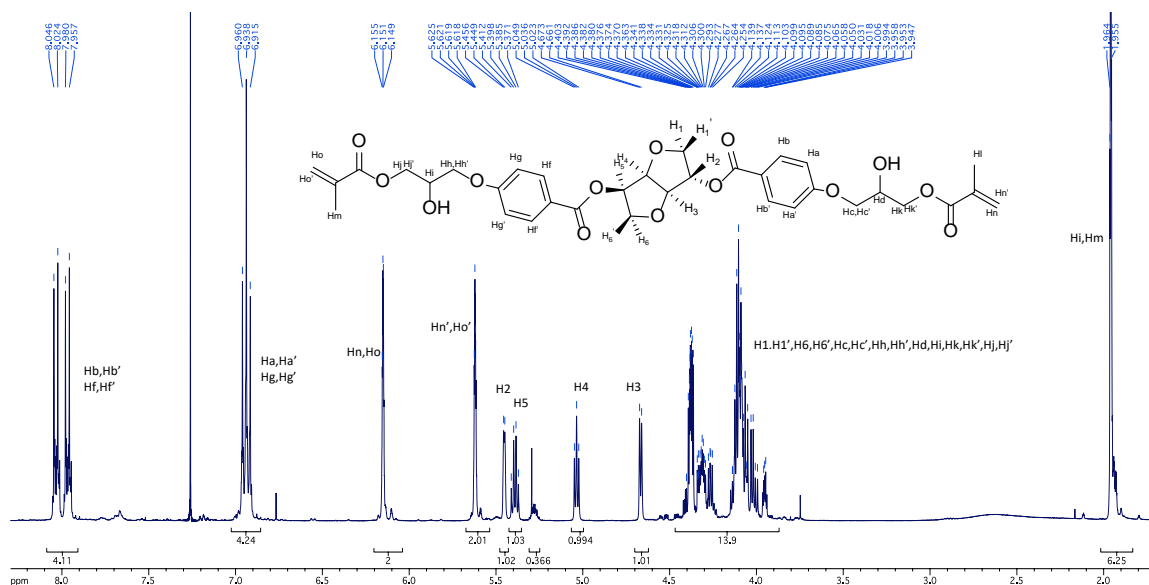


Figure 5.8 ^1H NMR spectrum of isosorbide 2,5-bis(4-glyceryloxybenzoate) dimethacrylate in CDCl_3 .

^1H -NMR (CDCl_3 , δ -ppm): 8.03-7.93 (2d, $J = 8.98, 8.99$ Hz, 4H-Hb,Hb',Hf,Hf'), 6.98-6.90 (m, 4H-Ha,Ha',Hg,Hg'), 6.15-6.10 (m, 2H-Hn,Ho), 5.63-6.62 (m, 2H-Hn',Ho'), 5.45 (d, $J = 2.7$ Hz, 1H-H2), 5.39 (q, $J = 5.4$ Hz, 1H-H5), 5.04 (t, $J = 5.1$ Hz, 1H-H4), 4.67 (d, $J = 4.7$ Hz, 1H-H3), 4.40-3.95 (m, 14H - H1,H1',H6,H6',Hc,Hc',Hh,Hh',Hd,Hi,Hk,Hk',Hj,Hj'), 1.96 (m, 6H-Hi,Hm).

5.1.3 NMR Analysis of ISB3GBMA and Reaction Intermediates

The ^1H NMR spectrum of isosorbide 2,5-bis(3-allyloxybenzoate) is depicted in **Figure 5.9**.

The integration ratio of the isosorbide cyclic protons, H3 and H4, to the allyl methine protons Hi/Hd is (1:1:2), and this corresponds to the desired structure.

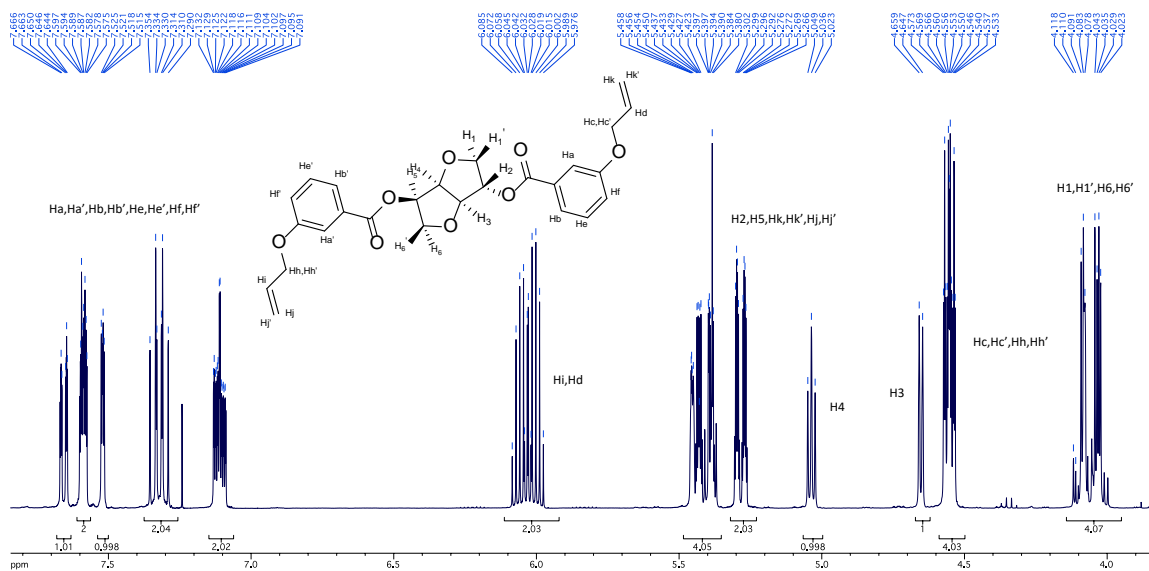


Figure 5.9 ^1H NMR spectrum of isosorbide 2,5-bis(3-allyloxybenzoate) in CDCl_3 . ^1H -NMR (CDCl_3 , δ -ppm): [7.67-7.64 (dt, $J = 7.68, 1.26$ Hz, 1H), 7.59 (m, 2H), 7.52 (dd, $J = 2.6, 1.5$ Hz, 1H), 7.32 (2t, $J = 8.01, 8.01$ Hz, 2H), and 7.11 (m, 2H) - $\text{Ha,Ha}',\text{Hb,Hb}',\text{He,He}',\text{Hf,Hf}'$], 6.03 (m, 2H- Hi,Hd), [5.46-5.38 (m, 4H) and 5.28 (m, 2H) - $\text{H2,H5,Hk,Hk}',\text{Hj,Hj}'$], 5.04 (t, $J = 5.1$ Hz, 1H- H4), 4.65 (d, $J = 4.8$ Hz, 1H- H3), 4.58-4.53 (m, 4H- $\text{Hc,Hc}',\text{Hh,Hh}'$), 4.12-4.02 (m, 4H - $\text{H1,H1}',\text{H6,H6}'$).

The ^1H NMR spectrum of isosorbide 2,5-bis(3-glycidyloxybenzoate) is shown in **Figure 5.10**. The integration ratios of the isosorbide protons, H3 to H4 and H2 to H5 are both 1:1, which indicates that the isosorbide is doubly substituted. The integration ratio of the isosorbide protons to the epoxide protons Hd/Hi , Hk/Hj , and Hk'/Hj' is (1:1:2:2:2) and this confirms that the epoxidation is complete at both ends of the isosorbide core.

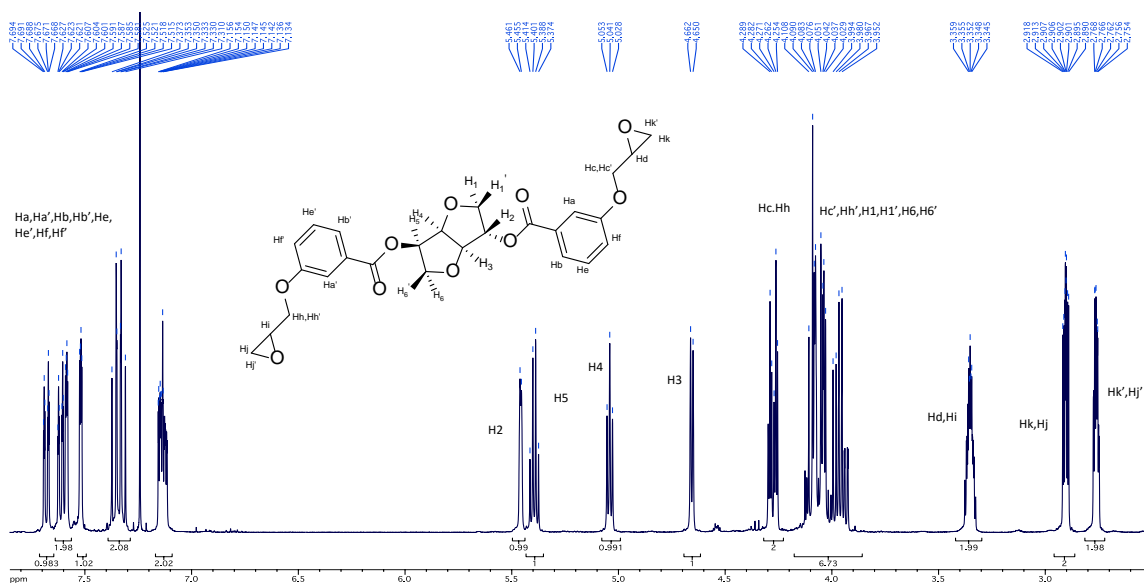


Figure 5.10 ^1H NMR spectrum of isosorbide 2,5-bis(3-glycidyloxybenzoate) in CDCl_3 . ^1H -NMR (CDCl_3 , δ -ppm): [7.68 (dt, $J = 7.7, 1.2$ Hz, 1H), 7.63-7.58 (m, 2H), 7.52 (dd, $J = 2.6, 1.5$ Hz, 1H), 7.37-7.31 (m, 2H), 7.16-7.11 (m, 2H), Ha,Ha',Hb,Hb',He,He',Hf,Hf'], 5.46 (d, $J = 2.6$ Hz, 1H - H2), 5.39 (q, $J = 5.3$ Hz, 1H-H5), 5.04 (t, $J = 5.1$ Hz, 1H-H4), 4.66 (d, $J = 4.7$ Hz, 1H - H3), 4.29-4.25 (m, 2H - Hc,Hh), 4.11-3.95 (m, 7H - [6H - Hc',Hh',H1,H1',H6,H6']), 3.35 (m, 2H - Hd,Hi), 2.90 (m, 2H - Hk,Hj), 2.76 (m, 2H - Hk',Hj').

A higher than expected proton area integration in the region of 4.11-3.95 (1H) is believed to be attributed to the remnants of ethyl acetate. This was confirmed from the singlet proton signal of the acetate methyl group at 2.02 ppm, and the triplet proton signal of the CH_3 moiety of the ethyl group at 1.23 ppm, where both signals integrated for 1.5 (not shown).

Figure 5.11 shows the disappearance of the epoxide protons and the formation of the methacrylate functionality at 5.6/6.1 ppm. The integration ratios of the isosorbide protons, H3 to H4 and H2 to H5, are both 1:1, indicating dual substitution. The integration ratio of the isosorbide cyclic protons to the vinyl and methyl protons of the methacrylate is 1:1:2:2:6 (H3:H4:Hn,o':Hn',o':Hi,m), which indicates complete dimethacrylation. The methine signal present at 5.3 ppm suggests the presence of Iso-ISB3GBMA.

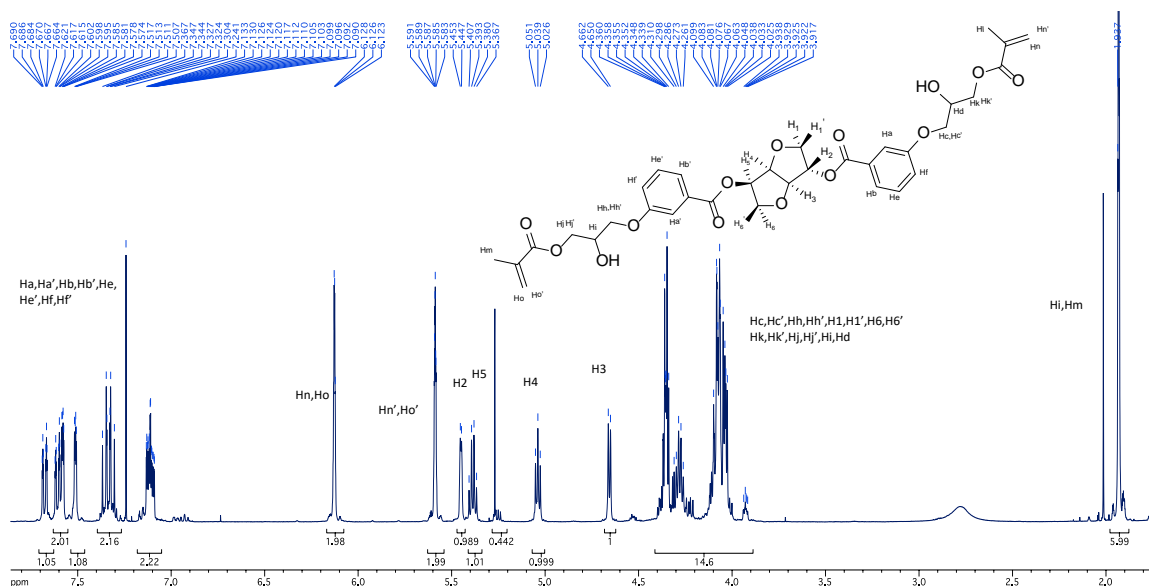


Figure 5.11 ^1H NMR spectrum of isororbide 2,5-bis(3-glyceryloxymethacrylate) in CDCl_3 .

^1H -NMR (CDCl_3 , δ -ppm): [7.67 (dt, $J = 7.71$, 1.20 Hz, 1H), 7.62-7.57 (m, 2H), 7.51 (dd, $J = 2.56$, 1.50 Hz, 1H), 7.33 (m, 2H), 7.11 (m, 2H), Ha,Ha',Hb,Hb',He,He',Hf,Hf'], 6.16-6.10 (m, 2H – Hn,Ho), 5.62-5.58 (m, 2H – Hn',Ho'), 5.45 (d, $J = 2.6$ Hz, 1H – H2), 5.39 (q, $J = 5.3$ Hz, 1H – H5), 5.04 (dd, $J = 6.27$, 3.97 Hz, 1H – H4), 4.66 (d, $J = 4.7$ Hz, 1H – H3), 4.40-3.92 (m, 15H – [14H – H1,H1',H6,H6',Hc,Hc',Hh,Hh',Hd,Hi,Hk,Hk',Hj,Hj'], 1.97-1.9 (m, 6H – Hl,Hm, 2- CH_3).

A higher than expected proton integration in the region of 4.40-3.92 (1H) is believed to be attributed to the remnants of ethyl acetate. This was confirmed from the singlet proton signal of the acetate methyl group at 2.01 ppm, and the triplet proton signal of the CH_3 moiety of the ethyl group at 1.23 ppm, where both signals integrated for 1.5 (not shown).

5.1.4 NMR Analysis of ISB2GBMA and Reaction Intermediates

The ^1H NMR spectrum of isororbide 2,5-bis(2-allyloxybenzoate) is depicted in **Figure 5.12**. The integration ratio of H3/H4 to the allyl methines Hd/Hi is (1:0.97:2), which is close to the expected (1:1:2), and this confirms the formation of the desired structure.

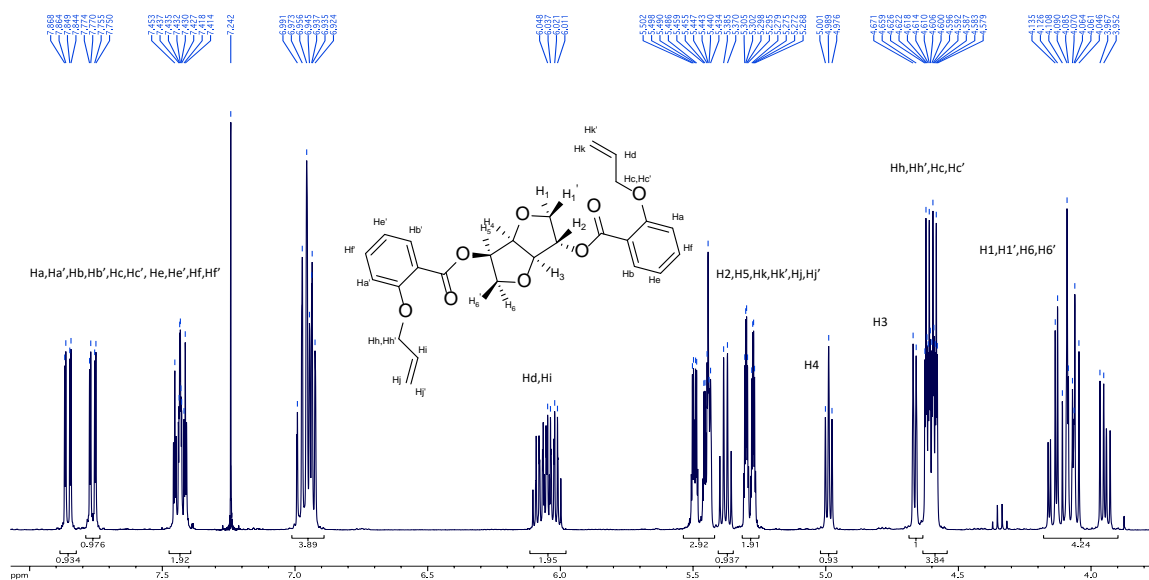


Figure 5.12 ^1H NMR spectrum of isorborne 2,5-bis(2-allyloxybenzoate) in CDCl_3 . ^1H -NMR (CDCl_3 , δ -ppm): [7.86 (dd, $J = 7.74$, 1.82 Hz, 1H), 7.76 (dd, $J = 7.7$, 1.8 Hz, 1H), 7.45-7.41 (m, 2H), 6.99-6.92 (m, 4H), Ha,Ha',Hb,Hb',He,He',Hf,Hf'], 6.10-6.0 (m, 2H – Hi,Hd), [5.50-5.43 (m, 3H), 5.38 (q, $J = 5.7$ Hz, 1H), 5.29 (ddq, $J = 10.57$, 2.82, 1.42 Hz, 2H), H2,H5,Hk,Hk',Hh,Hh'], 4.99 (t, $J = 5.0$ Hz, 1H – H4), 4.66 (d, $J = 4.6$ Hz, 1H – H3), 4.60 (ddt, $J = 10.5$, 5.0, 1.6 Hz, 4H – Hc,Hc,Hi,Hi), 4.14-3.95 (m, 4H – H1,H1',H6,H6').

Figure 5.13 displays the ^1H NMR spectrum of isorborne 2,5-bis(2-glycidyloxybenzoate) where the integration ratio of the epoxide protons to the H3/H4 isorborne protons is (3.8:1.9:1.0:0.99); while this ratio is slightly lower than the theoretical ratio (4:2:1:1), this still confirms the epoxide structure at both ends of the isorborne core.

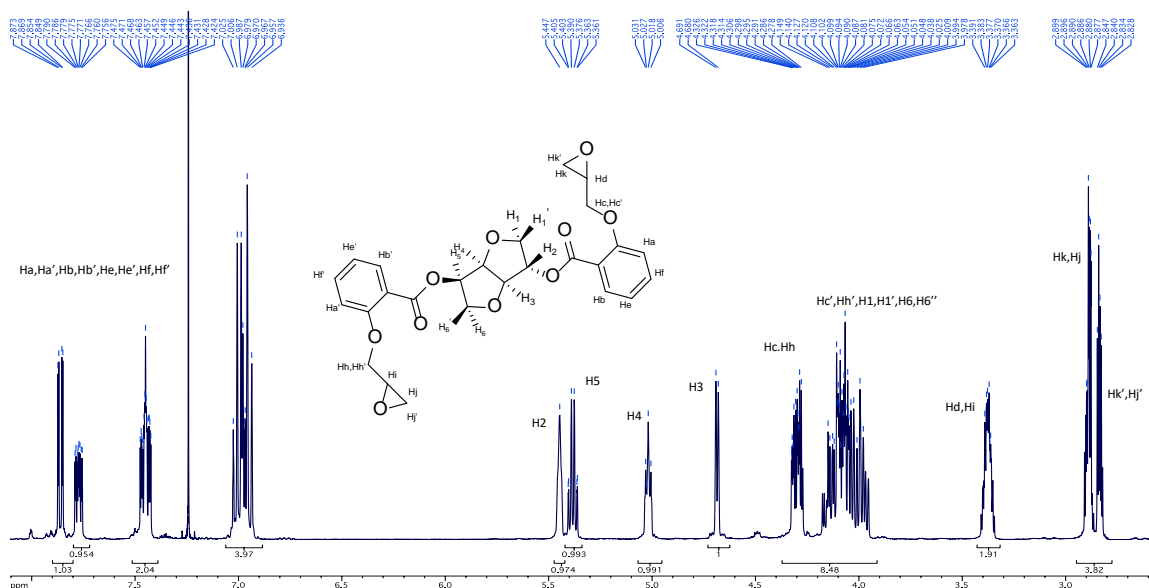


Figure 5.13 ^1H NMR spectrum of isosorbide 2,5-bis(2-glycidyoxybenzoate) in CDCl_3 . ^1H -NMR (CDCl_3 , δ -ppm): [7.86 (dd, $J = 7.7, 1.8$ Hz, 1H), 7.77 (m, 1H), 7.48-7.42 (m, 2H), 7.03-6.94 (m, 4H), $\text{Ha,Ha',Hb,Hb',He,He',Hf,Hf'}$], 5.45-5.42 (m, 1H – H2), 5.41-5.36 (m, 1H – H5), 5.03-5.01 (m, 1H – H4), 4.69 (d, $J = 4.6$ Hz, 1H – H3), 4.33-3.98 (m, 8H – $\text{Hc,Hc',Hh,Hh',H1,H1',H6,H6'}$), 3.93-3.36 (m, 2H – Hd,Hi), 2.90-2.83 (m, 4H – Hk,Hj,Hk',Hj').

The ^1H NMR spectrum of isosorbide 2,5-bis(2-glycidyoxybenzoate) dimethacrylate is displayed in **Figure 5.14**. The integration ratio of the isosorbide protons H3 to H4 is 1:0.94 and H2 to H5 is 0.95:1, suggesting that the molecule is largely disubstituted with up to 2.5 mole% monosubstituted. The integration ratio of H3/H4 to the methacrylate vinyl protons at 5.6/6.1 ppm is about (1:0.94:1.98:1.96) and it is close to the theoretical ratio (1:1:2:2). An excess in proton integration is observed in the region 3.8-4.4ppm, where the integration is 16 protons instead of 14. This excess can be attributed to the possibility of the presence of mono-substituted isosorbides and some trapped solvent (ethyl acetate). Further analysis by means of carbon NMR is necessary for further verification. The methine signal at 5.25 ppm is present as well, and it suggests the presence of Iso-ISB2GBMA.

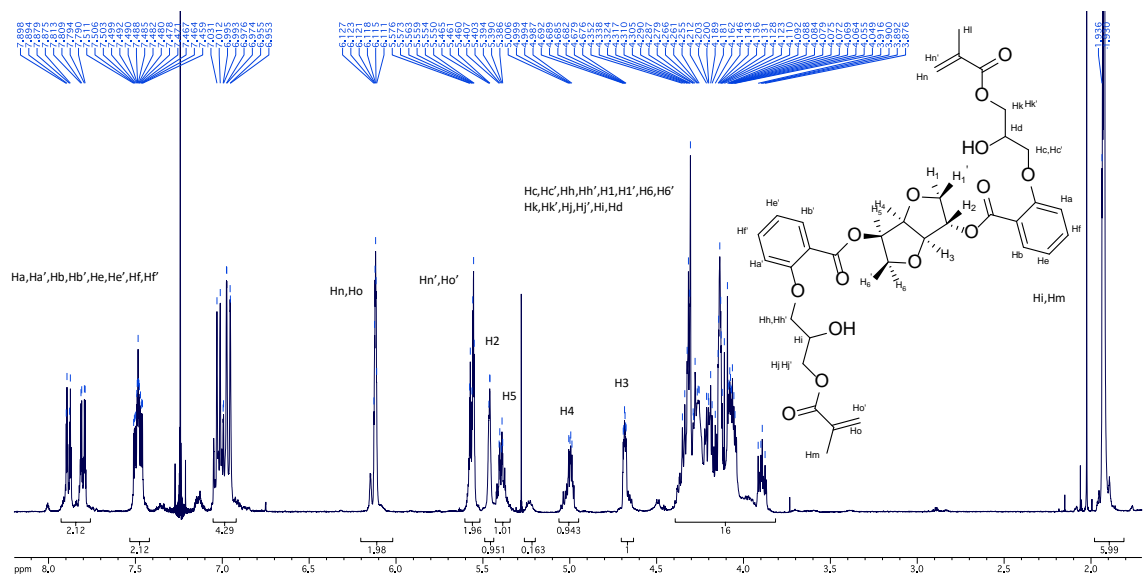


Figure 5.14 ^1H NMR spectrum of isosorbide 2,5-bis(2-glyceryloxybenzoate) dimethacrylate in CDCl_3 .

^1H -NMR (CDCl_3 , δ -ppm): [7.9-7.79 (m, 2H), 7.51-7.43 (m, 2H), 7.06-6.89 (m, 4H), $\text{Ha,Ha}',\text{Hb,Hb}',\text{He,He}',\text{Hf,Hf}'$], 6.16-6.08 (m, 2H – Hn,Ho), 5.60-5.52 (m, 2H – Hn',Ho'), 5.47-5.44 (m, 1H – H_2), 5.42-5.34 (m, 1H – H_5), 5.05-4.98 (m, 1H – H_4), 4.69-4.64 (m, 1H – H_3), 4.39-3.87 (m, 16H – [$\text{H}_1,\text{H}_1',\text{H}_6,\text{H}_6',\text{Hc,Hc}',\text{Hh,Hh}',\text{Hd,Hi,Hk,Hk}',\text{Hj,Hj}'$], 1.97-1.86 (m, 6H – Hl,Hm).

A higher than expected proton integration in the region of 4.35-3.88 (2H) is observed. The presence of residual ethyl acetate was confirmed from the singlet proton signal of the acetate methyl group at 2.01 ppm, and the triplet proton signal of the CH_3 moiety of the ethyl group at 1.23 ppm, where both signals integrate for 1.5 and account for 1H (not shown).

5.1.5 NMR Comparison of the Isosorbide Cyclic Protons H_3 and H_4

The splitting pattern and the shape of the H_3 and H_4 protons appear to differ between the various isosorbide dimethacrylates presented in this chapter. The shape is more defined in ISB4GBMA and ISB3GBMA, Figure 5.15, than in ISB2GBMA and ISDGBMA Figure 5.16.

The change in peak shape or splitting pattern occurs largely during the methacrylation step, which suggests that the proximity of the methacrylate protons to the isosorbide core, as in ISDGMA, or their isomeric position, as in ISB2GBMA, can affect the isosorbide core and induce a change of the dihedral angle between H3 and H4. Further spectroscopic evidence is needed to confirm this hypothesis.

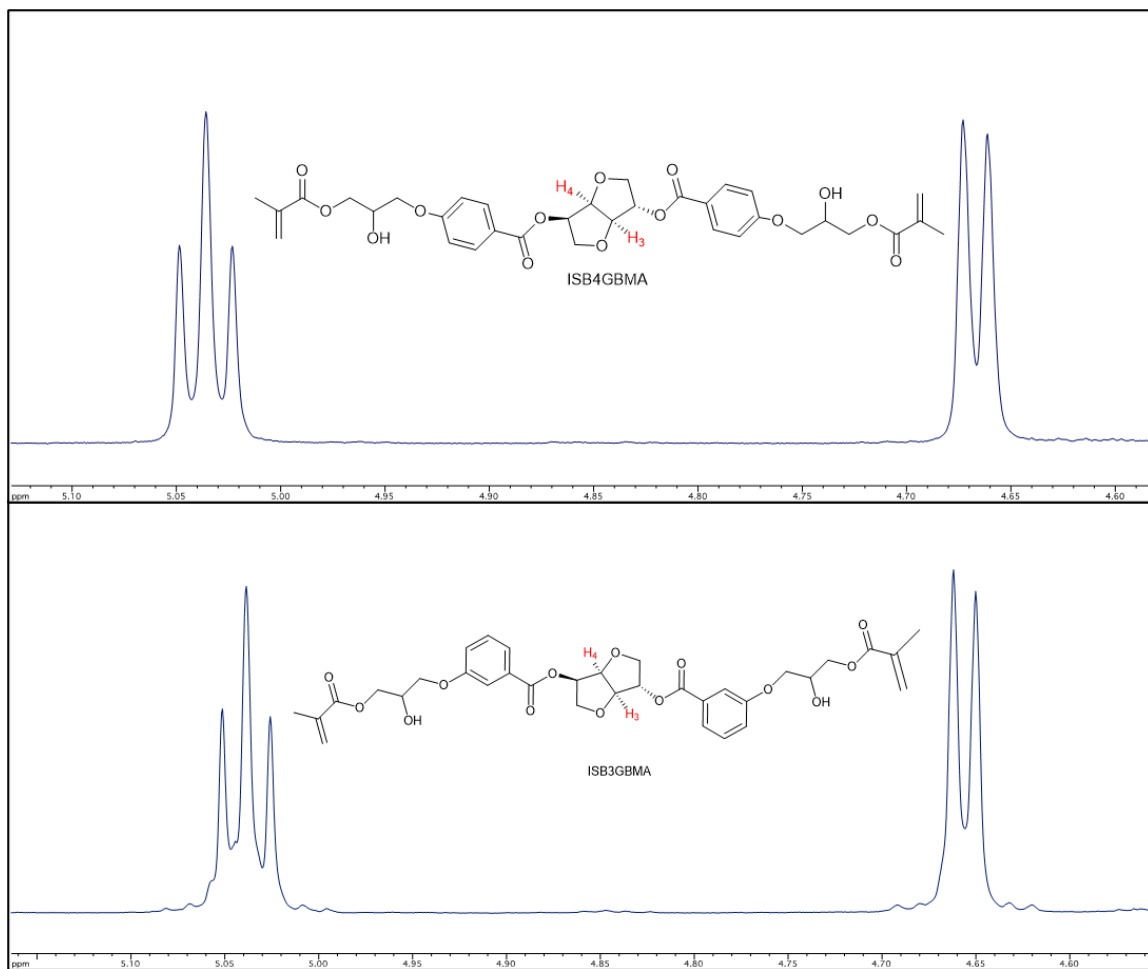


Figure 5.15 ¹H NMR peak shape comparison of H3/H4 as a result of methacrylation in ISB4GBMA and ISB3GBMA.

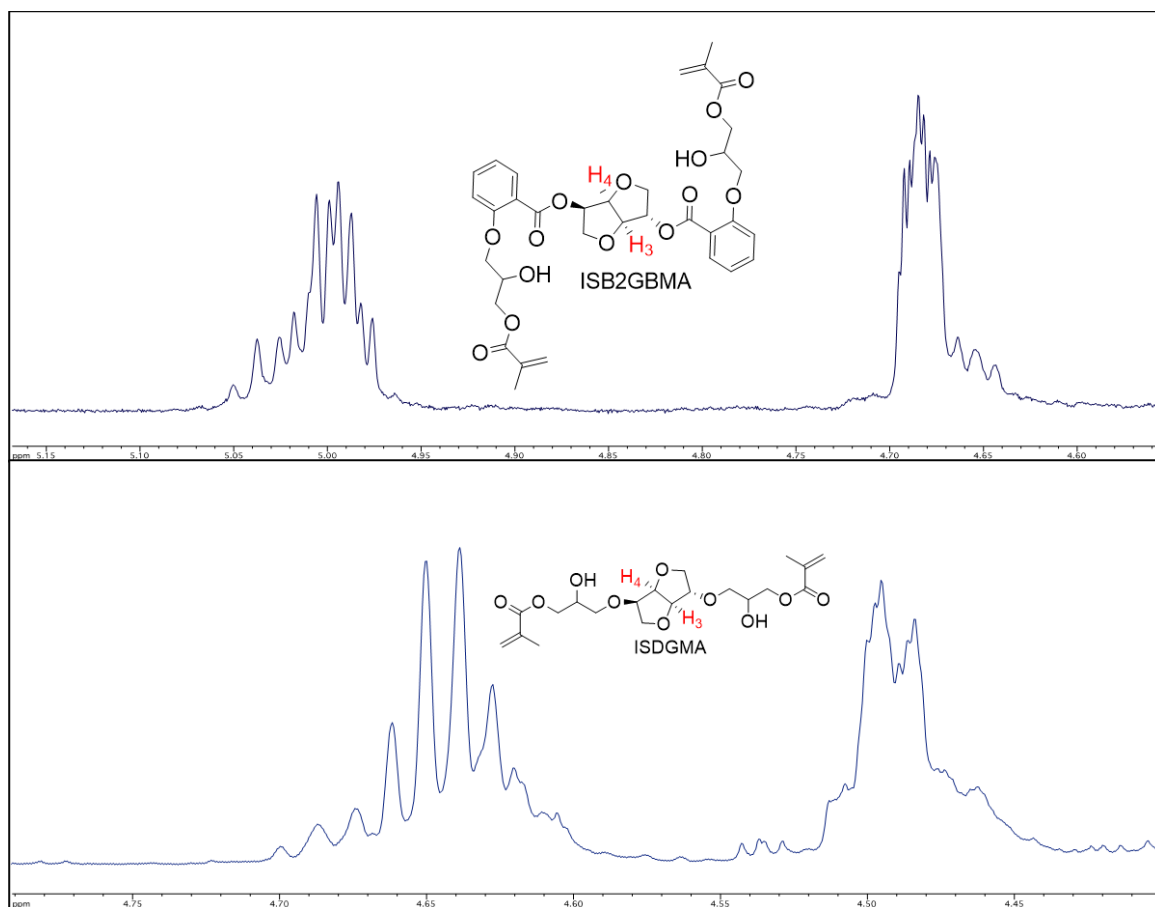


Figure 5.16 ¹H NMR peak shape comparison of H3/H4 as a result of methacrylation in ISB2GBMA and ISDGMA.

5.2 Hydrophobicity

The benzoate functionality in the *para*, *meta*, and *ortho* substituted isosorbide dimethacrylates was incorporated to improve the hydrophobicity of the resulting isosorbide monomers over the non-hydrophobically modified isosorbide dimethacrylate (ISDGMA). Therefore, contact angle measurements and cLogP estimations of ISBGBMA monomers, ISDGMA, and BisGMA were carried out to verify the hydrophobicity of each monomer, and the values are reported in **Table 5.2**.

Table 5.2 Contact Angle Measurements and cLogP Estimations of BisGMA, ISB4GBMA, ISB3GBMA, ISB2GBMA, and ISDGMA

| Sample | Contact Angle (degrees °) | cLogP |
|-----------------------|-----------------------------------|-------|
| BisGMA ^a | 76.97 (2.84) ^[b,c,d,e] | 5.09 |
| ISB4GBMA ^b | 63.21 (4.08) ^[a,e] | 2.75 |
| ISB3GBMA ^c | 62.65 (1.33) ^[a,e] | 2.75 |
| ISB2GBMA ^d | 62.82 (1.74) ^[a,e] | 2.75 |
| ISDGMA ^e | 13.41 (1.76) ^[a,b,c,d] | -0.53 |

Note: Letters indicate statistically significant difference (P<0.05) based on group. Standard deviation in parenthesis.

Hydrophobic materials or surfaces are typically characterized with a water contact angle (θ) $> 90^\circ$, while hydrophilic materials have a contact angle (θ) $< 90^\circ$; therefore, the higher the contact angle, the more hydrophobic the material is [179,180]. The mean contact angle (θ) of ISBGBMA monomers at ($\sim 62.9^\circ$) is significantly higher than the contact angle of ISDGMA at 13.41° , which indicates that the new monomers are more hydrophobic than ISDGMA but less hydrophobic than BisGMA at 77° [181].

The partition coefficient is the ratio of the compound's solubility in two immiscible solvents. The logarithm of the octanol/water partition coefficient is typically used to assess hydrophobicity and various other biological properties of developmental drugs by pharmaceutical companies [182]. As the hydrophobicity of the molecule increases, the LogP value increases. Various computational methods to predict LogP were developed and verified against experimental data [183]. The cLogP estimations in this study also indicate that the ISBGBMA monomers (2.75) are more hydrophobic than ISDGMA (-0.53) but less hydrophobic than BisGMA (5.09) [182].

5.3 Viscosity

Monomer mixture viscosity is an important parameter that can affect other properties such as the degree of conversion and the amount of filler that can be incorporated into the composite. The size and shape of the monomer, its molecular weight, and its ability for inter- and intramolecular interactions have an impact on its viscosity [30]. It is typically preferred to have resin mixtures with lower viscosities as long as polymerization shrinkage and water sorption are kept to a minimum [36,66].

The viscosities of the monomeric mixtures are reported in **Figure 5.17**. The ISDGMA/TEGDMA mixture exhibited the least viscosity at 0.06 Pa·s, while the viscosity increased for the ISBGBMA/TEGDMA monomer mixtures in the order of *ortho* (0.63 Pa·s) < *meta* (1.26 Pa·s) < *para* (2.48 Pa·s). The viscosity of the reference BisGMA/TEGDMA mixture at 0.48 Pa·s was near to that of the *ortho* ISBGBMA/TEGDMA mixture.

The ISBGBMA monomers have a higher molecular weight (~671 g/mol) and are larger than ISDGMA (~430 g/mol) and BisGMA (~513 g/mol) and can cause more friction and increase the mixture's viscosity.

On the other hand, since all of the ISBGBMA monomers have the same molecular weight, the differences in their monomeric mixture viscosity is probably related to the conformation or the radius of gyration of the isosorbide monomer. ISB4GBMA is relatively planar while ISB2GBMA is sterically hindered; planar aromatic molecules are known to closely align in parallel, in what is referred to as π -stacking [184]. The steric hindrance and lower potential of ISB2GBMA for packing is believed to result in lower friction and lower viscosity for ISB2GBMA/TEGDMA.

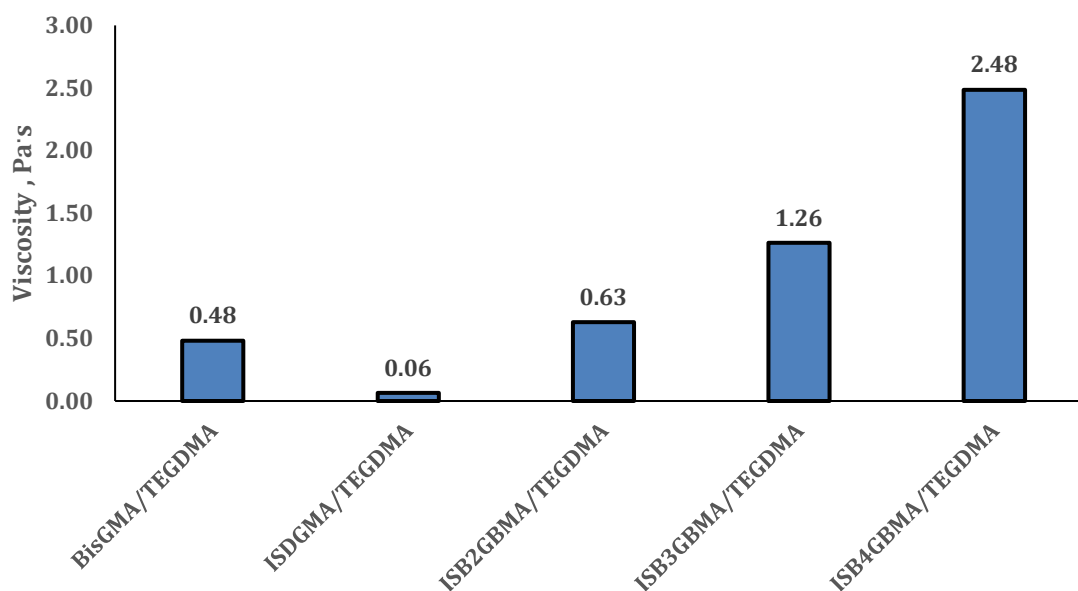


Figure 5.17 Viscosity of BisGMA/TEGDMA, ISDGMA/TEGDMA, ISB4GBMA/TEGDMA, ISB3GBMA/TEGDMA, and ISB2GBMA/TEGDMA monomer mixtures (60:40 wt%) at 25°C and 200 rpm.

5.4 Degree of Double Bond Conversion

The average degree of double bond conversion is reported in **Figure 5.18**. Poly(ISB2GBMA/TEGDMA) had a degree of conversion of 52% and was statistically different from poly(ISB4GBMA/TEGDMA) at 47% but statistically similar to the reference, poly(BisGMA/TEGDMA) at 54% and poly(ISB3GBMA/TEGDMA) at 51%. Poly(ISDGMA/TEGDMA) does not contain an aromatic ring to be used as an internal standard, and, as such, its degree of conversion was not calculated in this study. On the other hand, Łukaszczyk et al. reported the degree of conversion of poly(ISDGMA/TEGDMA) at 60:40 weight% to be slightly higher than that of poly(BisGMA/TEGDMA) by means of photo-DSC in their studies [163].

The higher degree of conversion of poly(ISB2GBMA/TEGDMA) and poly(ISB3GBMA/TEGDMA) at 52 and 51%, respectively, are attributed to the lower viscosity of their monomeric mixtures in comparison to the monomer viscosity of poly(ISB4GBMA/TEGDMA). As stated before, Sideridou et al. and Pfifer et al. demonstrated improving degree of conversion with improving monomer viscosity [31,34]. The addition of a diluent reduces viscosity and increases diffusion [54]. A degree of conversion less than 50% can indicate the presence of unreacted residual monomers which can leach and irritate the soft tissue [34].

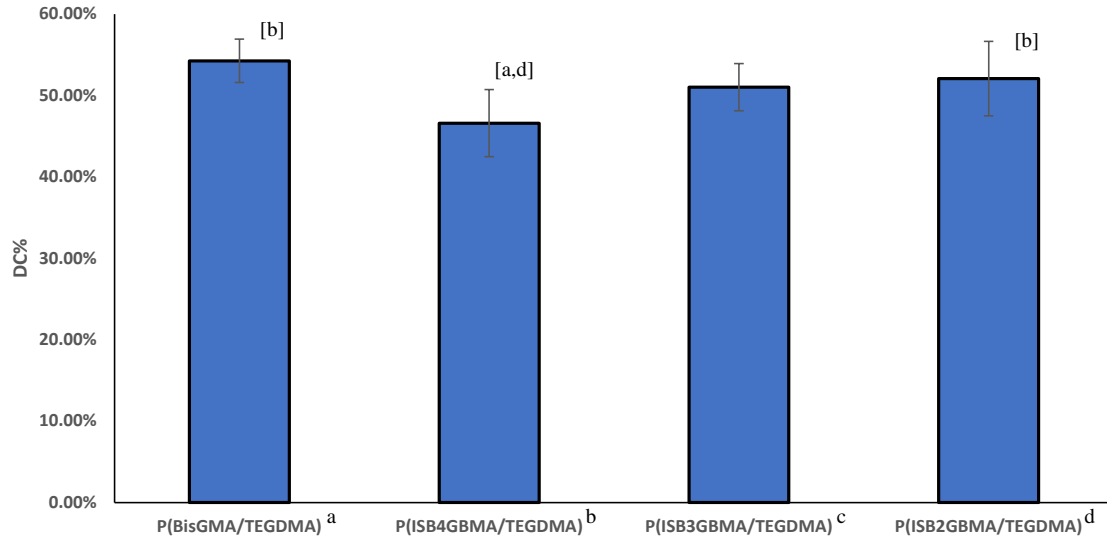


Figure 5.18 Degree of monomeric conversion of P(BisGMA/TEGDMA), P(ISB4GBMA/TEGDMA), P(ISB3GBMA/TEGDMA), P(ISB2GBMA/TEGDMA) at 60:40 wt%.

Note: Letters indicate statistically significant difference ($P < 0.05$) based on group.

Figure 5.19 shows the comparison of the degree of conversion between the top and bottom layer for every sample series. The degree of conversion of the top layer was relatively higher for every sample. Depth of cure can be affected by the light output and uniformity, distance to the sample and transmittance through the sample [185].

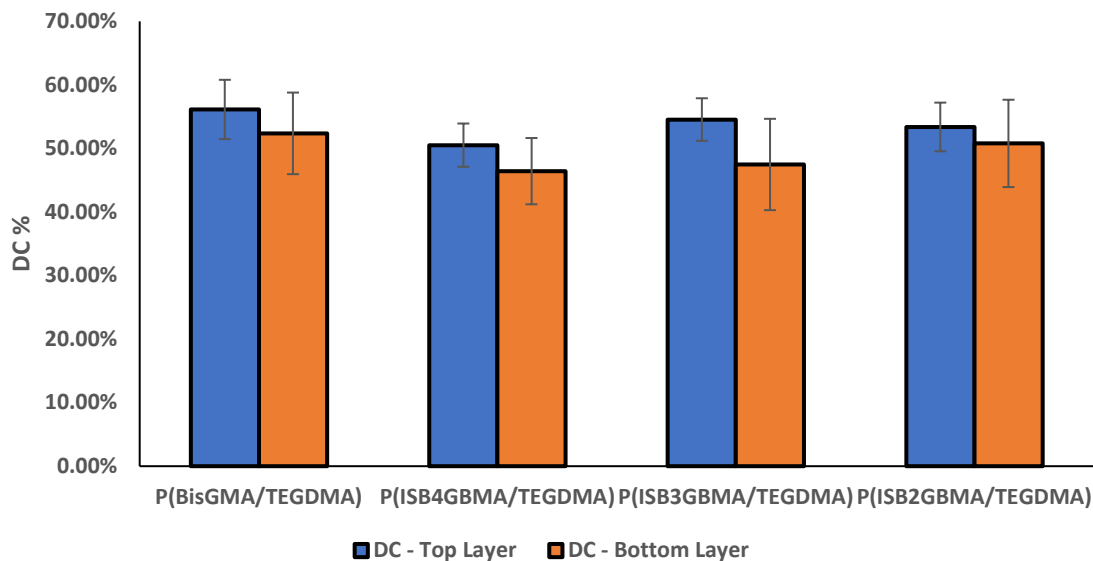


Figure 5.19 Comparison of the degree of conversion between top and bottom specimen layers.

5.5 Polymerization Shrinkage

The polymerization shrinkage of poly(ISB2GBMA/TEGDMA), poly(BISGMA/TEGDMA), and poly(ISDGMA/TEGDMA) was around 7% and was statistically higher than that of poly(ISB4GBMA/TEGDMA) at 4.5%, **Figure 5.20**.

The lower degree of conversion for the para ISBGBMA and its bulky nature is believed to result in lower shrinkage. This also correlates with the work of Pfifer et al., where higher degrees of conversion resulted in higher degrees of polymerization shrinkage in poly(BisGMA/TEGDMA) [31].

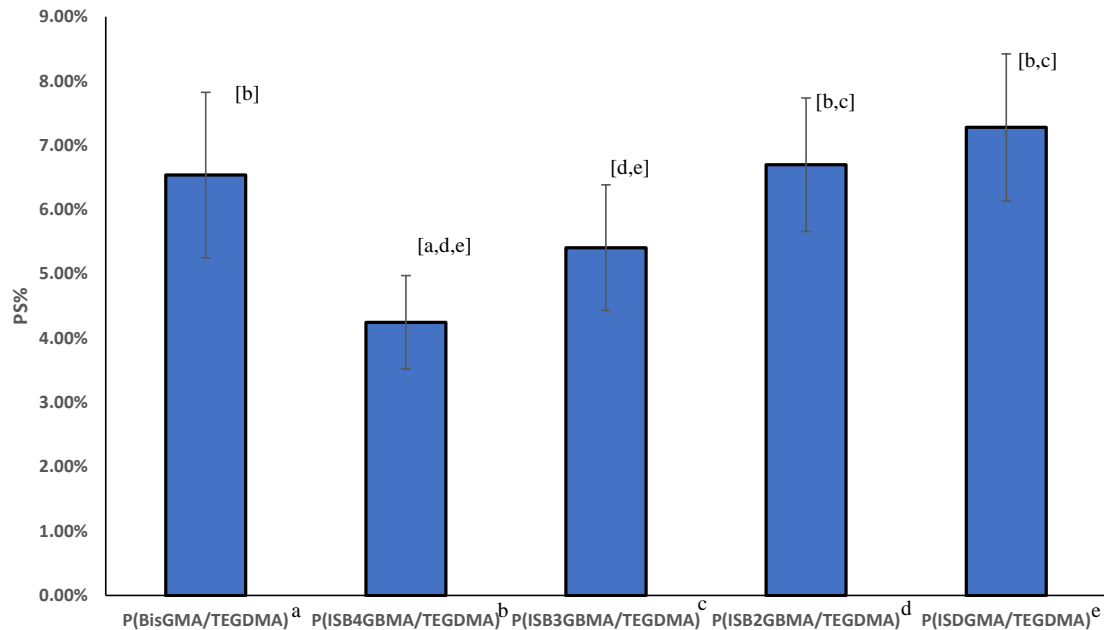


Figure 5.20 Polymerization shrinkage for P(BisGMA/TEGDMA), P(ISB4GBMA/TEGDMA), P(ISB3GBMA/TEGDMA), P(ISB2GBMA/TEGDMA), and P(ISDGMA/TEGDMA) at 60:40 wt%.

Note: Letters indicate statistically significant difference ($P < 0.05$) based on group.

5.6 Glass Transition Temperature

Glass transition temperatures were determined from the maxima of tan delta curves through a 3-point bending test, **Figure 5.21**, and the values are displayed in **Table 5.3**. For the materials to be clinically viable, the glass transition temperature must exceed cure temperature and temperature ranges in the oral cavity [30].

The glass transition temperature of poly(ISB2GBMA/TEGDMA) was the highest among the poly(ISBGBMA/TEGDMA) series at 85°C. This is believed to be due to its higher degree of double-bond conversion and the presumed rigidity of the crosslinked network due to the *ortho* isomer's relative lack of internal rotational freedom.

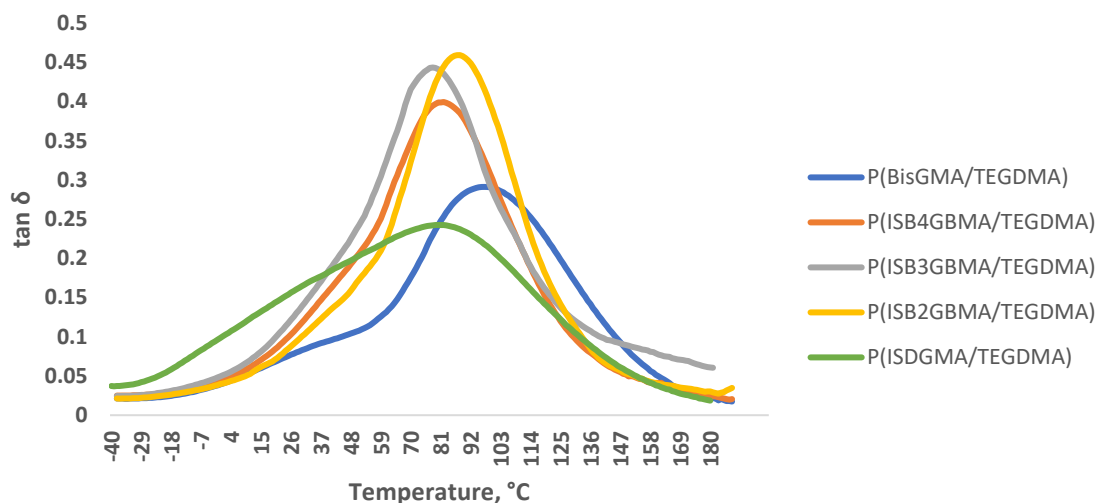


Figure 5.21 Tan delta curves for P(BisGMA/TEGDMA), P(ISB4GBMA/TEGDMA), P(ISB3GBMA/TEGDMA), P(ISB2GBMA/TEGDMA), and P(ISDGMA/TEGDMA) at 60:40 wt%.

Table 5.3 Glass Transition Temperature of P(BisGMA/TEGDMA), P(ISB4GBMA/TEGDMA), P(ISB3GBMA/TEGDMA), P(ISB2GBMA/TEGDMA), and P(ISDGMA/TEGDMA) at 60:40 wt%

| Sample | Glass Transition Temperature (°C) |
|---------------------------------|-----------------------------------|
| p(BisGMA/TEGDMA) ^a | 95.73 (3.73) ^[b,c,e] |
| p(ISB4GBMA/TEGDMA) ^b | 80.57 (0.46) ^[a] |
| p(ISB3GBMA/TEGDMA) ^c | 77.38 (3.86) ^[a] |
| p(ISB2GBMA/TEGDMA) ^d | 86.52 (1.18) |
| p(ISDGMA/TEGDMA) ^e | 85.56 (7.30) ^[a] |

Note: Letters indicate statistically significant difference ($P < 0.05$) based on group. Standard deviation in parenthesis.

The glass transition temperature of poly(BisGMA/TEGDMA) was the highest around 95°C. However, statistical analysis did not indicate it to be significantly different from the T_g of poly(ISB2GBMA/TEGDMA). This may be explained from the corresponding storage modulus, which is shown in **Figure 5.22**, where a near overlap is observed between the two samples. This suggests the corresponding crosslinked networks

to be structurally similar. The storage modulus is also the highest for these two samples as well.

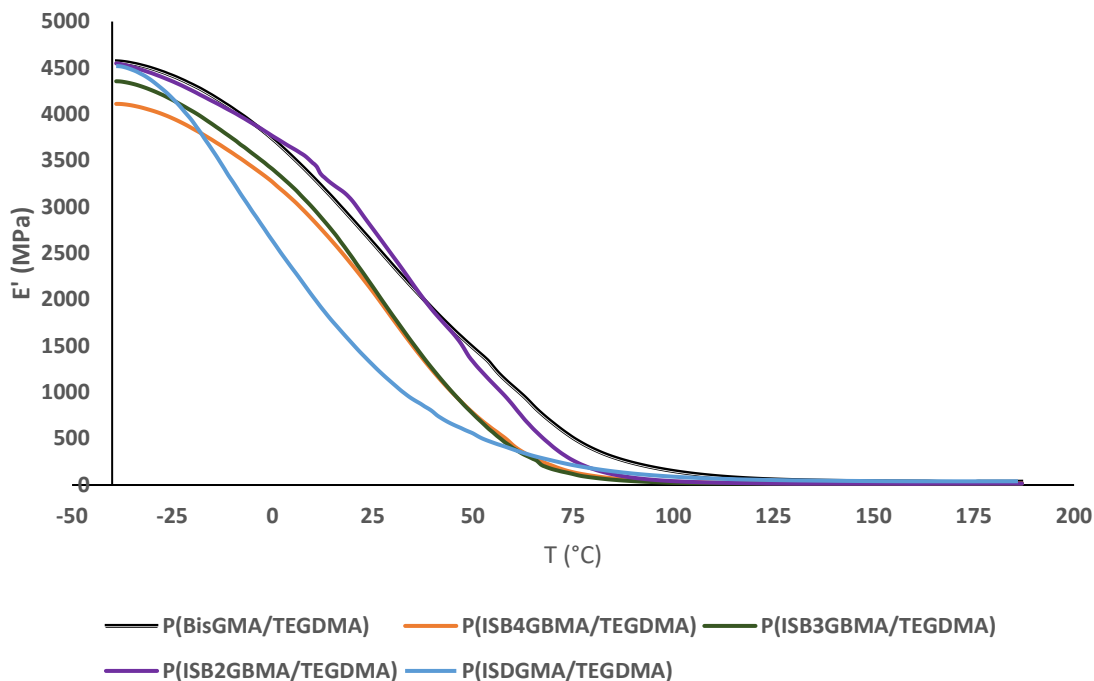


Figure 5.22 Storage modulus as a function of temperature for P(BisGMA/TEGDMA), P(ISB4GBMA/TEGDMA), P(ISB3GBMA/TEGDMA), P(ISB2GBMA/TEGDMA), and P(ISDGMA/TEGDMA).

The glass transition temperature of poly(ISDGMA/TEGDMA) at 85 $^{\circ}\text{C}$ was statistically significant only for the T_g of poly(BisGMA/TEGDMA). Its corresponding modulus was the lowest and might be attributed to the structural flexibility of ISDGMA. However, in the work of Łukaszczyk et al., the T_g of poly(ISDGMA/TEGDMA) and poly(BisGMA/TEGDMA) were reported to be comparable, and it was attributed to similar degrees of conversion between the two polymers. Different curing and T_g characterization methods were used in that study [163].

Higher glass transition temperatures are expected to be achieved with an improved degree of monomeric conversion for the ortho sample, in accordance with the work done by Sideridou et al. and Stansbury et al., where improved glass transition temperatures were obtained by improving the degree of conversion [30,34].

5.7 Water Sorption

The water sorption of poly(ISB2GBMA/TEGDMA) was the lowest among the ISBGBMA derived polymers at $39 \mu\text{g}/\text{mm}^3$ and was statistically different from the water sorption of poly(ISB4GBMA/TEGDMA) at $44 \mu\text{g}/\text{mm}^3$. However, poly(BisGMA/TEGDMA) had the lowest water sorption, overall, at $26 \mu\text{g}/\text{mm}^3$, and poly(ISDGMA/TEGDMA) had the highest at $73 \mu\text{g}/\text{mm}^3$, **Figure 5.23**.

When ISDGMA/TEGDMA samples were initially cured similar to other resin samples for water sorption, the results obtained were inconsistent. The curing method may not have produced an acceptable degree of conversion, leading to sample deterioration and dissolution. In order to overcome this, the curing conditions were optimized further by curing the samples longer. As a result, the water sorption of p(ISDGMA/TEGDMA) was consistent, and this is shown in the appendix, **Figure C.1**.

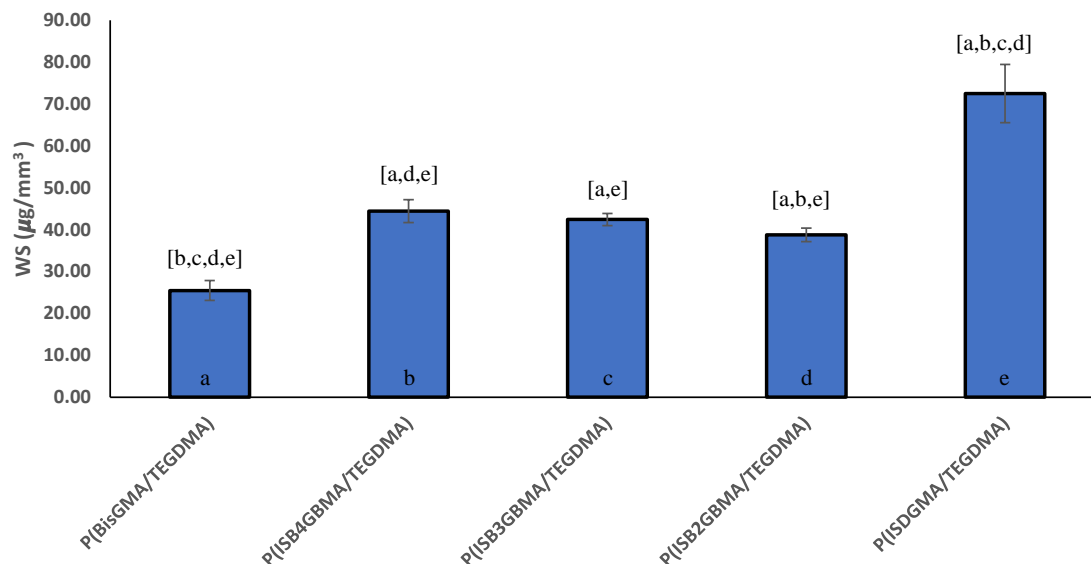


Figure 5.23 Water sorption of P(BisGMA/TEGDMA), P(ISB4GBMA/TEGDMA), P(ISB3GBMA/TEGDMA), P(ISB2GBMA/TEGDMA), and P(ISDGMA/TEGDMA) at 60:40 wt%.

Note: Letters indicate statistically significant difference ($P < 0.05$) based on group. Individual groups are represented by (a-e).

Hygroscopic expansion due to water sorption can weaken mechanical properties, increase wear rate, and reduce dimensional stability [117-119]. Polymer samples derived from the hydrophilic ISDGMA deteriorated and cracked as a result of water uptake after immersion in buffer solution. This behavior was also noted by Kim et al., where resins and resin-based composites of poly(ISDGMA) exhibited surface cracks after buffer storage [165].

On the other hand, the polymers derived from the ISBGBMA monomers did not show any signs of network deterioration or cracking and exhibited greater stability due to improved hydrophobicity and reduced water sorption, similar to the BisGMA reference, and this is shown in **Figure 5.24**.

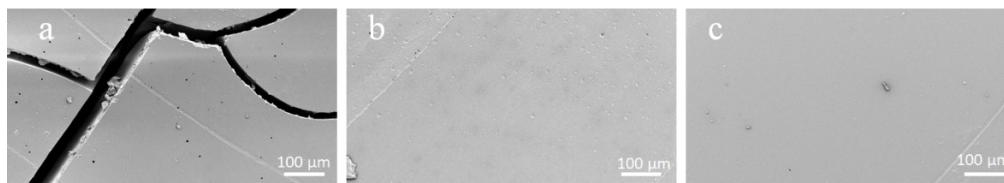
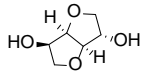
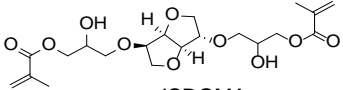
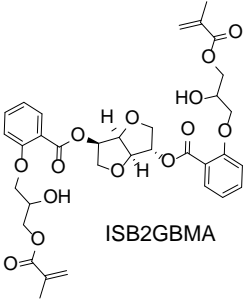
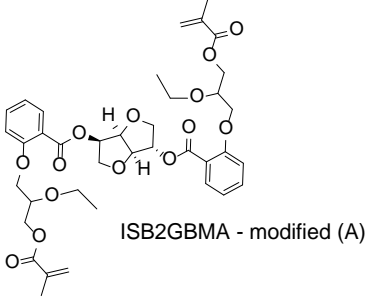
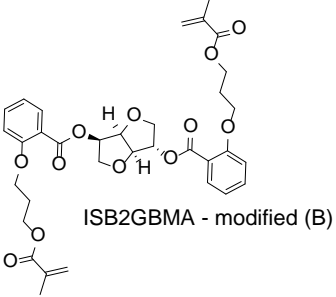
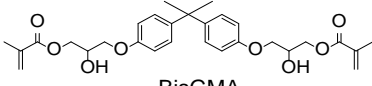


Figure 5.24 SEM images at 150X and 2.5 kV of a) P(ISDGMA/TEGDMA), b) P(ISB2GBMA/TEGDMA), and c) P(BisGMA/TEGDMA) after buffer immersion for 7 days at 37°C.

Note: ISB2GBMA is only shown as an example of the ISBGBMA series.

The improved hydrophobicity of the ISBGBMA series over ISDGMA helped lower the water sorption by about 40% and improved the overall network stability. However, the hydrophobicity of the ISBGBMA series was not enough for water sorption to match or be lower than the water sorption of poly(BisGMA/TEGDMA). The isosorbide core is hygroscopic with hydrophilicity similar to that of diethylene glycol [153,186]. Improving the hydrophobicity of the isosorbide dimethacrylate monomers, by means of eliminating or reacting the hydroxyl groups, as indicated by cLogP estimations in **Table 5.4**, is expected to lower the water sorption of the ISBGBMA series further.

Table 5.4 cLogP Values for Isosorbide, Isosorbide Derivatives and BisGMA

| Structure | clogP |
|--|-------|
|  <p data-bbox="574 407 672 432">Isosorbide</p> | -1.67 |
|  <p data-bbox="558 567 649 592">ISDGMA</p> | -0.53 |
|  <p data-bbox="552 856 669 882">ISB2GBMA</p> | 2.75 |
|  <p data-bbox="506 1201 753 1226">ISB2GBMA - modified (A)</p> | 4.15 |
|  <p data-bbox="487 1537 740 1562">ISB2GBMA - modified (B)</p> | 4.04 |
|  <p data-bbox="542 1747 626 1772">BisGMA</p> | 5.09 |

5.5 Flexural Strength and Modulus

Dental restorative materials should have sufficient mechanical integrity to function properly. It is generally recognized that the higher the mechanical strength, the better is the performance [187].

Flexural strength analysis for dried and buffer-immersed samples is shown in **Figure 5.25**. Flexural strength decreased for all samples once immersed in PBS for 24 hours. Poly(ISDGMA/TEGDMA) had the highest decrease in flexural strength (80%), where signs of sample cracking and degradation were observed. All other samples had a comparable 50% loss.

The flexural strength of poly(BisGMA/TEGDMA) was statistically different only from that of poly(ISDGMA/TEGDMA) in both dried and immersed states. The flexural strength of poly(ISDGMA/TEGDMA) was statistically different from that of all other samples in the immersed state.

Yiu et al. investigated the tensile strength of unfilled dental resins as a result of water storage. Hydrophilic materials had the lowest tensile strength, where water sorption was highest and water acted as a plasticizer [188]. Similarly, the improved hydrophobicity of the ISBGBMA monomers over ISDGMA and increased rigidity due the presence of the aromatic rings is believed to improve the flexural strength by reducing the water uptake of the sample.

Table 5.5 shows the water uptake with respect to mass after 24 hours of sample storage. The hydrophilic poly(ISDGMA/TEGDMA) had the highest water uptake and lowest flexural strength. Since the storage time was only 24 hours, it is unclear if saturation was obtained and caused such significant decrease in flexural strength. Therefore, longer

storage times are needed to verify this concept further. Similarly, Kim et al. reported a decrease in flexural strength in resins and resin-based composites of poly(BisGMA/TEGDMA) and poly(ISDGMA) after PBS buffer storage for 7 days at 37°C [165].

The lower flexural strength for poly(ISBGBMA/TEGDMA) series, in comparison to that of poly(BisGMA/TEGDMA), is due to the lower degree of conversion and corresponding lower cross-link density, where the concentration of double bonds is 4.59 mol/Kg for ISBGBMA/TEGDMA and 5.13 mol/Kg for BisGMA/TEGDMA. This is in accordance with the work reported by Gajewski et al., where higher monomeric conversion and crosslink density led to improved flexural strength [97].

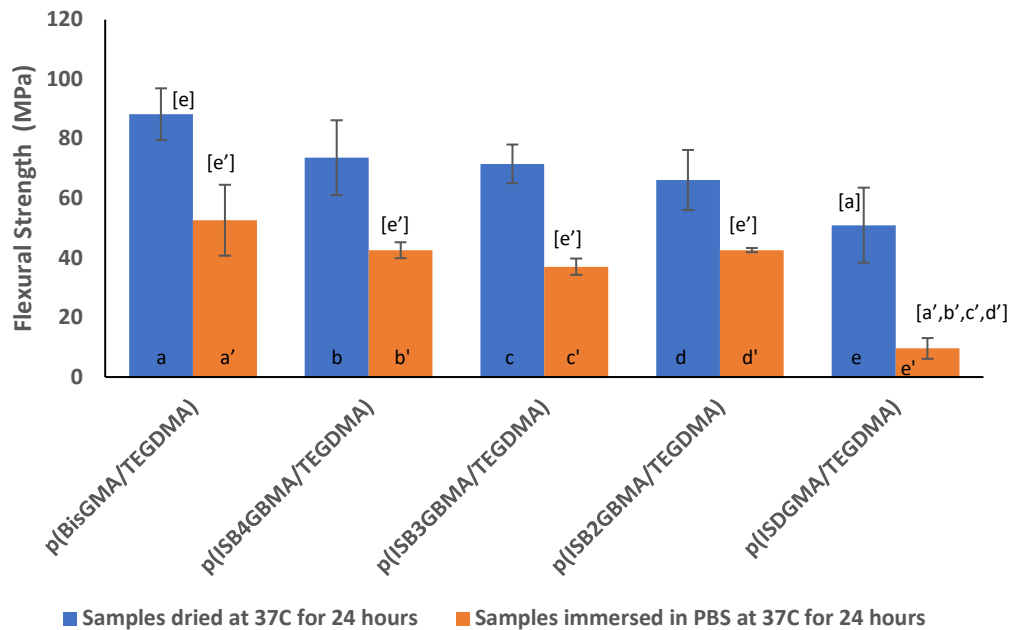


Figure 5.25 Flexural strength analysis of P(BisGMA/TEGDMA), P(ISB4GBMA/TEGDMA), P(ISB3GBMA/TEGDMA), P(ISB2GBMA/TEGDMA), and P(ISDGMA/TEGDMA) at 60:40 wt% at RT.

Note: Letters indicate statistically significant difference ($P < 0.05$) based on group. Individual groups are represented by (a-e).

Table 5.5 Water Uptake After 24 Hours and at 37°C for P(BisGMA/TEGDMA), P(ISB4GBMA/TEGDMA), P(ISB3GBMA/TEGDMA), P(ISB2GBMA/TEGDMA) and P(ISDGMA/TEGDMA)

| Test | p(BisGMA /TEGDMA) | p(ISB4GBMA /TEGDMA) | p(ISB3GBMA /TEGDMA) | p(ISB2GBMA /TEGDMA) | p(ISDGMA /TEGDMA) |
|------|-------------------|---------------------|---------------------|---------------------|-------------------|
| WU% | 0.91% (0.05) | 1.48% (0.09) | 1.35% (0.13) | 1.19% (0.06) | 4.20% (0.17) |

Note: WU%: water uptake percentage. Standard deviation in parenthesis.

The flexural modulus of dried and immersed samples is presented in **Figure 5.26**. poly(BisGMA/TEGDMA) and poly(ISB4GBM/TEGDMA) exhibited the highest modulus in the dried state while all samples had lower modulus once immersed in PBS for 24 hours. In the work of Ito et al., the modulus of elasticity was lower for samples with higher water sorption. The more hydrophilic the material, the higher is the water sorption, and the lower is the modulus of elasticity [188]. The flexural modulus of poly(ISDGMA/TEGDMA) was statistically different from that of all other samples in the immersed state, but all samples were statistically similar in the dried state.

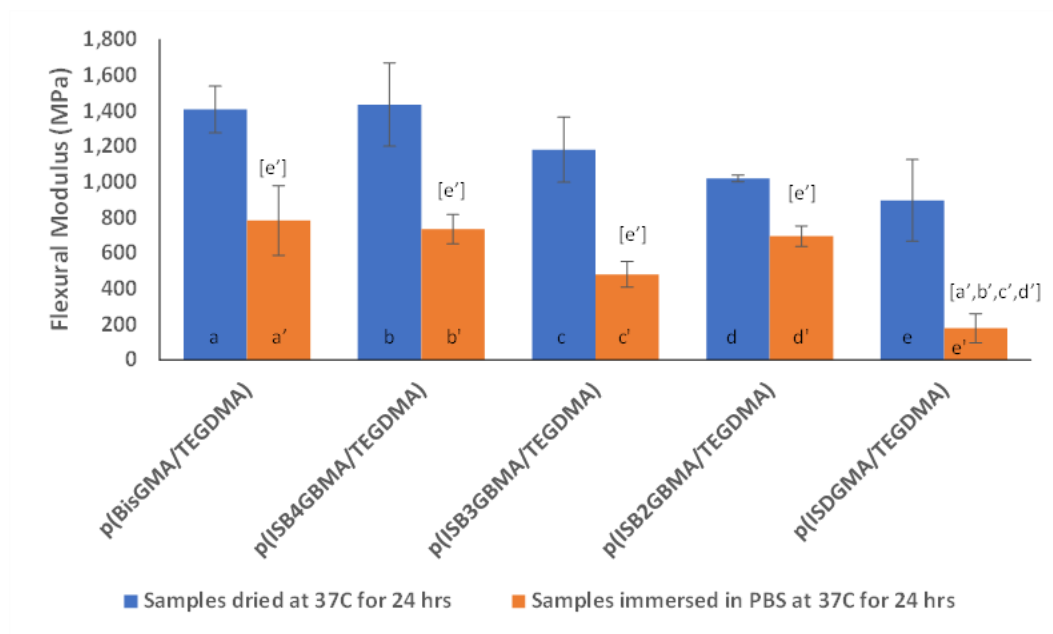


Figure 5.26 Flexural modulus of P(BisGMA/TEGDMA), P(ISB4GBMA/TEGDMA), P(ISB3GBMA/TEGDMA), P(ISB2GBMA/TEGDMA), and P(ISDGMA/TEGDMA) at 60:40 wt% at RT.

Note: Letters indicate statistically significant difference ($P < 0.05$) based on group. Individual groups are represented by (a-e).

CHAPTER 6

SUMMARY AND FUTURE WORK

6.1 Summary

There is a constantly growing need for bio-derived materials in all aspects of our daily lives including dentistry. Therefore, the objective of this dissertation was to identify and evaluate bio-based, BPA-free, dental resin methacrylates with key performances similar to the industry standard, BisGMA. As such, three hydrophobically modified bio-based isosorbide isomers (ISBGBMA) were synthesized, characterized, and evaluated in the context of copolymers with TEGDMA as potential dental filling materials.

The new monomers were shown to be much more hydrophobic than the isosorbide BisGMA analogue, ISDGMA, but less hydrophobic than BisGMA, based on contact angle measurements and cLogP estimations. The ISBGBMA series had a contact angle measurement around 63° with a cLogP estimate of 2.75. On the other hand, ISDGMA had a contact angle measurement of only 13° and a cLogP estimate of -0.53. The contact angle and cLogP estimate of BisGMA were 77° and 5.09, respectively.

The *ortho*, *meta*, and *para* substitution of the benzoate group resulted in different properties as well. In this series, the monomer mixture of the *ortho* substituted isomer, isosorbide 2,5-bis(2-glyceryloxybenzoate) dimethacrylate, along with the diluent TEGDMA exhibited the least viscosity at 0.62 Pa·s. This viscosity was similar to that of the reference BisGMA/TEGDMA monomer mixture at 0.48 Pa·s but higher than that of ISDGMA/TEGDA at 0.06 Pa·s. Lower viscosities are preferred for ease of handling and filler incorporation.

The corresponding copolymer of poly(ISB2GBMA/TEGDMA) had the highest monomeric degree of conversion among the ISBGBMA/TEGDMA polymer series at 52%, trailing that of poly(BisGMA/TEGDMA) at 54%. Monomeric degree of conversion near 55% and higher is needed to minimize the effect of unreacted residual monomers.

The polymer derived from ISB2GBMA and TEGDMA had the highest polymerization shrinkage, near 7%, similar to that of poly(BisGMA/TEGDMA) and poly(ISDGMA/TEGDMA). Lower polymerization shrinkage rates are needed to prevent debonding, gap formation, and secondary caries.

The highest glass transition temperature among the ISBGBMA series was also that of poly(ISB2GBMA/TEGDMA) at 86°C, which was near that of poly(ISDGMA/TEGDMA) at 85°C but less than that of poly(BisGMA/TEGDMA) at 95°C. However, the storage moduli were nearly identical between the *ortho*-configured polymer, and the polymer derived from the reference BisGMA.

The water sorption of the polymers derived from the ISBGBMA series ranged from 39 to 44 $\mu\text{g}/\text{mm}^3$ with the *ortho* derived polymer having the lowest water sorption. The polymer derived from ISDGMA was the highest at 73 $\mu\text{g}/\text{mm}^3$ and the reference poly(BisGMA/TEGDMA) was the lowest at 26 $\mu\text{g}/\text{mm}^3$. The lower water sorption obtained with the new monomers over ISDGMA is due to the increased hydrophobicity of the ISBGBMA monomers. This improved hydrophobicity resulted in lower water sorption, and improved polymer stability in buffer solution, with no signs of deterioration or cracking, similar to the reference BisGMA derived polymer.

The flexural strength of the poly(ISBGBMA/TEGDMA) series ranged from 37 to 42 MPa and was superior to that of the 10 MPa for poly(ISDGMA/TEGDMA) but less

than that of poly(BisGMA/TEGDMA) at 52 MPa after buffer immersion. Similar to water sorption, the improved hydrophobicity and lower water uptake resulted in improved mechanical properties and polymer stability. The drop in flexural strength for buffer immersed samples was about 50% for the ISBGBMA derived polymers and the reference BisGMA derived polymer. However, the ISDGMA derived polymer had a near 80% drop in flexural strength. A similar trend was observed in the flexural modulus as well. Materials with high flexural strength and modulus are needed to withstand the various forces at play in the oral cavity.

Considered together, the data suggests the performance of the monomer mixture and polymer derived from the *ortho* ISBGBMA monomer was close to that of the reference BisGMA. Therefore, it is a potential bio-based, BPA-free replacement of BisGMA and should be the focus of future studies.

6.2 Future Work

Future work should take advantage of the available prediction methods and calculations. For example, cLogP estimations have shown that, by eliminating the hydroxyl groups, the predicted hydrophobicity of the material increases. Therefore, further synthesis should focus on a number of factors which include first eliminating or alkylating the hydroxyl groups of the *ortho* ISBGBMA monomer and, second, replacing the ester linkage with an ether linkage to improve hydrolytic stability.

Additionally, the polymerization efficiency can be improved by further investigating the light source, photo-initiator type, concentration, and curing method.

The water sorption analysis should be expanded and include daily water uptake for extended periods of time, for example up to 21 days. This will validate saturation levels and their impact on network stability. Similarly, while this dissertation has not addressed solubility levels, it should be included in any future studies as well since dental resins should not be soluble or have very limited solubility.

Methods for determining the degree of conversion ought to use the heat of polymerization through photo-differential scanning calorimetry for accurate evaluation. The mechanical properties should be expanded to include micro-hardness and compressive strength.

Finally, the materials need to be evaluated as resin-based composites through the incorporation of inorganic fillers. This is an important step to validate the real-world effectiveness of these materials.

APPENDIX A
PROTON NMR SPECTRA

Figures A.1 to A.2 depict proton NMR spectra of isosorbide and BisGMA.

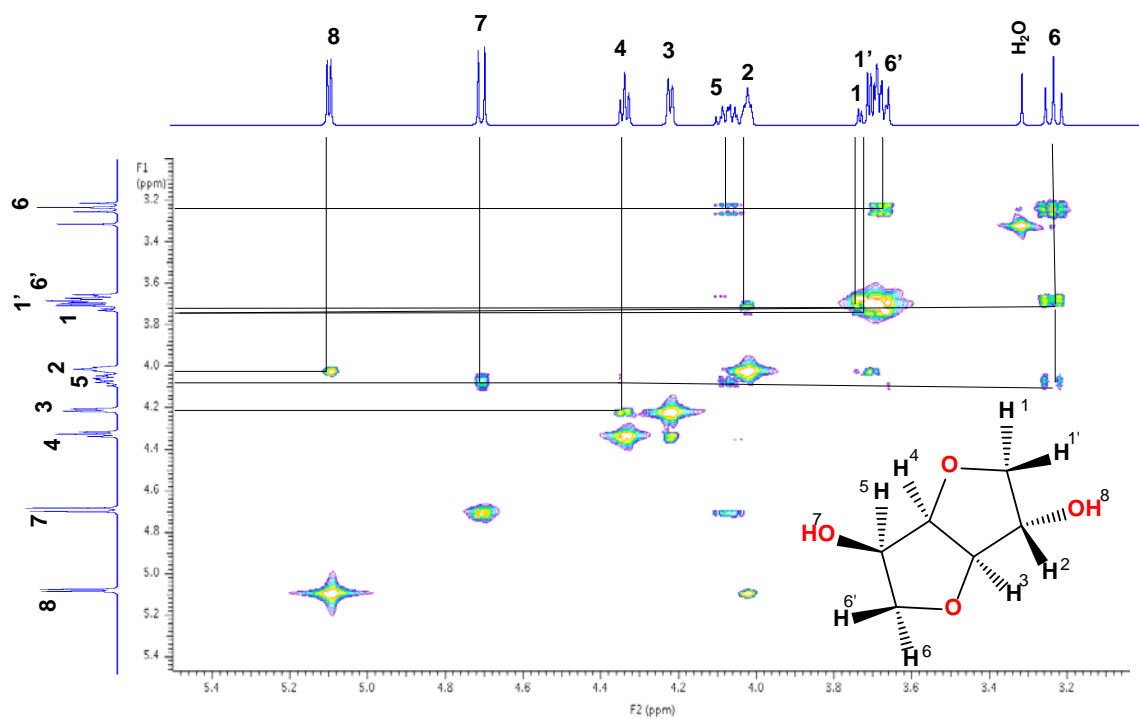


Figure A.1 ^1H - ^1H COSY of isosorbide.

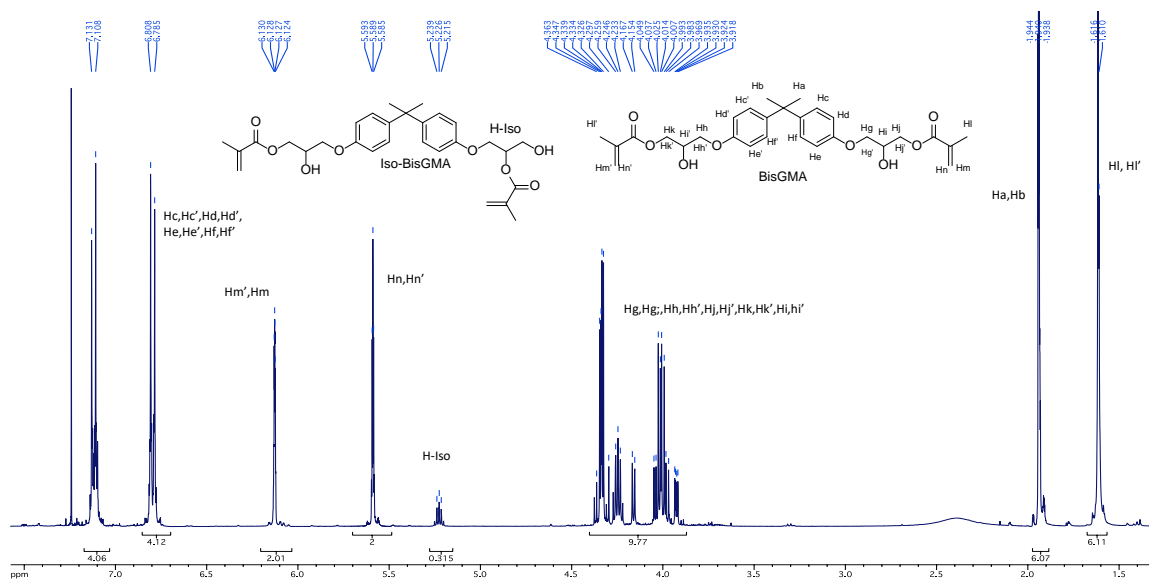


Figure A.2 ^1H NMR Spectrum of BisGMA in CDCl_3

^1H -NMR (CDCl_3 , δ -ppm): 7.14-7.09 (m, 4H), 6.82-6.78 (m, 4H), 6.13 (m, 2H), 5.59 (m, 2H), 5.23 (m, H-iso), 4.38-3.92 (m, 10H), 1.97-1.91 (m, 6H), 1.65-1.58 (m, 6H).

APPENDIX B
ATR-FTIR SPECTRA

Figures B.1 to B.20 show ATR-FTIR spectra of isosorbide, isosorbide dimethacrylates and monomer mixtures.

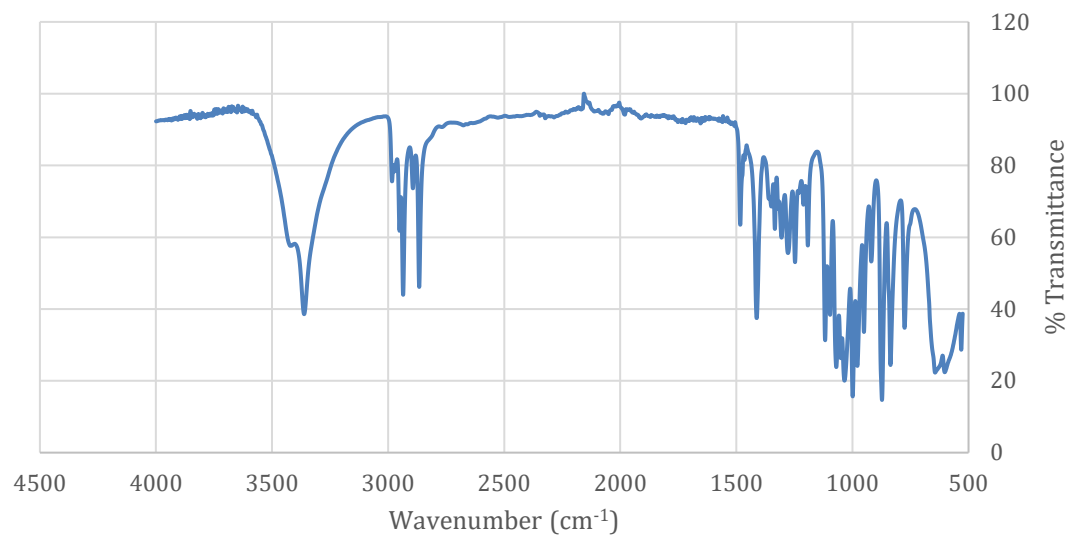


Figure B.1 ATR-FTIR Spectrum of isosorbide.

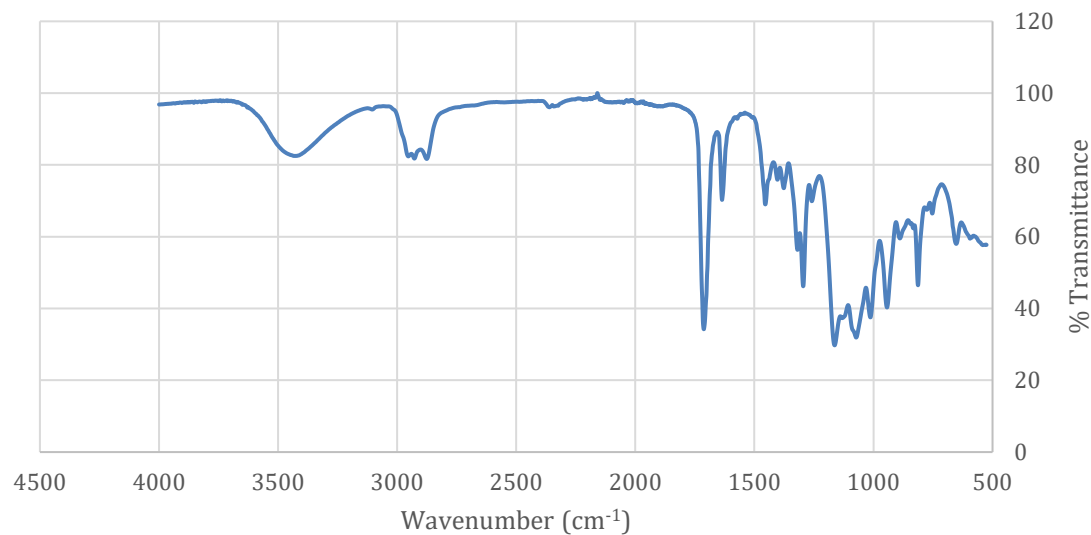


Figure B.2 ATR-FTIR spectrum of isosorbide 2,5-bis(glyceryloxy) dimethacrylate.
 ATR-FTIR (ν , cm^{-1}) = 1712 (C=O, methacrylate), 1636 (C=C, methacrylate).

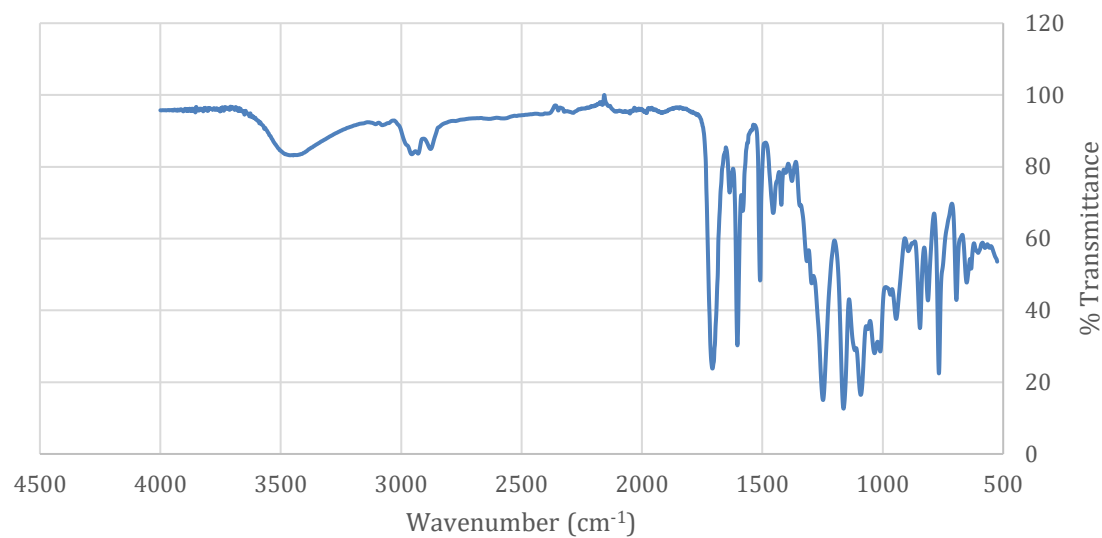


Figure B.3 ATR-FTIR spectrum of isosorbide 2,5-bis(4-glyceryloxybenzoate) dimethacrylate.
 ATR-FTIR (ν , cm^{-1}) = 1706 (C=O, methacrylate), 1635 (C=C, methacrylate), 1604 (C=C, aromatic).

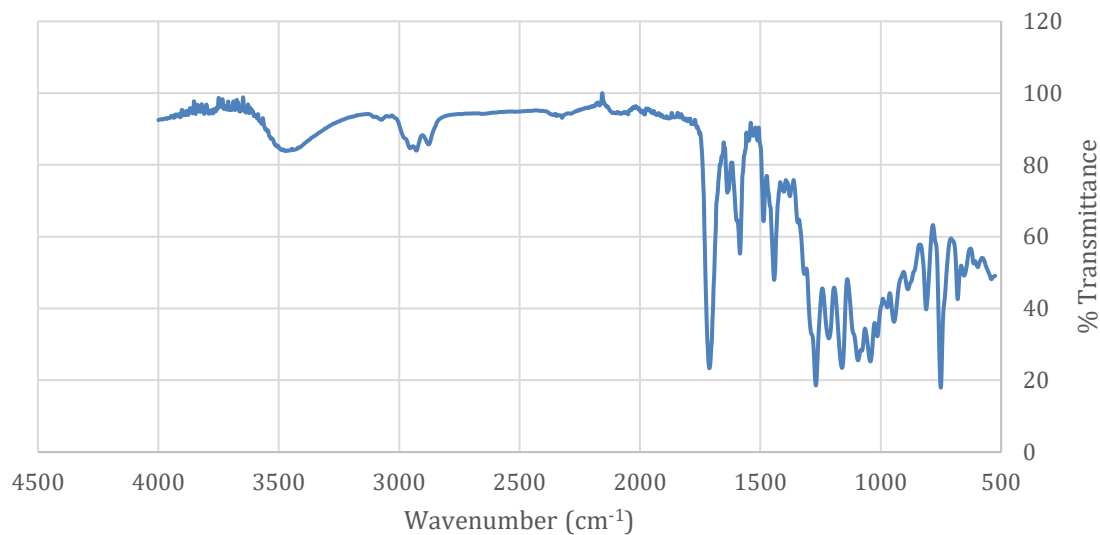


Figure B.4 ATR-FTIR spectrum of isosorbide 2,5-bis(3-glyceryloxybenzoate) dimethacrylate.

ATR-FTIR (ν , cm^{-1}) = 1711 (C=O, methacrylate) 1637 (C=C, methacrylate), 1606 (C=C, aromatic).

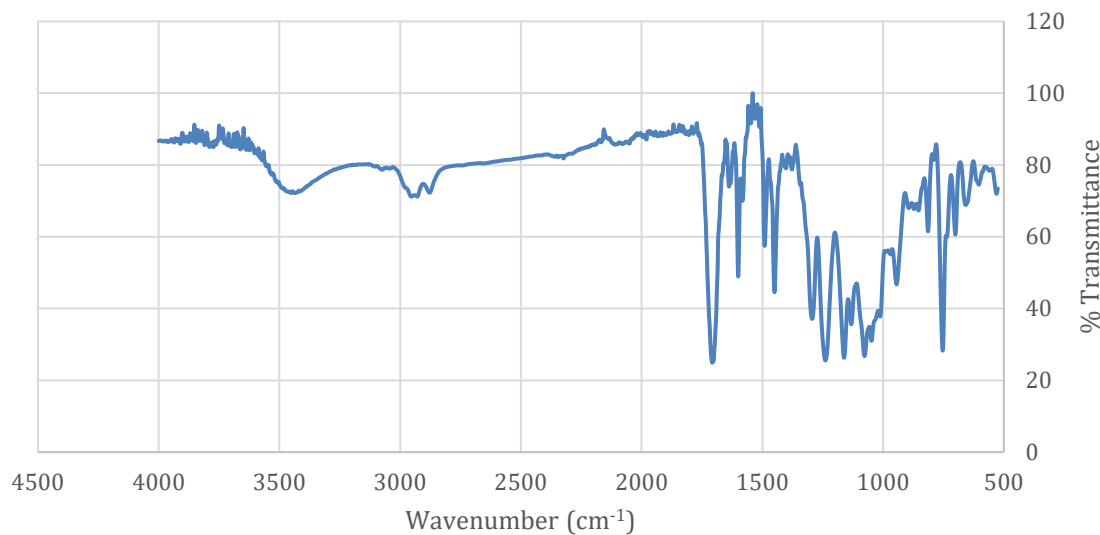


Figure B.5 ATR-FTIR spectrum of isosorbide 2,5-bis(2-glyceryloxybenzoate) dimethacrylate.

ATR-FTIR (ν , cm^{-1}) = 1704 (C=O, methacrylate) 1632 (C=C, methacrylate), 1600 (C=C, aromatic).

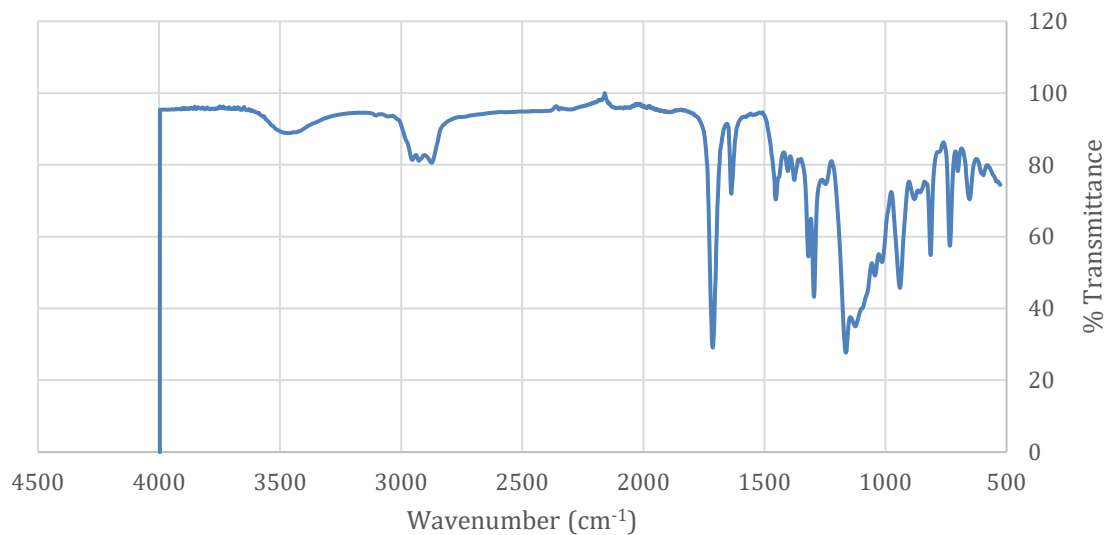


Figure B.6 ATR-FTIR spectrum of ISDGMA/TEGDMA 60:40 wt%.
 ATR-FTIR (ν , cm^{-1}) = 1713 (C=O, methacrylate) 1636 (C=C, methacrylate).

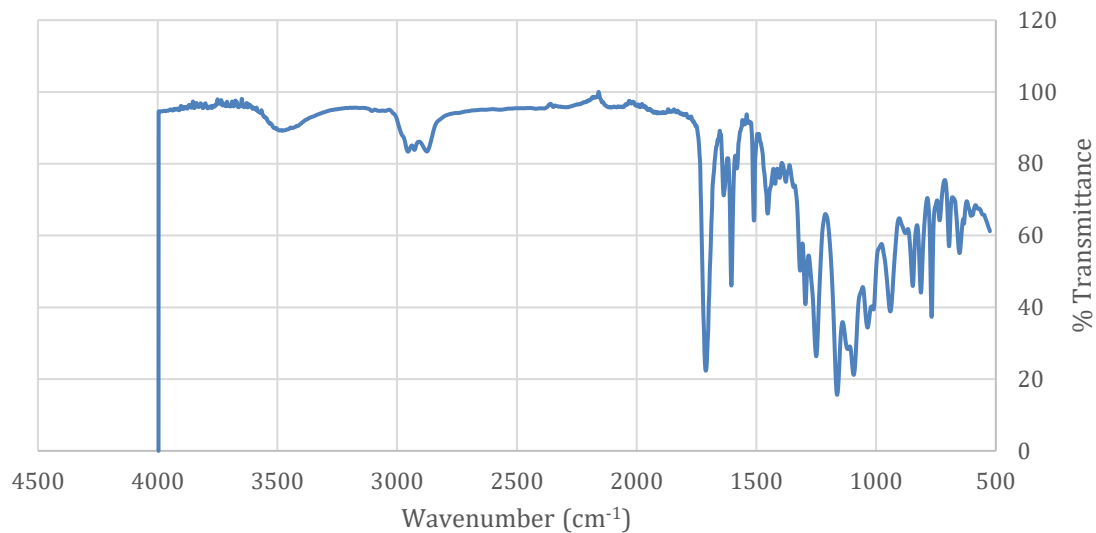


Figure B.7 ATR-FTIR spectrum of ISB4GBMA/TEGDMA 60:40 wt%.
 ATR-FTIR (ν , cm^{-1}) = 1710 (C=O, methacrylate) 1635 (C=C, methacrylate), 1604 (C=C, aromatic).

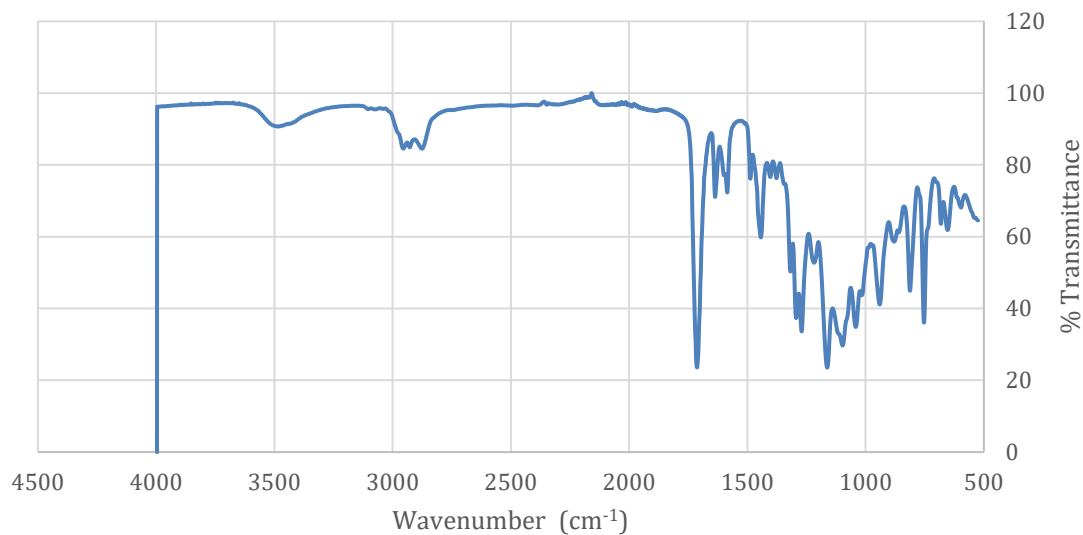


Figure B.8 ATR-FTIR spectrum of ISB3GBMA/TEGDMA 60:40 wt%.
 ATR-FTIR (ν , cm^{-1}) = 1710 (C=O, methacrylate) 1635 (C=C, methacrylate), 1602 (C=C, aromatic).

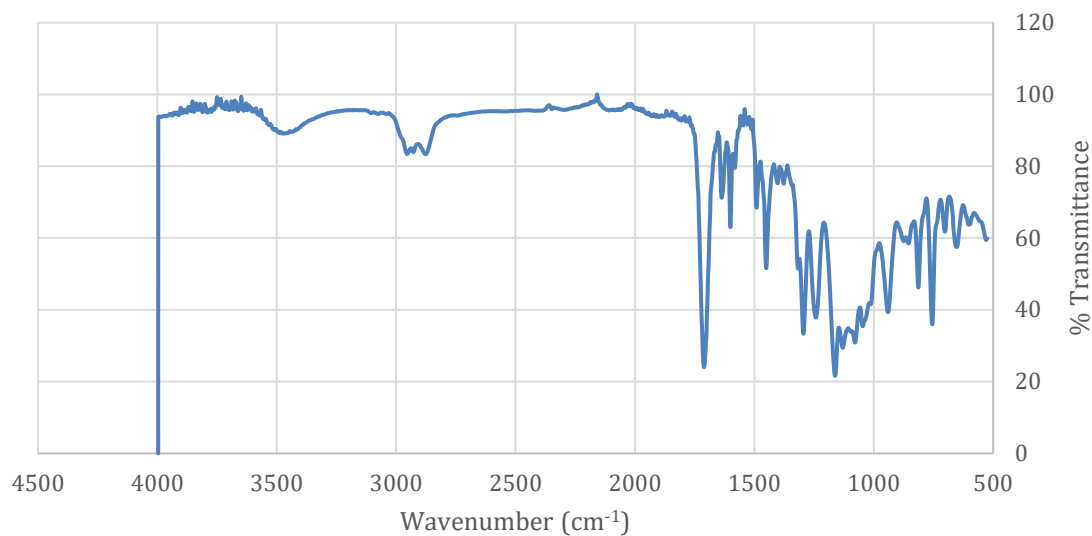


Figure B.9 ATR-FTIR spectrum of ISB2GBMA/TEGDMA 60:40 wt%.
 ATR-FTIR (ν , cm^{-1}) = 1710 (C=O, methacrylate) 1635 (C=C, methacrylate), 1600 (C=C, aromatic).

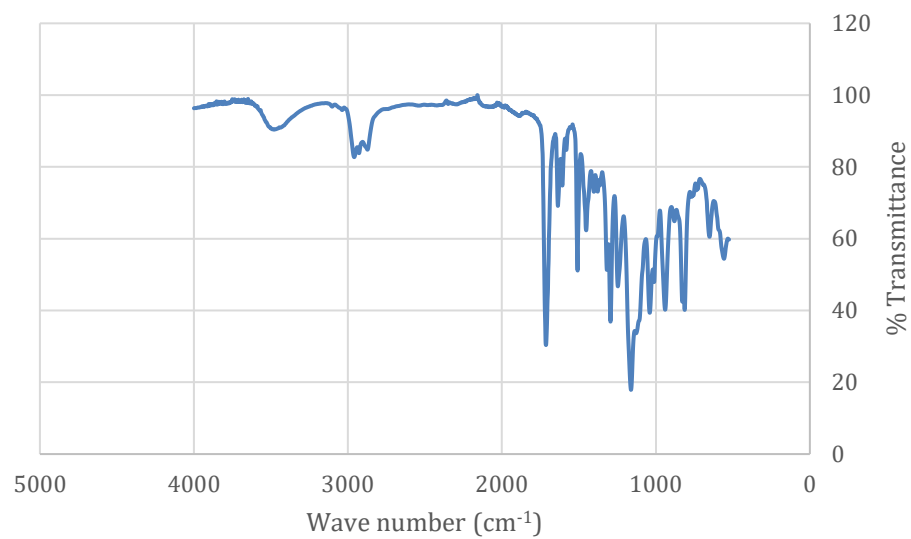


Figure B.10 ATR-FTIR spectrum of BisGMA/TEGDMA 60:40 wt%.
ATR-FTIR (ν , cm^{-1}) = 1713 (C=O, methacrylate) 1635 (C=C, methacrylate), 1607 (C=C, aromatic).

APPENDIX C

EFFECT OF CURING DURATION ON WATER SORPTION OF P(ISDGMA/TEGDMA)

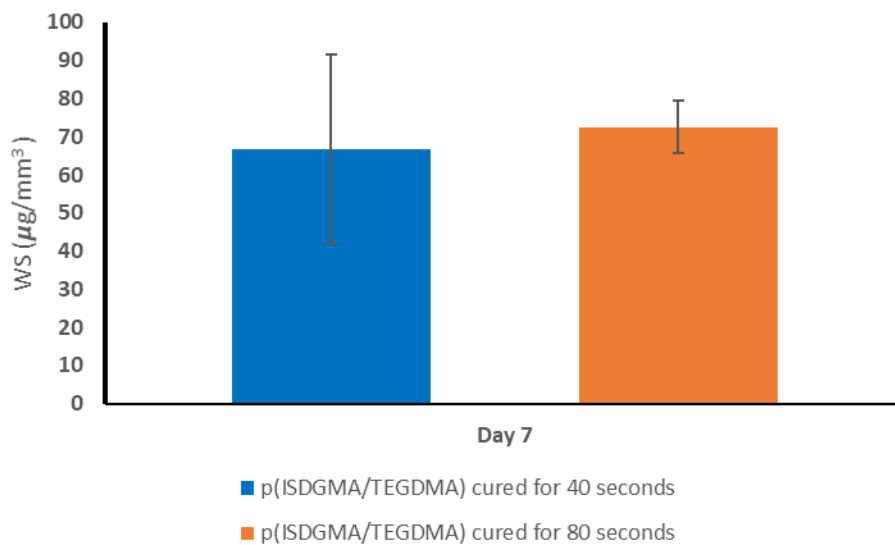


Figure C.1 Water sorption of P(ISDGMA/TEGDMA) when cured at different time lengths.

APPENDIX D

DATA CORRELATIONS

Tables D.1-D.4 summarize data correlations between the various resin properties

Table D.1 Monomer Mixture Viscosity, Degree of Conversion, Polymerization Shrinkage for P(BisGMA/TEGDMA), P(ISB4GBMA/TEGDMA), P(ISB3GBMA/TEGDMA), P(ISB2GBMA/TEGDMA), and P(ISDGMA/TEGDMA)

| | Monomer mixture viscosity (Pa·S) | Degree of Conversion (%) | Polymerization Shrinkage (%) |
|---------------------------------|----------------------------------|--------------------------|------------------------------|
| P(BisGMA/TEGDMA) ^a | 0.48 | 54 (3) ^[b] | 6.54 (1) ^[b] |
| P(ISB4GBMA/TEGDMA) ^b | 2.48 | 47 (4) ^[a,d] | 4.25 (1) ^[a,d,e] |
| P(ISB3GBMA/TEGDMA) ^c | 1.26 | 51 (3) | 5.41 (1) ^[d,e] |
| P(ISB2GBMA/TEGDMA) ^d | 0.63 | 52 (5) ^[b] | 6.7 (1) ^[b,c] |
| P(ISDGMA/TEGDMA) ^e | 0.06 | N/A | 7.28 (1) ^[b,c] |

Note: Letters indicate statistically significant difference (P<0.05) based on group. Standard deviation in parenthesis.

Table D.2 Degree of Conversion, Glass Transition Temperature, and Water Sorption for P(BisGMA/TEGDMA), P(ISB4GBMA/TEGDMA), P(ISB3GBMA/TEGDMA), P(ISB2GBMA/TEGDMA), and P(ISDGMA/TEGDMA)

| | Degree of Conversion (%) | Glass Transition Temperature (°C) | Water sorption (μg/mm ³) |
|---------------------------------|--------------------------|-----------------------------------|--------------------------------------|
| P(BisGMA/TEGDMA) ^a | 54 (3) ^[b] | 95.73 | 26 ^[b,c,d,e] |
| P(ISB4GBMA/TEGDMA) ^b | 47 (4) ^[a,d] | 80.57 (0.46) ^[a] | 44 ^[a,d,e] |
| P(ISB3GBMA/TEGDMA) ^c | 51 (3) | 77.38 (3.86) ^[a] | 42 ^[a,e] |
| P(ISB2GBMA/TEGDMA) ^d | 52 (5) ^[b] | 86.52 (1.18) | 39 ^[a,b,e] |
| P(ISDGMA/TEGDMA) ^e | N/A | 85.56 (7.30) ^[a] | 73 ^[a,b,c,d] |

Note: Letters indicate statistically significant difference (P<0.05) based on group. Standard deviation in parenthesis.

Table D.3 Degree of Conversion, and Flexural Strength for P(BisGMA/TEGDMA), P(ISB4GBMA/TEGDMA), P(ISB3GBMA/TEGDMA), P(ISB2GBMA/TEGDMA), and P(ISDGMA/TEGDMA)

| | Degree of Conversion (%) | Flexural Strength (MPa) dry | Flexural Strength (MPa) wet |
|---------------------------------|--------------------------|-----------------------------|-----------------------------|
| P(BisGMA/TEGDMA) ^a | 54 (3) ^[b] | 88 (9) ^[e] | 53 (12) ^[e] |
| P(ISB4GBMA/TEGDMA) ^b | 47 (4) ^[a,d] | 74 (12) | 43 (3) ^[e] |
| P(ISB3GBMA/TEGDMA) ^c | 51 (3) | 72 (6) | 37 (3) ^[e] |
| P(ISB2GBMA/TEGDMA) ^d | 52 (5) ^[b] | 66 (10) | 43 (1) ^[e] |
| P(ISDGMA/TEGDMA) ^e | N/A | 51(13) ^[a] | 10 (4) ^[a,b,c,d] |

Note: Letters indicate statistically significant difference (P<0.05) based on group. Standard deviation in parenthesis.

Table D.4 Degree of Conversion, and Flexural Modulus for P(BisGMA/TEGDMA), P(ISB4GBMA/TEGDMA), P(ISB3GBMA/TEGDMA), P(ISB2GBMA/TEGDMA), and P(ISDGMA/TEGDMA)

| | Degree of Conversion (%) | Flexural Modulus (MPa) dry | Flexural Modulus (MPa) wet |
|---------------------------------|--------------------------|----------------------------|-----------------------------|
| P(BisGMA/TEGDMA) ^a | 54 (3) ^[b] | 88 (9) | 53 (12) ^[e] |
| P(ISB4GBMA/TEGDMA) ^b | 47 (4) ^[a,d] | 74 (12) | 43 (3) ^[e] |
| P(ISB3GBMA/TEGDMA) ^c | 51 (3) | 72 (6) | 37 (3) ^[e] |
| P(ISB2GBMA/TEGDMA) ^d | 52 (5) ^[b] | 66 (10) | 43 (1) ^[e] |
| P(ISDGMA/TEGDMA) ^e | N/A | 51 (13) | 10 (4) ^[a,b,c,d] |

Note: Letters indicate statistically significant difference (P<0.05) based on group. Standard deviation in parenthesis.

REFERENCES

1. James, S.L.; Abate, D.; Abate, K.H.; Abay, S.M.; Abbafati, C.; Abbasi, N.; Abbastabar, H.; Abd-Allah, F.; Abdela, J.; Abdelalim, A.; et al. Global, Regional, and National Incidence, Prevalence, and Years Lived with Disability for 354 Diseases and Injuries for 195 Countries and Territories, 1990–2017: A systematic Analysis for the Global Burden of Disease Study 2017. *The Lancet* (2018) 392, 1789-1858.
2. Featherstone, J. Dental Caries: a Dynamic Disease Process. *Australian Dental Journal* (2008) 53, 286-291.
3. Heng, C. Tooth Decay Is the Most Prevalent Disease. *Fed Pract* (2016) 33, 31-33.
4. Pitts, N.B.; Zero, D.T.; Marsh, P.D.; Ekstrand, K.; Weintraub, J.A.; Ramos-Gomez, F.; Tagami, J.; Twetman, S.; Tsakos, G.; Ismail, A. Dental Caries. *Nature Reviews Disease Primers* (2017) 3, 17030.
5. Forssten, S.D.; Björklund, M.; Ouwehand, A.C. *Streptococcus mutans*, Caries and Simulation Models. *Nutrients* (2010) 2, 290-298.
6. Lamont, R.J.; Demuth, D.R.; Davis, C.A.; Malamud, D.; Rosan, B. Salivary-Agglutinin-Mediated Adherence of *Streptococcus mutans* to Early Plaque Bacteria. *Infect Immun* (1991) 59, 3446-3450.
7. Davey, M.E.; O'Toole, G.A. Microbial Biofilms: From Ecology to Molecular Genetics. *Microbiol Mol Biol Rev* (2000) 64, 847-867.
8. Marsh, P.D. Dental plaque as a Biofilm and a Microbial community - implications for health and disease. *BMC Oral Health* (2006) 6 Suppl 1, S14-S14.
9. Ten Cate, J.M.; Featherstone, J.D.B. Mechanistic Aspects of the Interactions Between Fluoride and Dental Enamel. *Critical Reviews in Oral Biology & Medicine* (1991) 2, 283-296.

10. Abou Neel, E.A.; Aljabo, A.; Strange, A.; Ibrahim, S.; Coathup, M.; Young, A.M.; Bozec, L.; Mudera, V. Demineralization-remineralization Dynamics in Teeth and Bone. *Int J Nanomedicine* (2016) 11, 4743-4763.
11. Selwitz, R.H.; Ismail, A.I.; Pitts, N.B. Dental Caries. *The Lancet* (2007) 369, 51-59.
12. Ekstrand, K.R. Improving Clinical Visual Detection—Potential for Caries Clinical Trials. *Journal of Dental Research* (2004) 83, 67-71.
13. Anusavice, K.J., Ralph W. Phillips, Chiayi Shen, and H. Ralph Rawls. *Phillips' Science of Dental Materials*.; Elsevier/Saunders.: St. Louis, Mo, (2013).
14. Chadwick, B.L.; Dummer, P.M.; Dunstan, F.D.; Gilmour, A.S.; Jones, R.J.; Phillips, C.J.; Rees, J.; Richmond, S.; Stevens, J.; Treasure, E.T. What Type of Filling? Best Practice in Dental Restorations. *Qual Health Care* (1999), 8, 202-207.
15. Narayan, R. *Biomedical Materials*, 1 ed.; Springer US: New York, NY, (2009).
16. Singh, H.; Kaur, M.; Dhillon, J.; Mann, J.; Kumar, A. Evolution of Restorative Dentistry from Past to Present. *Indian Journal of Dental Sciences* (2017) 9, 38.
17. Knosp, H.; Holliday, R.J.; Corti, C.W. Gold in Dentistry: Alloys, Uses and Performance. *Gold Bulletin* (2003) 36, 93-102.
18. Leistevuo, J.; Leistevuo, T.; Helenius, H.; Pyy, L.; Österblad, M.; Huovinen, P.; Tenovuo, J. Dental Amalgam Fillings and the Amount of Organic Mercury in Human Saliva. *Caries Research* (2001) 35, 163-166.
19. Mackert, J.R.; Berglund, A. Mercury Exposure From Dental Amalgam Fillings: Absorbed Dose and the Potential for Adverse Health Effects. *Critical Reviews in Oral Biology & Medicine* (1997) 8, 410-436.
20. Bates, M.N. Dental Amalgam Fillings: A Source of Mercury Exposure. In *Encyclopedia of Environmental Health*, Nriagu, J.O., Ed.; Elsevier: Burlington (2011) pp. 11-20.

21. Rathore, M.; Singh, A.; Pant, V.A. The Dental Amalgam Toxicity Fear: a Myth or Actuality. *Toxicol Int* (2012) 19, 81-88.
22. Taut, C. Dental Amalgam: Is This the End? *Journal of the Irish Dental Association* (2013) 59, 311-317.
23. Epidemiological Evidence on the Adverse Health Effects Reported in Relation to Mercury from Dental Amalgam: Systematic Literature Review, U.S. Food and Drug Administration, Center for Devices and Radiological Health (2019).
24. Fisher, J.; Varenne, B.; Narvaez, D.; Vickers, C. The Minamata Convention and the Phase Down of Dental Amalgam. *Bull World Health Organ* (2018) 96, 436-438.
25. Moncada, G.; Silva, F.; Angel, P.; Oliveira, O., Jr; Fresno, M.; Cisternas, P.; Fernandez, E.; Estay, J.; Martin, J. Evaluation of Dental Restorations: A Comparative Study Between Clinical and Digital Photographic Assessments. *Operative Dentistry* (2014) 39, e45-e56.
26. Sideridou, I. "Trends in Dental Polymer Nanocomposites" Irini D. Sideridou, Chapter in *Encyclopedia of Dentistry Research*. Nova Science, Hauppauge, NY 11788 USA, (2012).
27. Moszner, N.; Hirt, T. New Polymer-chemical Developments in Clinical Dental Polymer Materials: Enamel-dentin Adhesives and Restorative Composites. *J. Polym. Sci., Part A: Polym. Chem* (2012) 50, 4369-4402
28. Ferracane, J.L. Resin Composite—State of the Art. *Dental Materials* (2011) 27, 29-38.
29. Ferracane, J.L. Current Trends in Dental Composites. *Critical Reviews in Oral Biology & Medicine* (1995) 6, 302-318.
30. Stansbury, J.W. Dimethacrylate Network Formation and Polymer Property Evolution as Determined by the Selection of Monomers and Curing Conditions. *Dental Materials* (2012) 28, 13-22.

31. Pfeifer, C.S.; Shelton, Z.R.; Braga, R.R.; Windmoller, D.; Machado, J.C.; Stansbury, J.W. Characterization of Dimethacrylate Polymeric Networks: A study of the Crosslinked Structure Formed by Monomers Used in Dental Composites. *European Polymer Journal* (2011) 47, 162-170.
32. Bowen, R.L. Dental Dilling Material Comprising Vinyl-silane Treated Fused Silica and a Binder Consisting of the Reaction Product of Bisphenol and Glycidyl Methacrylate. 26 June (1962) US3066112A.
33. Pratap, B.; Gupta, R.K.; Bhardwaj, B.; Nag, M. Resin Based Restorative Dental Materials: Characteristics and Future Perspectives. *Japanese Dental Science Review* (2019) 55, 126-138.
34. Sideridou, I.; Tserki, V.; Papanastasiou, G. Effect of Chemical Structure on Degree of Conversion in Light-cured Dimethacrylate-based Dental Resins. *Biomaterials* (2002) 23, 1819-1829.
35. Asmussen, E.; Peutzfeldt, A. Influence of UEDMA, BisGMA and TEGDMA on Selected Mechanical Properties of Experimental Resin Composites. *Dental Materials* (1998) 14, 51-56.
36. Pereira, S.G.; Nunes, T.G.; Kalachandra, S. Low Viscosity Dimethacrylate Comonomer Compositions [Bis-GMA and CH3Bis-GMA] for Novel Dental Composites; Analysis of the Network by Stray-field MRI, Solid-state NMR and DSC & FTIR. *Biomaterials* (2002) 23, 3799-3806.
37. Sideridou, I.D.; Karabela, M.M.; Vouvoudi, E.C. Volumetric Dimensional Changes of Dental Light-cured Dimethacrylate Resins After Sorption of Water or Ethanol. *Dental Materials* (2008) 24, 1131-1136.
38. Sideridou, I.D.; Karabela, M.M. Sorption of Water, Ethanol or Ethanol/Water Solutions by Light-cured Dental Dimethacrylate Resins. *Dental Materials* (2011) 27, 1003-1010.
39. Polydorou, O.; König, A.; Hellwig, E.; Kümmerer, K. Uthethane Dimethacrylate: A molecule that May Cause Confusion in Dental Research. *Journal of Biomedical Materials Research Part B: Applied Biomaterials* (2009) 91B, 1-4.

40. Barszczewska-Rybarek, I.M. Characterization of Urethane-dimethacrylate Derivatives as Alternative Monomers for the Restorative Composite Matrix. *Dental Materials* (2014) 30, 1336-1344.
41. Peutzfeldt, A. Resin Composites in Dentistry: the Monomer Systems. *European Journal of Oral Sciences* (1997) 105, 97-116.
42. Khatri, C.A.; Stansbury, J.W.; Schultheisz, C.R.; Antonucci, J.M. Synthesis, Characterization and Evaluation of Urethane Derivatives of Bis-GMA. *Dental Materials* (2003) 19, 584-588.
43. Moszner, N.; Salz, U. New Developments of Polymeric Dental Composites. *Progress in Polymer Science* (2001) 26, 535-576.
44. Sideridou, I.D.; Achilias, D.S.; Karava, O. Reactivity of Benzoyl Peroxide/Amine System as an Initiator for the Free Radical Polymerization of Dental and Orthopaedic Dimethacrylate Monomers: Effect of the Amine and Monomer Chemical Structure. *Macromolecules* (2006) 39, 2072-2080.
45. Lal, J.; Green, R. Effect of Amine Accelerators on the Polymerization of Methyl methacrylate with Benzoyl Peroxide. *Journal of Polymer Science* (1955) 17, 403-409.
46. Kim, K.; Singstock, N.R.; Childress, K.K.; Sinha, J.; Salazar, A.M.; Whitfield, S.N.; Holder, A.M.; Stansbury, J.W.; Musgrave, C.B. Rational Design of Efficient Amine Reductant Initiators for Amine–Peroxide Redox Polymerization. *Journal of the American Chemical Society* (2019) 141, 6279-6291.
47. Fouassier, J.P.; Allonas, X.; Burget, D. Photopolymerization Reactions Under Visible Lights: Principle, Mechanisms and Examples of Applications. *Progress in Organic Coatings* (2003) 47, 16-36.
48. Jakubiak, J.; Allonas, X.; Fouassier, J.P.; Sionkowska, A.; Andrzejewska, E.; Linden, L.Å.; Rabek, J.F. Camphorquinone–amines Photoinitiating Systems for the Initiation of Free Radical Polymerization. *Polymer* (2003) 44, 5219-5226.

49. Chen, Y.-C.; Ferracane, J.L.; Prah, S.A. Quantum Yield of Conversion of the Dental Photoinitiator Camphorquinone. In Proceedings of the Saratov, Russia, (2005) p. 11.
50. Abdalla, M.; Larisa-Milena, P.-T.; Leopold, N.; Cimpean, S.; Chis, V. Excited State Properties of the Camphorquinone Photoinitiator. *Studia UBB Physica* 2065-9415 (2016) 61 (LXI), 7-20.
51. Kamoun, E.A.; Winkel, A.; Eisenburger, M.; Menzel, H. Carboxylated Camphorquinone as Visible-light Photoinitiator for Biomedical Application: Synthesis, Characterization, and Application. *Arabian Journal of Chemistry* (2016) 9, 745-754.
52. Stansbury, J.W. Curing Dental Resins and Composites by Photopolymerization. *Journal of Esthetic and Restorative Dentistry* (2000) 12, 300-308.
53. Cosola, A.; Chiappone, A.; Martinengo, C.; Grützmaier, H.; Sangermano, M. Gelatin Type A from Porcine Skin Used as Co-Initiator in a Radical Photo-Initiating System. *Polymers* (2019) 11, 1901.
54. Leprince, J.G.; Palin, W.M.; Hadis, M.A.; Devaux, J.; Leloup, G. Progress in Dimethacrylate-based Dental Composite Technology and Curing Efficiency. *Dental Materials* (2013) 29, 139-156.
55. Cramer, N.B.; Stansbury, J.W.; Bowman, C.N. Recent Advances and Developments in Composite Dental Restorative Materials. *Journal of Dental Research* (2011) 90, 402-416.
56. Johnston-Hall, G.; Monteiro, M.J. Bimolecular Radical Termination: New Perspectives and Insights. *Journal of Polymer Science Part A: Polymer Chemistry* (2008) 46, 3155-3173.
57. Anseth, K.S.; Newman, S.M.; Bowman, C.N. *Polymeric Dental Composites: Properties and Reaction Behavior of Multimethacrylate Dental Restorations*. Berlin, Heidelberg (1995) pp. 177-217.

58. Lovell, L.G.; Stansbury, J.W.; Syrpes, D.C.; Bowman, C.N. Effects of Composition and Reactivity on the Reaction Kinetics of Dimethacrylate/Dimethacrylate Copolymerizations. *Macromolecules* (1999) 32, 3913-3921.
59. Barszczewska-Rybarek, I.M. A Guide Through the Dental Dimethacrylate Polymer Network Structural Characterization and Interpretation of Physico-Mechanical Properties. *Materials* (2019) 12.
60. Barszczewska-Rybarek, I.M. Structure–property Relationships in Dimethacrylate Networks based on Bis-GMA, UDMA and TEGDMA. *Dental Materials* (2009) 25, 1082-1089.
61. Musanje, L.; Ferracane, J.L.; Sakaguchi, R.L. Determination of the Optimal Photoinitiator Concentration in Dental Composites based on Essential Material Properties. *Dental Materials* (2009) 25, 994-1000.
62. Pfeifer, C.S.; Ferracane, J.L.; Sakaguchi, R.L.; Braga, R.R. Photoinitiator Content in Restorative Composites: Influence on Degree of Conversion, Reaction Kinetics, Volumetric Shrinkage and Polymerization Stress. *American journal of dentistry* (2009) 22, 206-210.
63. Neumann, M.G.; Schmitt, C.C.; Ferreira, G.C.; Corrêa, I.C. The Initiating Radical Yields and the Efficiency of Polymerization for Various Dental Photoinitiators Excited by Different Light Curing Units. *Dental Materials* (2006) 22, 576-584.
64. Decker, C. Kinetic Study and New Applications of UV Radiation Curing. *Macromolecular Rapid Communications* (2002) 23, 1067-1093.
65. Beun, S.; Bailly, C.; Dabin, A.; Vreven, J.; Devaux, J.; Leloup, G. Rheological properties of experimental Bis-GMA/TEGDMA flowable resin composites with various macrofiller/microfiller ratio. *Dental Materials* 2009, 25, 198-205.
66. Flávia, G.; Yoshio, K.; Carmem, P.; W., S.J.; R., B.R. Influence of BisGMA, TEGDMA, and BisEMA Contents on Viscosity, Conversion, and Flexural Strength of Experimental Resins and Composites. *European Journal of Oral Sciences* (2009) 117, 442-446.

67. Shortall, A.C.; Wilson, H.J.; Harrington, E. Depth of Cure of Radiation - Activated Composite Restoratives- Influence of Shade and Opacity. *Journal of Oral Rehabilitation* (1995) 22, 337-342.
68. Watts, D.C.; Cash, A.J. Analysis of optical transmission by 400-500 nm visible light into aesthetic dental biomaterials. *J Dent* 1994, 22, 112-117.
69. Musanje, L.; Darvell, B.W. Curing-light Attenuation in Filled-resin Restorative Materials. *Dental Materials* (2006) 22, 804-817.
70. Ogunyinka, A.; Palin, W.M.; Shortall, A.C.; Marquis, P.M. Photoinitiation Chemistry Affects Light Transmission and Degree of Conversion of Curing Experimental Dental Resin Composites. *Dental Materials* (2007) 23, 807-813.
71. Shortall, A.C.; Palin, W.M.; Burtscher, P. Refractive Index Mismatch and Monomer Reactivity Influence Composite Curing Depth. *Journal of Dental Research* (2008) 87, 84-88.
72. Howard, B.; Wilson, N.D.; Newman, S.M.; Pfeifer, C.S.; Stansbury, J.W. Relationships Between Conversion, Temperature and Optical Properties During Composite Photopolymerization. *Acta Biomaterialia* (2010) 6, 2053-2059.
73. Emami, N.; Sjö Dahl, M.; Söderholm, K.-J.M. How Filler Properties, Filler Fraction, Sample Thickness and Light Source Affect Light Attenuation in Particulate Filled Resin Composites. *Dental Materials* (2005) 21, 721-730.
74. AlShaafi, M.M. Factors Affecting Polymerization of Resin-based Composites: A Literature Review. *The Saudi Dental Journal* (2017) 29, 48-58.
75. Rueggeberg, F.A.; Caughman, W.F.; Curtis, J.W., Jr. Effect of Light Intensity and Exposure Duration on Cure of Resin Composite. *Oper Dent* (1994) 19, 26-32.
76. Rueggeberg, F.A.; Craig, R.G. Correlation of Parameters Used to Estimate Monomer Conversion in a Light-Cured Composite. *J Dent Res* (1988) 67, 932-937.

77. Price, R.; Dérand, T.; Loney, R.; Andreou, P. Effect of Light Source and Specimen Thickness on the Surface Hardness of Resin Composite. *American Journal of Dentistry* (2002) 15, 47-53.
78. Flury, S.; Peutzfeldt, A.; Lussi, A. Influence of Increment Thickness on Microhardness and Dentin Bond Strength of Bulk Fill Resin Composites. *Dental Materials* (2014) 30, 1104-1112.
79. Althoff, O.; Hartung, M. Advances in Light Curing. *American Journal of Dentistry* (2000) 13, 77d-81d.
80. Rueggeberg, F. Contemporary Issues in Photocuring. *Compendium of Continuing Education in Dentistry*. (Jamesburg, N.J. : 1995). Supplement 1999, S4-15.
81. Mills, R.W.; Jandt, K.D.; Ashworth, S.H. Dental Composite Depth of Cure with Halogen and Blue Light Emitting Diode Technology. *British Dental Journal* (1999) 186, 388-391.
82. Jandt, K.D.; Mills, R.W. A Brief History of LED Photopolymerization. *Dental Materials* (2013) 29, 605-617.
83. Leprince, J.; Devaux, J.; Mullier, T.; Vreven, J.; Leloup, G. Pulpal-Temperature Rise and Polymerization Efficiency of LED Curing Lights. *Oper Dent* (2010) 35, 220-230.
84. Price, R.B.; Murphy, D.G.; Dérand, T. Light Energy Transmission Through Cured Resin Composite and Human Dentin. *Quintessence International* (1985) 2000, 31, 659-667.
85. Price, R.B.T.; Felix, C.A.; Andreou, P. Effects of Resin Composite Composition and Irradiation Distance on the Performance of Curing Lights. *Biomaterials* (2004) 25, 4465-4477.
86. Price, R.B.; Whalen, J.M.; Price, T.B.; Felix, C.M.; Fahey, J. The Effect of Specimen Temperature on the Polymerization of a Resin-Composite. *Dental Materials* (2011) 27, 983-989.

87. Daronch, M.; Rueggeberg, F.A.; De Goes, M.F.; Giudici, R. Polymerization kinetics of Pre-Heated Composite. *J Dent Res* (2006) 85, 38-43.
88. Fonseca, A.S.Q.S.; Labruna Moreira, A.D.; de Albuquerque, P.P.A.C.; de Menezes, L.R.; Pfeifer, C.S.; Schneider, L.F.J. Effect of Monomer Type on the CC Degree of Conversion, Water Sorption and Solubility, and Color Stability of Model Dental Composites. *Dental Materials* (2017) 33, 394-401.
89. Herrera-González, A.M.; Caldera-Villalobos, M.; Pérez-Mondragón, A.A.; Cuevas-Suárez, C.E.; González-López, J.A. Analysis of Double Bond Conversion of Photopolymerizable Monomers by FTIR-ATR Spectroscopy. *Journal of Chemical Education* (2019) 96, 1786-1789.
90. Collares, F.M.; Portella, F.F.; Leitune, V.C.B.; Samuel, S.M.W. Discrepancies in Degree of Conversion Measurements by FTIR. *Brazilian Oral Research* (2014) 28, 9-15.
91. Khalil, S.K.H.; Allam, M.A.; Tawfik, W.A. Use of FT-Raman Spectroscopy to Determine the Degree of Polymerization of Dental Composite Resin Cured with a New Light Source. *Eur J Dent* (2007) 1, 72-79.
92. Soares, L.E.S.; Rocha, R.; Martin, A.A.; Pinheiro, A.L.B.; Zampieri, M. Monomer Conversion of Composite Dental Resins Photoactivated by a Halogen Lamp and a LED: a FT-Raman Spectroscopy Study. *Química Nova* (2005) 28, 229-232.
93. Soh, M.S.; Yap, A.U.J. Influence of Curing Modes on Crosslink Density in Polymer Structures. *Journal of Dentistry* (2004) 32, 321-326.
94. Asmussen, E.; Peutzfeldt, A. Influence of Selected Components on Crosslink Density in Polymer Structures. *European Journal of Oral Sciences* (2001) 109, 282-285.
95. Benetti, A.R.; Asmussen, E.; Munksgaard, E.C.; Dewaele, M.; Peutzfeldt, A.; Leloup, G.; Devaux, J. Softening and Elution of Monomers in Ethanol. *Dental Materials* (2009) 25, 1007-1013.

96. Moraes, J.; Sostena, M.M.D.S.; Grandini, C. The Glass Transition Temperature in Dental Composites (2011).
97. Gajewski, V.E.S.; Pfeifer, C.S.; Fróes-Salgado, N.R.G.; Boaro, L.C.C.; Braga, R.R. Monomers Used in Resin Composites: Degree of Conversion, Mechanical Properties and Water Sorption/Solubility. *Brazilian Dental Journal* (2012) 23, 508-514.
98. McCabe, J.F.; Rusby, S. Water Absorption, Dimensional Change and Radial Pressure in Resin Matrix Dental Restorative Materials. *Biomaterials* (2004) 25, 4001-4007.
99. Ferracane, J.L. Hygroscopic and Hydrolytic Effects in Dental Polymer Networks. *Dental Materials* (2006) 22, 211-222.
100. Örtengren, U.; Wellendorf, H.; Karlsson, S.; Ruyter, I.E. Water Sorption and Solubility of Dental Composites and Identification of Monomers Released in an Aqueous Environment. *Journal of Oral Rehabilitation* (2001) 28, 1106-1115.
101. Sevkusic, M.; Schuster, L.; Rothmund, L.; Dettinger, K.; Maier, M.; Hickel, R.; Van Landuyt, K.L.; Durner, J.; Högg, C.; Reichl, F.-X. The Elution and Breakdown Behavior of Constituents from Various Light-Cured Composites. *Dental Materials* (2014) 30, 619-631.
102. Ito, S.; Hashimoto, M.; Wadgaonkar, B.; Svizero, N.; Carvalho, R.M.; Yiu, C.; Rueggeberg, F.A.; Foulger, S.; Saito, T.; Nishitani, Y.; et al. Effects of Resin Hydrophilicity on Water Sorption and Changes in Modulus of Elasticity. *Biomaterials* (2005) 26, 6449-6459.
103. Asaoka, K.; Hirano, S. Diffusion Coefficient of Water through Dental Composite Resin. *Biomaterials* (2003) 24, 975-979.
104. Braden, M.; Causton, E.E.; Clarke, R.L. Diffusion of Water in Composite Filling Materials. *Journal of Dental Research* (1976) 55, 730-732.
105. Pearson, G.J. Long Term Water Sorption and Solubility of Composite Filling Materials. *Journal of Dentistry* (1979) 7, 64-68.

106. Neumann, M.G.; Schmitt, C.C.; Catalina, F.; Goi, B.E. The Relation Between the Polymerization Rates and Swelling Coefficients for Copolymers Obtained by Photoinitiation. *Polymer Testing* (2007) 26, 189-194.
107. Palin, W.M.; Fleming, G.J.P.; Burke, F.J.T.; Marquis, P.M.; Randall, R.C. The Influence of Short and Medium-Term Water Immersion on the Hydrolytic Stability of Novel Low-Shrink Dental Composites. *Dental Materials* (2005) 21, 852-863.
108. Wei, Y.-j.; Silikas, N.; Zhang, Z.-t.; Watts, D.C. The Relationship between Cyclic Hygroscopic Dimensional Changes and Water Sorption/Desorption of Self-Adhering and New Resin-Matrix Composites. *Dental Materials* (2013) 29, e218-e226.
109. Sideridou, I.; Tserki, V.; Papanastasiou, G. Study of Water Sorption, Solubility and Modulus of Elasticity of Light-Cured Dimethacrylate-based Dental Resins. *Biomaterials* (2003) 24, 655-665.
110. T., A.; H., M.; T., H. The Effects of Cross-Linking Agents on the Water Sorption and Solubility Characteristics of Denture Base Resin. *Journal of Oral Rehabilitation* (1996) 23, 476-480.
111. J., P.R.; A., D. Model of Sorption of Simple Molecules in Polymers. *Journal of Polymer Science: Polymer Physics Edition* (1980) 18, 1103-1124.
112. Santos, C.; Clarke, R.L.; Braden, M.; Guitian, F.; Davy, K.W.M. Water Absorption Characteristics of Dental Composites Incorporating Hydroxyapatite Filler. *Biomaterials* (2002) 23, 1897-1904.
113. Musanje, L.; Shu, M.; Darvell, B.W. Water Sorption and Mechanical Behaviour of Cosmetic Direct Restorative Materials in Artificial Saliva. *Dental Materials* (2001) 17, 394-401.
114. Bastioli, C.; Romano, G.; Migliaresi, C. Water Sorption and Mechanical Properties of Dental Composites. *Biomaterials* (1990) 11, 219-223.
115. Göhring, T.N.; Besek, M.J.; Schmidlin, P.R. Attritional Wear and Abrasive Surface Alterations of Composite Resin Materials in Vitro. *Journal of Dentistry* (2002) 30, 119-127.

116. Munksgaard, E.C. Changes in Expansion and Mechanical Strength During Water Storage of a Traditional and Three Modified Resin Composites. *Acta Odontologica Scandinavica* (2002) 60, 203-207.
117. Ferracane, J.L.; Berge, H.X.; Condon, J.R. In Vitro Aging of Dental Composites in Water—Effect of Degree of Conversion, Filler Volume, and Filler/Matrix Coupling. *Journal of Biomedical Materials Research* (1998) 42, 465-472.
118. Momoi, Y.; McCabe, J.F. Hygroscopic Expansion of Resin Based Composites During 6 Months of Water Storage. *British Dental Journal* (1994) 176, 91.
119. Sarrett, D.C.; Ray, S. The Effect of Water on Polymer Matrix and Composite Wear. *Dental Materials* (1994) 10, 6-10.
120. Feilzer, A.J.; De Gee, A.J.; Davidson, C.L. Relaxation of Polymerization Contraction Shear Stress by Hygroscopic Expansion. *Journal of Dental Research* (1990) 69, 36-39.
121. Versluis, A.; Tantbirojn, D.; Lee, M.S.; Tu, L.S.; DeLong, R. Can Hygroscopic Expansion Compensate Polymerization shrinkage? Part I. Deformation of Restored Teeth. *Dental Materials* (2011) 27, 126-133.
122. Meriwether, L.A.; Blen, B.J.; Benson, J.H.; Hatch, R.H.; Tantbirojn, D.; Versluis, A. Shrinkage Stress Compensation in Composite-Restored Teeth: Relaxation or Hygroscopic Expansion? *Dental Materials* (2013) 29, 573-579.
123. Hansen, E.K.; Asmussen, E. Marginal Adaptation of Posterior Resins: Effect of Dentin-Bonding Agent and Hygroscopic Expansion. *Dental Materials* (1989) 5, 122-126.
124. Koike, T.; Hasegawa, T.; Manabe, A.; Itoh, K.; Wakumoto, S. Effect of Water Sorption and Thermal Stress on Cavity Adaptation of Dental Composites. *Dental Materials* (1990) 6, 178-180.
125. Rüttermann, S.; Krüger, S.; Raab, W.H.M.; Janda, R. Polymerization Shrinkage and Hygroscopic Expansion of Contemporary Posterior Resin-based Filling Materials—A Comparative Study. *Journal of Dentistry* (2007) 35, 806-813.

126. Attin, T.; Buchalla, W.; Kielbassa, A.M.; Hellwig, E. Curing Shrinkage and Volumetric Changes of Resin-modified Glass Ionomer Restorative Materials. *Dental Materials* (1995) 11, 359-362.
127. Feilzer, A.J.; Kakaboura, A.I.; de Gee, A.J.; Davidson, C.L. The Influence of Water Sorption on the Development of Setting Shrinkage Stress in Traditional and Resin-modified Glass Ionomer Cements. *Dental Materials* (1995) 11, 186-190.
128. Watts, D.C.; Kisumbi, B.K.; Toworfe, G.K. Dimensional Changes of Resin/Ionomer Restoratives in Aqueous and Neutral Media. *Dental Materials* (2000) 16, 89-96.
129. Tilbrook, D.A.; Pearson, G.J.; Braden, M.; Coveney, P.V. Prediction of Polymerization Shrinkage Using Molecular Modeling. *J. Polym. Sci., Part B: Polym. Phys* (2003) 41, 528-548.
130. Tantbirojn, D.; Versluis, A.; Pintado, M.R.; DeLong, R.; Douglas, W.H. Tooth Deformation Patterns in Molars After Composite Restoration. *Dental Materials* (2004) 20, 535-542.
131. Pearson, G.J.; Hegarty, S.M. Cusp Movement in Molar Teeth Using dentine Adhesives and Composite Filling Materials. *Biomaterials* (1987) 8, 473-476.
132. Martin, N.; Jedyakiewicz, N.M.; Williams, D.F. Cuspal Deflection During Polymerisation of Composite Lutes of Ceramic Inlays1Work presented at the IADR/CED Conference in Madrid, September 1997 and submitted as a component of a Ph.D. thesis by N. Martin.1. *Journal of Dentistry* 1999, 27, 29-36.
133. Suliman, A.-H.; Boyer, D.B.; Lakes, R.S. Polymerization Shrinkage of Composite Resins: Comparison with Tooth Deformation. *The Journal of Prosthetic Dentistry* (1994) 71, 7-12.
134. Kemp-Scholte, C.M.; Davidson, C.L. Marginal Sealing of Curing Contraction Gaps in Class V Composite Resin Restorations. *Journal of Dental Research* (1988) 67, 841-845.
135. Lutz, F.; Krejci, I.; Barbakow, F. Quality and Durability of Marginal Adaptation in Bonded Composite Restorations. *Dental Materials* (1991) 7, 107-113.

136. Kidd, E.A.; Joyston-Bechal, S.; Beighton, D. Diagnosis of Secondary Caries: a Laboratory Study. *British Dental Journal* (1994) 176, 135.
137. Moharamzadeh, K.; Brook, I.M.; Van Noort, R. Biocompatibility of Resin-based Dental Materials. *Materials* (2009) 2, 514-548.
138. Yoshii, E. Cytotoxic Effects of Acrylates and Methacrylates: Relationships of Monomer Structures and Cytotoxicity. *Journal of Biomedical Materials Research* (1997) 37, 517-524.
139. Gupta, S.K.; Saxena, P.; Pant, V.A.; Pant, A.B. Release and Toxicity of Dental Resin Composite. *Toxicol Int* (2012) 19, 225-234.
140. Batarseh, G.; Windsor, L.; Labban, N.; Liu, Y.; Gregson, K. Triethylene Glycol Dimethacrylate Induction of Apoptotic Proteins in Pulp Fibroblasts. *Operative Dentistry* (2014) 39, E1-E8.
141. Chang, H.-H.; Chang, M.-C.; Wang, H.-H.; Huang, G.-F.; Lee, Y.-L.; Wang, Y.-L.; Chan, C.-P.; Yeung, S.-Y.; Tseng, S.-K.; Jeng, J.-H. Urethane Dimethacrylate Induces Cytotoxicity and Regulates Cyclooxygenase-2, Hemeoxygenase and Carboxylesterase Expression in Human Dental Pulp Cells. *Acta Biomaterialia* (2014) 10, 722-731.
142. Santerre, J.P.; Shajii, L.; Tsang, H. Biodegradation of Commercial Dental Composites by Cholesterol Esterase. *Journal of Dental Research* (1999) 78, 1459-1468.
143. METTE, F.; CHRISTIAN, M.E. Enzymatic Degradation of BISGMA/TEGDMA-Polymers Causing Decreased Microhardness and Greater Wear in Vitro. *European Journal of Oral Sciences* (1990) 98, 351-355.
144. CHRISTIAN, M.E.; METTE, F. Enzymatic Hydrolysis of (di)Methacrylates and their Polymers. *European Journal of Oral Sciences* (1990) 98, 261-267.
145. A., B.T.; C., Z.W.; Y., T.P.; D., E.J.; M., Y.D. Effect of Esterase on Methacrylates and Methacrylate Polymers in an Enzyme Simulator for Biodurability and

- Biocompatibility Testing. *Journal of Biomedical Materials Research* (1994) 28, 59-63.
146. Finer, Y.; Santerre, J.P. The Influence of Resin Chemistry on a Dental Composite's biodegradation. *Journal of Biomedical Materials Research Part A* (2004) 69A, 233-246.
147. Finer, Y.; Santerre, J.P. Biodegradation of a Dental Composite by Esterases: Dependence on Enzyme Concentration and Specificity. *Journal of Biomaterials Science, Polymer Edition* (2003) 14, 837-849.
148. Schmalz, G.; Preiss, A.; Arenholt-Bindslev, D. Bisphenol-A Content of Resin Monomers and Related Degradation Products. *Clinical Oral Investigations* (1999) 3, 114-119.
149. Imai, Y.; Watanabe, M.; Ohsaki, A. Analysis of Major Components and Bisphenol A in Commercial Bis-GMA and Bis-GMA-based Resins Using High Performance Liquid Chromatography. *Dental Materials Journal* (2000) 19, 263-269.
150. Rubin, B.S. Bisphenol A: An Endocrine Disruptor with Widespread Exposure and Multiple Effects. *The Journal of Steroid Biochemistry and Molecular Biology* (2011) 127, 27-34.
151. Rochester, J.R. Bisphenol A and Human Health: A Review of the Literature. *Reproductive Toxicology* (2013) 42, 132-155.
152. Marcus, R.; Regina, P. Isosorbide as a Renewable Platform chemical for Versatile Applications—Quo Vadis? *ChemSusChem* (2012) 5, 167-176.
153. Fenouillot, F.; Rousseau, A.; Colomines, G.; Saint-Loup, R.; Pascault, J.P. Polymers from Renewable 1,4:3,6-dianhydrohexitols (isosorbide, isomannide and isoidide): A review. *Progress in Polymer Science* (2010) 35, 578-622.
154. Saxon, D.J.; Luke, A.M.; Sajjad, H.; Tolman, W.B.; Reineke, T.M. Next-generation polymers: Isosorbide as a renewable alternative. *Progress in Polymer Science* (2020) 101, 101196.

155. Fleche .G; Huchette .M. Isosorbide. Preparation, Properties and Chemistry. *Starch - Stärke* (1986) 38, 26-30.
156. Jones, M.; Inkielewicz, I.; Medina, C.; Santos-Martinez, M.J.; Radomski, A.; Radomski, M.W.; Lally, M.N.; Moriarty, L.M.; Gaynor, J.; Carolan, C.G.; et al. Isosorbide-Based Aspirin Prodrugs: Integration of Nitric Oxide Releasing Groups. *Journal of Medicinal Chemistry* (2009) 52, 6588-6598.
157. Gilmer, J.F.; Clune-Moriarty, L.; Lally, M. Efficient Aspirin Prodrugs US8486974B2, 2013.
158. Chrysant, S.G.; Glasser, S.P.; Bittar, N.; Shahidi, F.E.; Danisa, K.; Ibrahim, R.; Watts, L.E.; Garutti, R.J.; Ferraresi, R.; Casareto, R. Efficacy and Safety of Extended-Release Isosorbide Mononitrate for Stable Effort Angina Pectoris. *The American Journal of Cardiology* (1993) 72, 1249-1256.
159. García-Pagán, J.C.; Villanueva, C.; Vila, M.C.; Albillos, A.; Genescà, J.; Ruiz-Del-Arbol, L.; planas, R.; Rodriguez, M.; Calleja, J.L.; González, A.; et al. Isosorbide Mononitrate in the Prevention of First Variceal Bleed in Patients Who Cannot Receive β -blockers. *Gastroenterology* (2001) 121, 908-914.
160. Gilmer, J.F.; Lally, M.N.; Gardiner, P.; Dillon, G.; Gaynor, J.M.; Reidy, S. Novel Isosorbide-based Substrates for Human Butyrylcholinesterase. *Chemico-Biological Interactions* (2005) 157-158, 317-319.
161. Okada, M.; Tsunoda, K.; Tachikawa, K.; Aoi, K. Biodegradable Polymers based on Renewable Resources. IV. Enzymatic Degradation of Polyesters Composed of 1,4:3.6-dianhydro-D-glucitol and Aliphatic Dicarboxylic Acid Moieties. *Journal of Applied Polymer Science* (2000) 77, 338-346.
162. Gogolewski, S.; Gorna, K.; Zaczynska, E.; Czarny, A. Structure–Property Relations and Cytotoxicity of Isosorbide-based Biodegradable Polyurethane Scaffolds for Tissue Repair and Regeneration. *Journal of Biomedical Materials Research Part A* (2008) 85A, 456-465.
163. Łukaszczyk, J.; Janicki, B.; Frick, A. Investigation on Synthesis and Properties of Isosorbide based bis-GMA Analogue. *Journal of Materials Science: Materials in Medicine* (2012) 23, 1149-1155.

164. Shin, S.; Kim, Y.-J.; Toan, M.; Kim, J.-G.; Nguyen, T.; Ku Cho, J. Property Enhancement of Dental Composite Prepared with an Isosorbide-based Photocurable Compound by Mixing with TEGDMA. *European Polymer Journal* (2017) 92, 338-345.
165. Kim, J.S.; Park, H.W.; Lee, J.-H.; Lee, S.-H.; Cho, J.K.; Shin, S. Synthesis of a Novel Isosorbide-based Dental Material with Improved Water Sorption. *European Polymer Journal* (2019) 112, 629-635.
166. Berlanga Duarte María, L.; Reyna Medina Luis, A.; Reyes Patricia, T.; González Pérez Sergio, E.; Herrera González Ana, M. Biobased Isosorbide Methacrylate Monomer as an Alternative to Bisphenol A Glycerolate Dimethacrylate for Dental Restorative Applications. *Journal of Applied Polymer Science* (2016) 134.
167. Łukaszczyk, J.; Janicki, B.; Kożuch, J.; Wojdyła, H. Synthesis and Characterization of Low Viscosity Dimethacrylic Resin Based on Isosorbide. *Journal of Applied Polymer Science* (2013) 130, 2514-2522.
168. Vazifehasl, Z.; Hemmati, S.; Zamanloo, M.; Jaymand, M. Synthesis and Characterization of Novel Diglycidyl Methacrylate-based Macromonomers on Isosorbide for Dental Composites. *Macromolecular Research* (2013) 21, 427-434.
169. Jun, S.-K.; Cha, J.-R.; Knowles, J.C.; Kim, H.-W.; Lee, J.-H.; Lee, H.-H. Development of Bis-GMA-free Biopolymer to Avoid Estrogenicity. *Dental Materials* (2020) 36, 157-166.
170. Feng, X.; East, A.; Hammond, W.; Ophir, Z.; Zhang, Y.; Jaffe, M. Thermal Analysis Characterization of Isosorbide-containing Thermosets. *Journal of Thermal Analysis and Calorimetry* (2012) 109, 1267-1275.
171. Introduction to NMR spectroscopy. Available online: https://www.structbio.pitt.edu/images/sbl2014/notes/nmr_ref_notes_2011.pdf
172. Silverstein, R.M., Webster, F. X., & Kiemle, D. J. *Spectrometric identification of organic compounds.*, Sevinth Edition ed.; John Wiley & Sons.: Hoboken, NJ (2005).

173. Edwards, J. Principles of NMR. Available online: <https://www.researchgate.net/publication/268026544> Principles of NMR (Accessed on December 10th 2021)
174. NMR. Available online: <https://www2.chemistry.msu.edu/faculty/reusch/orgpage/nmr.htm> (Accessed on December 10th 2021)
175. Dentistry-Polymer-Based Restorative Materials; International Organization for Standardization. ISO 4049-2009.
176. Park, J.; Ye, Q.; Topp, E.M.; Misra, A.; Kieweg, S.L.; Spencer, P. Effect of Photoinitiator System and Water Content on Dynamic Mechanical Properties of a Light-Cured bisGMA/HEMA Dental Resin. *Journal of Biomedical Materials Research Part A* (2010) 93A, 1245-1251.
177. Plastics - Determination of Flexural Properties; International Organization for Standardization. ISO 178-2010.
178. Fujisawa, S. Nuclear Magnetic Resonance Spectra of Bis-GMA and Iso-bis-GMA. *Dent Mater J* (1994) 13, 251-255.
179. Law, K.-Y. Definitions for Hydrophilicity, Hydrophobicity, and Superhydrophobicity: Getting the Basics Right. *The Journal of Physical Chemistry Letters* (2014) 5, 686-688.
180. Ahmad, D.; van den Boogaert, I.; Miller, J.; Presswell, R.; Jouhara, H. Hydrophilic and Hydrophobic Materials and their Applications. *Energy Sources, Part A: Recovery, Utilization, and Environmental Effects* (2018) 40, 2686-2725.
181. Namen, F.; Galan Jr., J.; Oliveira, J.F.d.; Cabreira, R.D.; Costa e Silva Filho, F.; Souza, A.B.; Deus, G.d. Surface Properties of Dental Polymers: Measurements of Contact Angles, Roughness and Fluoride Release. *Materials Research* (2008) 11, 239-243.

182. Ghose, A.K.; Viswanadhan, V.N.; Wendoloski, J.J. Prediction of Hydrophobic (Lipophilic) Properties of Small Organic Molecules Using Fragmental Methods: An Analysis of ALOGP and CLOGP Methods. *The Journal of Physical Chemistry A* (1998) 102, 3762-3772.
183. Machatha, S.G.; Yalkowsky, S.H. Comparison of the Octanol/Water Partition Coefficients Calculated by ClogP®, ACDlogP and KowWin® to Experimentally Determined Values. *International Journal of Pharmaceutics* (2005) 294, 185-192.
184. Nakano, T. Synthesis, Structure and Function of π -stacked Polymers. *Polymer Journal* (2010) 42, 103-123.
185. Pongprueksa, P.; De Munck, J.; Duca, R.C.; Poels, K.; Covaci, A.; Hoet, P.; Godderis, L.; Van Meerbeek, B.; Van Landuyt, K.L. Monomer Elution in Relation to Degree of Conversion for Different Types of Composite. *Journal of Dentistry* (2015) 43, 1448-1455.
186. Zhu, Y.; Durand, M.; Molinier, V.; Aubry, J.-M. Isosorbide as a Novel Polar Head Derived from Renewable Resources. Application to the Design of Short-Chain Amphiphiles with Hydrotropic Properties. *Green Chemistry* (2008) 10, 532-540.
187. Ilie, N.; Hilton, T.J.; Heintze, S.D.; Hickel, R.; Watts, D.C.; Silikas, N.; Stansbury, J.W.; Cadenaro, M.; Ferracane, J.L. Academy of Dental Materials guidance—Resin composites: Part I—Mechanical properties. *Dental Materials* (2017) 33, 880-894.
188. Yiu, C.K.Y.; King, N.M.; Pashley, D.H.; Suh, B.I.; Carvalho, R.M.; Carrilho, M.R.O.; Tay, F.R. Effect of Resin Hydrophilicity and Water Storage on Resin Strength. *Biomaterials* (2004) 25, 5789-5796.